New Tools for Multimodal Imaging of Immune Cells

Giorgia Zambito

Lay-out and printing by Optima Grafische Communicatie (www.ogc.nl)

New Tools for Multimodal Imaging of Immune Cells

Doctoral Thesis

To obtain the degree of doctor
From Erasmus University of Rotterdam
On the authority of the Rector Magnificus

Prof.dr. F.A. van der Duijn Schouten

According to the decision if the Council of Deans
To be defended in public on

8th September 2021 at 10:30

By

Giorgia Zambito
Born in Palermo, Italy

Erasmus University Rotterdam

Promotor
Prof. dr. C.W.G.M Löwik

Other members
Prof. Dr. Riccardo Fodde
Prof. Dr. Frederick A. Verburg
Prof. Dr. Ferry Ossendorp
Piera di Martino, Ph.D.

Copromotor
Laura Mezzanotte, Ph.D.

CONTENTS

Chapter 1	General introduction Aim and thesis outline	7
Chapter 2	Emerging tools on Bioluminescence imaging	27
Chapter 3	Evaluating Brightness and Spectral Properties of Click Beetle and Firefly Luciferases Using Luciferin Analogues: Identification of Preferred Pairings of Luciferase and Substrate for In Vivo	45
Chapter 4	Red-shifted click beetle luciferase mutant expands the multicolor bioluminescent palette for deep tissue imaging	65
Chapter 5	Near-infrared bioluminescence imaging of two-cell populations in living mice	83
Chapter 6	Fluorinated Mannose-targeted PLGA nanoparticles for imaging tumor-associated Macrophages by MRI and optical imaging	99
Appendix	General discussion	123
	Future perspectives	133
	Nederlandse samenvatting	137
	Sommario	143
	About the author	147
	Portfolio	149
	List of publications	151
	Dankwoord (Acknowledgements)	153

1

General introduction
Aim and thesis outline

INTRODUCTION

How to follow cells with non-invasive techniques

Non-invasive cell tracking of cells is an emerging approach to visualize and study cells in their native environment and to produce the next-generation cell-based therapy for chronic conditions as cancer or autoimmune disease[1]. As immune cells are indispensable for immunotherapeutic interventions, tracking their presence in the body, organs or tissues can provide crucial information on their biological role. Indeed, immune cells like dendritic cells (DCs), macrophages, granulocytes and natural killer (NK) participate to the first line of defense forming the *innate immune system* and they are less specific compared to for instance T cells and B cells that instead act in *the adoptive immune system*.[2,3] Each immune cell type has a well-defined role in the cascade of events that occurs after the encounter with a pathogen or transformed cells. In particular, regulatory T cells (T regs) and tumor-associated macrophages (TAMs) are known to infiltrate and promote tumor growth[4].

As inflammation is one of the major hallmarks of cancer, monitoring the trafficking of immune cells in the tumor micro-environment (TME) provides fundamental insight on the status of pathophysiological conditions and on the success of administered therapies. It will also provide us opportune knowledge on possible physiological barriers that might interfere with the bio-distribution, release and accumulations of drugs in the TME[5].

Given the clear potentiality for non-invasive in vivo cell tracking, much progress has been made in the recent years. Most imaging methods require cell labelling prior cell visualization. Cell labelling can be broadly performed in two different ways: by direct and indirect labelling. Direct labelling consists of targeting a specific receptor or enzyme on the cell membrane or inside the cell. Indirect labelling relies on passive uptake of the label via i.e. endocytosis. Once labelled, the cells can be visualized by a variety of in vivo imaging modalities that are used in pre-clinal research:

1. **Fluorescence,** if cells are labelled with a fluorescent tag that after excitation with light of a certain wavelength will emit light of a higher wavelength that can be discriminated and detected using a specific filter and camera system.
2. **Bioluminescence (BL),** when cells are indirectly labelled with a bioluminescent reporter gene that is translated in to an enzyme (luciferase) that can generate light after addition of a substrate (luciferin). BL can be detected using a sensitive charge-coupled device (CCD) camera system
3. **Optoacoustic,** if cells are targeted with contrast agents with optical absorption properties that after excitation with pulsed light will transform the light into an ultra-sound wave that can be detected and imaged using an ultrasound scanner (sonography or echo)).

4. **Magnetic Resonance Imaging (MRI),** if cells incorporate a paramagnetic contrast agent that can be visualized in a scanner using a high magnetic field.
5. **Computed Tomography (CT),** when cells are labeled with gold or silver nanoparticles that can be imaged tomographically (in 3D) using X-Rays.
6. **Positron Emission Tomography (PET)** and **Single-Photon Emission Computerized Tomography** (**SPECT**) if cells are labelled with radioactive probes that can be detected with radioactive detectors in 3D.
7. **Ultrasound** if cells are targeted with bubbles filled with air, named microbubbles, that can be detected when the cells are exposed to an ultrasound wave and the echo is detected and transformed into an image.

Within the focus of this thesis, BLI and MRI techniques will be examined in detail and used as imaging techniques for cell labelling in vivo.

Visualize different glowing cells by in vivo bioluminescence imaging

Optical imaging modalities like bioluminescence offers a valuable research tool to explore and understand molecular mechanisms in health and diseases. It is largely applied in preclinical research to visualize molecular processes like e.g. gene expression, protein–protein interactions, cell proliferation, migration, and differentiation, but also to determine total cell distribution in small animals[6,7]. For cancer studies, BLI is routinely used to assess tumor formation, progression and metastasis but also for drug screening to assess therapeutic efficacy. BLI is more sensitive compared to fluorescence because it is not affected by auto-fluorescence and it does not require the use of an external excitation laser that can be toxic for living cells.

In general, the production of bioluminescent light occurs in nature when the luciferase-enzyme catalyzes the oxidation of a substrate typically named luciferin[8,9]. Relaxation of the luciferin oxidation product from its excited state is accompanied by a release of a quantum of light, which can be detected as an analytical signal by the appropriate device[10]. BL has become a common technique used in preclinical research because it is cheap and easy to perform compared to other imaging modalities. **In chapter 2,** a range of novel bioluminescent systems is described along with a plethora of novel luciferin analogues which expand the palette of colors (emission wavelengths) available for measuring the enzymatic activities[11,12]. Nevertheless, among several available luciferases, a few have been found to be useful for practical application. Luciferase size, the wavelength emitted, enzyme thermostability, optimal pH of the reaction, and the need for cofactors (Mg^{2+}, ATP and O_2) are parameters that may differ for luciferases from different groups of organisms, and this may affect the choice of the research area. Thus, it is crucial to consider the biochemical properties before choosing the best biolumi-

nescent probe suitable for the study[13,14]. **In chapter 3**, a valuable guidance of different BL systems using D-luciferin analogues in vitro and in vivo is provided. In general, it is convenient to broadly divide natural bioluminescence based on substrate affinity. Thus, we can list: D-luciferin dependent luciferases (Fireflies, click beetles and rail road worms); coelenterazine-dependent luciferases (Nanoluc, Renilla, Copepoda, shrimps); bacterial luciferases; fungal luciferases and Cypiridina luciferases[13,15,16,17,12].

For in vivo detection, BL, similar to the other optical imaging modalities, suffers from limited tissue penetration capability of the emitted light which is dependent on the wavelength and highest in the red and near infrared part of the spectrum. Therefore, by using engineered red-shifted luciferases and/or synthetic luciferin analogues, the light absorption by tissue components (hemoglobin, melanin etc.*)* will be considerably less increasing the detection of light *in vivo*[18,19]. To address this issue, bioluminescent luciferases have been mutated to emit longer wavelengths in the so-called "bio-optical window" (λ = 600 nm–800 nm)[20,21]. A stunning example of the power of red-shifted luciferase–luciferin pair is visualizing individual tumor cells in the lungs of mice and to detect small numbers of neurons in freely moving animals[22]. Another advance of an improved luciferase mutant is NanoLuc, a blue luciferase isolated form deep-sea shrimp and subsequently engineered to work optimally with furimazine and more recently with fluorofurimazine[17,23]. This system produces high-intensity and red-shifted glow-type luminescence that is successfully applied in vivo. In addition, the color of luciferases can also be red-shifted using bioluminescence probes via the resonance energy transfer (BRET) systems[10]. For instance, Antares luciferase is a fusion of NanoLuc luciferase and the orange fluorescent protein CyOFP, where the NanoLuc emitted light will exitate CyOFP leading to an auto-illuminated fluorescent probe with higher quantum yield (λ_{max} ~ 600 nm), extending the luciferase color palette[24]. BRET system represents a practical alternative to fluorescence overcoming issues related with phototoxicity and photobleaching[25,26,27].

Overall, BL imaging is a quite simple and relatively cheap technique to perform compared to the other imaging modalities **(Figure 1)**. Indeed, the detection of photons emitted relies mainly on the use of a CCD camera that processes the image and quantify the photons using a validated spectral unmixing algorithm as part of the instrument software[28–30]. The spectral unmixing algorithm is an essential tool if multiple luciferase-expressing cells emitting light with a different spectrum are injected in vivo. Thanks to the algorithm, it will possible to distinguish and quantify the photons emitted by the multicolored cells accumulated in specific sites in vivo[22,31].

Within the focus of this thesis, newly developed red-shifted click beetle luciferases will be accurately examined. Color variability and pH-insensitivity of click beetles within

the physiological range of pH (from 6 to 8), make them an attractive choice for in vivo multicolor BL imaging[32,33].

In chapter 4, we addressed the challenge to create a bioluminescent system where two luciferases are used with one single substrate for dual-color in vivo imaging. We introduced a novel click beetle mutant named CBG2 that can be used for near-infrared BLI imaging. CBG2 paired with NH_2-NpLH2 substrate (λ = 660 nm) can be used in conjunction with the near-infrared system CBR2/NH_2-NpLH2[32] (λ = 730 nm) and applied for dual-color near-infrared (NIR) BLI in vivo. Using this system avoids the use of sequential administration of 2 substrates with an interval, making imaging sessions shorter that also increases animal welfare [26,34]. **In chapter 5,** a detailed protocol to perform spectral unmixing algorithm for two-cell populations is described. Therefore, BL multispectral images can be resolved and quantified as single spectral contribution. This enables the visualization of multiple cell types in deep-tissue by injection of a single substrate. Experimental set-up for *in vitro* and *in vivo* tests are explained and recommendations or critical steps are also highlighted.

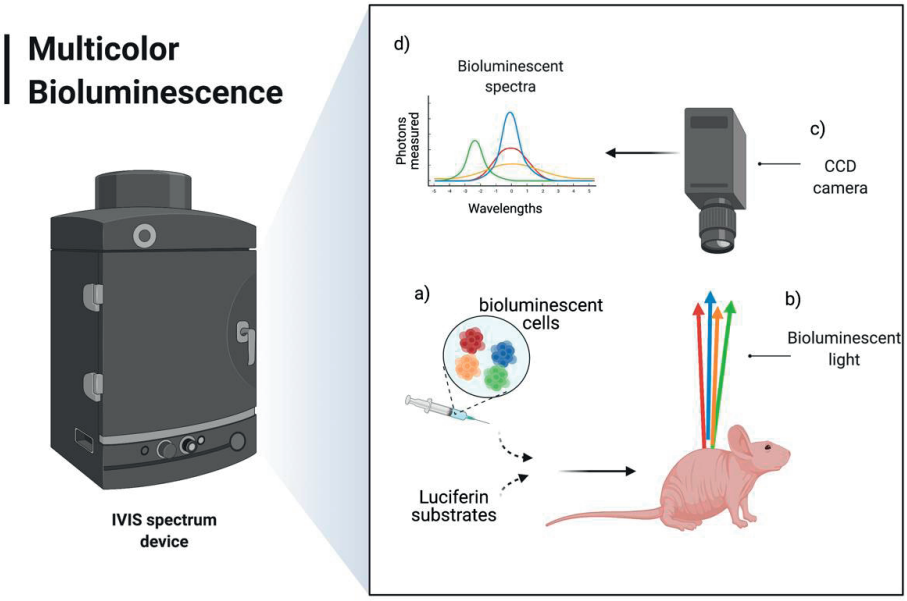

Figure 1. Multicolor Bioluminescence imaging scheme. a) Injection of bioluminescent cells can be done intravenously. Specific substrates are instead usually injected intraperitoneally. **b**) The mouse is then placed in the IVIS imaging device. **c)** Thanks to a sensitive CCD camera installed inside the machine, the luciferase emissions are registered and measured accurately. **d)** The spectral- unmixing algorithm tool enables to attribute the photons registered by the CCD camera at specific wavelength to a distinct luciferase. This allows to characterize and draw specific emission spectra for the luciferases tested. For complete details on Spectral unmixing tool, **chapters 4 and 5** may be consulted.

The importance of targeting tumor-associated macrophages in cancer

Tumors are comprised of heterogeneous cell populations including transformed cells and untransformed cells such as stromal, endothelial, and immune cells, that are indispensable in their microenvironment[35]. The evasion of immune function is commonly believed as one of the hallmarks of cancer. Therefore, understanding the status and interaction between the tumor and the immune system in the tumor microenvironment (TME) is of importance for future therapeutic interventions[36].

Amongst immune cells, macrophages play a pivotal role in autoimmune diseases, infections and cancers and they can act as pro-inflammatory M1 macrophages (classical activation) involved in the clearance of cell debris and pathogens. However, macrophages are cells with great plasticity that can modify their phenotype reversibly depending on stimuli like cytokines, chemokines, growth factors released in their surroundings[37]. Thus, they can skew away from the classical activation by proper stimuli and turn into M2 macrophages (alternative activation). M2-macrophages are involved in the clearance of apoptotic cells modulating the anti-inflammatory response. However, the dichotomy between M1 and M2 phenotypes represents an oversimplification of the possible scenario because due to their plasticity, macrophages might also express markers characteristic of both activation states[36,38].

In tumor progression, several types of inflammatory cells such as fibroblasts, granulocytes, lymphocytes, and macrophages, are recruited into the tumor site. Macrophages that reside inside the tumor or in the surrounding stroma are classified as tumor-associated macrophages (TAMs) that usually have an M2-phenotype. Their role consists on secreting pro-angiogenic factors promoting metastasis and neoplastic formation. They are beneficial to produce several proteolytic enzymes and motor-related proteins to support the invasion and metastasis of tumors[39,40].

TAMs are located in various types of tumors such as glioblastoma and lymphoma, breast, prostate, thyroid, and ovarian tumors leading to rapid cancer growth and a decrease in patient survival[2,41].

Indeed, high infiltration of tumor-associated macrophage has been correlated with increased tumor invasion and metastasis. TAMs can efficiently enter the hypoxic/necrotic areas of solid tumors (tumor nest) and still promoting tumor evasion. Hypoxic TAMs can also contribute to suppress T-cell activation in different ways like upregulation of IL-10 and negative checkpoint regulators such as PD-L1[42]. In recent studies, it has been shown that TAMs are able to shape metabolic circuitries via an intricate crosstalk with cancer-

associated fibroblasts (CAFs) and adipocytes that provide nutrients to support tumor progression[43,44].

In recent years, research on TAM-targeting therapies have focused on the following aspects: suppressing the recruitment of macrophages, activating the repolarization of the original tumorigenic M2-like into an anti-tumor M1-like phenotype, and depleting TAMs[45].

Given the crucial importance of tracking macrophages, the ability to label and observe TAMs non-invasively can tremendously help to understand the temporal and spatial localization of this population in the TME. Moreover, given their phagocytic nature, they may represent an attractive target when nanoparticle-based strategies are employed.

Labelling TAMs: passive and active targeting by nanoparticles

Nanoparticles (NPs) have many promising attributes for targeted imaging. They are commonly used for cell labelling, enabling sensitive and specific monitoring of targets associated with cancer growth and metastasis by molecular imaging. The great advantage of NPs is that they can deliver a larger amount of imaging contrast agents to its target allowing improvements in sensitivity for in vivo imaging.

In vivo visualization of cells can be performed when a pure contrast agent or NPs are injected into the bloodstream that a-specifically or specifically target circulating cells in the body. Another method is to use pre-labelled cells of interest with designed NPs that are then injected into the bloodstream[46]. In **Figure 2**, a scheme illustrating various modalities for targeting and visualizing cells by MRI technique is shown. Once in the bloodstream, NPs can reach the target site passively (via the EPR effects) or actively (accumulation due to the targeting ligand that is expressed on the surface of the NPs that will bind to its target) increasing the accumulation of the contrast agent[47]. In general, NPs can be customized enabling their use as amplifiers of the signal. Different types of labeling probes have been proposed against TAMs and in general, nanotechnology provides a plethora of nanocarrier platforms with different sizes, shapes, surface properties, and compositions that improve their solubility, stability, and reduce immunogenicity. Liposomes, polymeric particles (PLGA nanoparticles or dendrimers), iron oxide NPs like superparamagnetic iron oxide nanoparticles (SPIONs), antibodies, and peptides are the main nanocarriers proposed in the past years.

In this thesis, we have focused on the use of nanoparticles with magnetic resonance properties and with high potentiality to study cell migration or cell trafficking to the tumor site in vivo. Areas which contain magnetic-labeled inflammatory cells will then appear as regions in MR images.

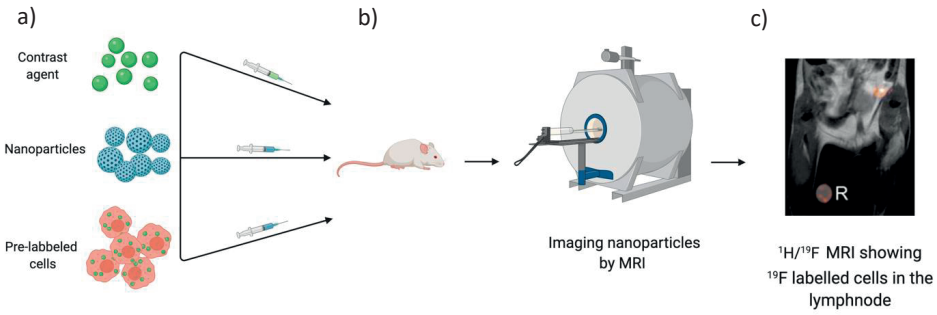

Figure 2. Schematic illustration for labelling and visualizing cells by in vivo MRI. Cells of interest can be targeted directly in the body via injection of the contrast agent or the nanoparticles incapsulating the contrast agent. An indirect targeting method is also possible when cells of interest are ex-vivo isolated, cultured and in vitro labelled with contrast agents/nanoparticles. Once the cells are positively labelled, the injection and imaging of cells is performed in vivo.

Passive targeting of TAMs relies on EPR effect

In regards of passive targeting, NP systems take advantage of irregular, disorganized and leaky tumor vasculature with high vascular density and impaired lymphatic drainage[47] **(Figure 3)**. These characteristics are attributed to solid tumors and inflamed tissue and is designated as the Enhanced Permeability and Retention (EPR)-effect. Thus, NPs can accumulate preferentially in tumor tissues guided by the leaky vasculature and passing through the interstitial vascular barrier and accumulate in the tumors helped by the pressure difference induced by poor lymphatic drainage resulting in their retention[48]. This requires a certain particle size to be generally between 10 and 200 nm, and its circulation time to be longer than 6 h[49]. Generally, passively targeted nanoparticles exploit the phagocytic activity of macrophages via cellular endocytosis. Once internalized, it will be possible to follow macrophage accumulation to their intended target in vivo. Macrophages can be imaged using in vivo cellular MRI techniques[50,51]. To do this, NPs are administered intravenously (i.v.) and are subsequently internalized by monocytes/macrophages in the reticuloendothelial system (specifically, the Kupffer cells of the liver and macrophages in the spleen, bone marrow and lymph nodes)[47]. MRI is typically performed 24h, 48 or 72h after the administration of the NPs, to allow the accumulation of labeled cells and to permit the clearance of non-internalized or bound NPs[52]. The in vivo labeling efficiency of macrophages is mainly dependent on nanoparticle composition like size, shape and surface coating. As will be discussed below, in order to actively target NPs and prevent rapid opsonization by the mononuclear phagocyte system (MPS), the NPs are often functionalized on the outside with polyethylene glycol (PEG) chains that also enhances the plasma half-life of nanoparticles and to which a targeting molecules can be attached [53,54].

For MRI in vivo imaging many different approaches might be cited[55]. For instance, gadolinium-based particles (~75-90 nm) for MRI imaging can be rapidly recognized and phagocytosed by macrophages leading to a positive MR signal effect on T1-weighted MR images and provide high detection sensitivity in assessing the progression of the tumor[56,57]. However, increased concerns about gadolinium deposition and toxicity of free gadolinium have been highlighted[58].

However, most studies are based on iron-based super-magnetic nanoparticles (SPIONs, ~80-150 nm) that provide darker contrast on T2-weighted magnetic strategy, useful for semi-quantitative assessment of TAM presence in cancer sites[59]. One strategy adopted is also to tag macrophages by using Ultra-small superparamagnetic iron oxide nanoparticles (USPIONs, ~ 20nm) for breast cancer[60]. USPIONs have a smaller size and longer circulation times compared to larger iron oxide agents, leading to greater uptake. An FDA approved USPIONs is Ferumoxytol (Feraheme™) (~30nm, -16mV) that has been found to be taken up passively by anti-inflammatory macrophages with a prolonged circulation half-life[61,62]. Interestingly, USPIOs have also been found to inhibit tumor growth by inducing pro-inflammatory macrophage polarization.[63]

However, passive targeting of cells by nanoparticles suffers from off-target outcomes. Circulation half-life time of these NPs can also be drastically decreased through uptake by the reticuloendothelial system (RES) located in the spleen, liver and bone marrow, further affecting NPs accumulation into tumor[51,47].

Active targeting of TAMs by tuning the surface functionality of nanoparticles

Active targeting is another approach to target cells via specific ligands presented on the surface of nanocarriers **(Figure 3).** In this way, the ligand will be recognized by the receptor that is over-expressed on the cellular membrane of the target cells. Moreover, decorated nanoparticles will also take advantage of the EPR effect but due to its targeting will be more retained in the tumor and therefore, deliver a greater amount of payload (contrast agent and/or drugs) to the desired cells compared to passive targeting only[64].

For tracking cells or delivering the contrast agent and/or drugs to specific regions, NPs such as antibodies[65], protease[66], aptamers and peptides [67–70].

Amongst targeted nanocarriers, poly-lactic-co-glycolic acid (PLGA) an FDA-approved copolymer, is one of the most exploited systems in preclinical research due to its biodegradability, biosafety, biocompatibility, versatility in formulation and functionalization and long shelf-life [71].

To visualize cell tracking and cell trafficking non-invasively in vivo, perfluorocarbons (PFCs) are emerging as a promising contrast agent for spectroscopic MRI. This is because fluorine-based contrast agents are found only in negligible traces in biological tissue meaning that the fluorine background is minimal and that the signal from exogenous fluorine is highly specific in vivo. Thus, the ^{19}F-agent functions like a tracer and it is able to detect the ^{19}F molecules that are associated with the labeled cells. The ^{19}F signal will be consequently proportional to the number of ^{19}F spins measured[72,73].

Amongst PFCs, perfluoro-15-crown-5-ether (PFCE) is one of the most attractive MRI contrast probes because it is FDA approved in a form of emulsion and therefore it is not toxic. In a recent study, USPIOs were compared with per-fluorocarbon (PFC) contrast agents for imaging TAMs in breast cancer. Imaging analysis showed that USPIO agents suffered from signal loss, whereas ^{19}F imaging provided more information on spatial distribution and density of TAMs in vivo[74]. However, one main limitation of ^{19}F-MRI cell tracking is the lower sensitivity compared to iron agents[51]. Indeed, relatively high concentration of

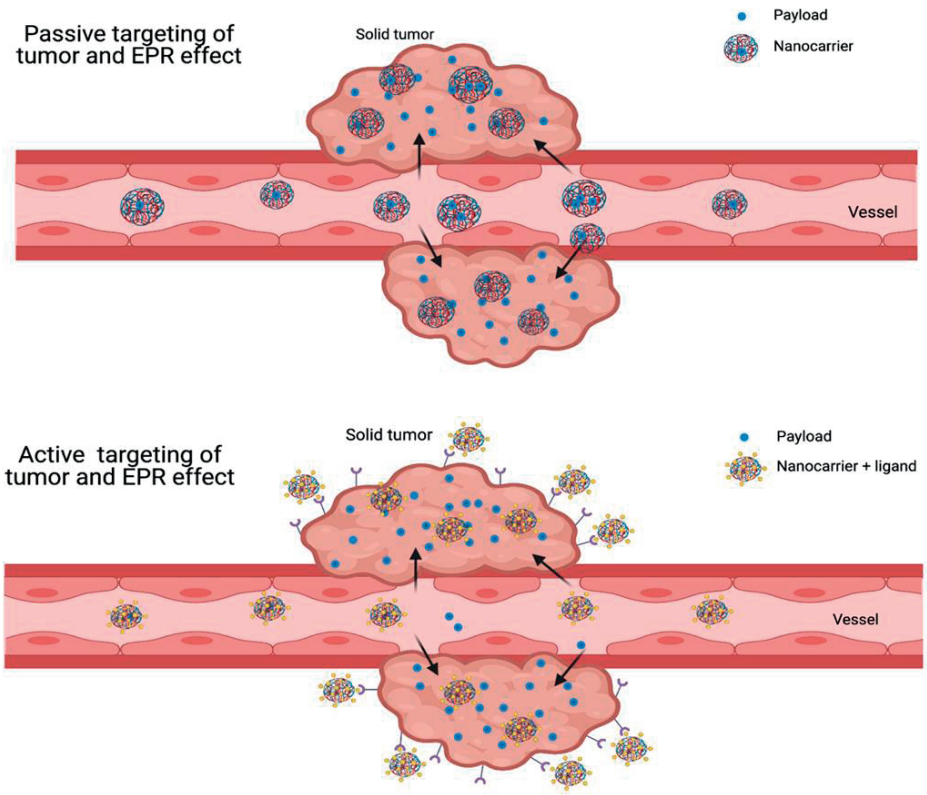

Figure 3. Schematic illustration for passive and active targeting of solid tumor by nanocarriers.

^{19}F signal must be reached to produce image quality comparable to proton images.[74,75]. Most studies have been performed at higher magnetic field strengths since low signal to noise ratios (SNR) present challenges due to the low ^{19}F concentrations in vivo.

Generally, most of PFCs in the form of a nano-emulsion are not miscible with hydrophilic or hydrophobic solvents and their surface decoration with ligands requires complex chemistry[76].

This also makes its combination with other functional molecules such as drugs, fluorescent tracker or surface ligand for specific targeting difficult. For these reasons we decided to encapsulate the PFCE in biodegradable organic-based nanocarriers like poly-lactic-co-glycolic acid (PLGA) NPs that act as protectors, provide good stability of the payload and are easy to functionalize.

In chapter 5, we focused on targeting macrophages with actively targeted PLGA nanoparticles, in breast cancer as a tumor model. This work has been performed in collaboration with the Chemistry department of the University of Camerino (Italy).

MRI as non-invasive imaging technique

MRI is a powerful non-invasive imaging technique that does no need ionizing radiation and characterized by high spatial-resolution. It is widely used to detect, follow, and define solid tumors, metastases and inflammation foci. As the human body predominantly consists of water, in the presence of an external magnetic field hydrogen nuclei (^{1}H or proton) will be aligned with the magnetic field. MRI will detect the small changes in spin frequencies of water hydrogen based on their surroundings when a high-magnetic field is applied.

Signals from fluorinated molecules (^{19}F) can also be detected using spectroscopic MRI. When ^{1}H or ^{19}F nuclei are disturbed from their equilibrium by pulsed radio frequency radiation (RF), the removal of the radio frequency radiation will bring the nuclei to the equilibrium (Relaxation). Once the receiver coil has measured the relaxation, the ^{1}H or ^{19}F values measured will be converted into a MR image. The time employed by the nuclei to reach their equilibrium is specific for each tissue and it depends on the main magnetic field strength in a measuring system.

The longitudinal (T_1) and transversal (T_2) relaxation times are used to characterize tissues in the body. **T_1 relaxation time**, also known as spin-lattice relaxation time, is a measure that determines the rate at which excited ^{1}H recovers to the equilibrium state. **T_2 relaxation time**, also known as spin-spin relaxation time, refers instead to the time

constant that measures the time taken from spinning hydrogen atoms to progressive dephasing resulting in decay in the magnetization in the transverse plane. Therefore, MRI contrast agents that are often administered to enhance the contrast between normal and diseased tissues are divided into two groups: T_1-weighted (positive) contrast agents, which produce brighter images by shortening the longitudinal relaxation time of protons; and, T_2-weighted (negative) contrast agents, which yield darker MRI images by shortening the protons' transverse relaxation time[77]. Contrast-enhanced MRI using positive (T_1) or negative (T_2) contrast agents aim to enhance the relaxation properties. Typically, the magnetic strength of a human MRI scanner is 1.5 and 3 T, and for small animal imaging 4.7 and 7 T—however, the scanners tuned to even higher field, such as 9.4 T, 11 even 20 T, can be found in dedicated research facilities. One of the main advantages of MRI is the ability to detect variations within soft tissues and cell populations that is enhanced when intravenous contrast agents are injected[78].

Aim and Thesis outline

The thesis describes mainly two non-invasive techniques used for imaging cells in mouse models. **In chapter 1** is introduced the overall aim of the study as to visualize cells using two imaging modalities as Bioluminescence and Magnetic resonance imaging (MRI) in order to monitor the functionality and the localization of cells and potentially study tumor progression at different stages.

In chapter 2, a general introduction of emerging strategies used for sensitive bioluminescence is given. A summary of recently published luciferase/luciferin pairs for labelling bacterial, fungi and mammalian cells is also highlighted. In vitro and in vivo applications are described along with new possible tools to further evaluate in vivo interventions. **In chapter 3**, we investigated different D-luciferin-dependent luciferases and we evaluated their brightness and spectral properties either in vitro and vivo. Such an approach was helpful to find a green click beetle luciferase mutant (CBG99) with great potentiality for dual-color BL in vivo. As a follow-up, in **chapter 4,** we explored whether the optimization of CBG99 luciferase could be exploited for dual-color bioluminescence imaging in deep tissues. Notably, the novel CBG2 mutant luciferase paired with CBR2 luciferase, that both use napthyl luciferin as a substrate, produced a dual-color luciferase system in the NIR window using one single substrate in vivo. This dual-color luciferase system enables simultaneous monitoring of different transplanted cells or their different functional state in one and the same mouse. **In chapter 5,** we described a detailed protocol to perform the spectral unmixing of two bioluminescent cell populations injected *in vivo*. This chapter presents an optimized approach on the set-up of the experiment including recommendations and critical steps to be considered.

Another strategy to label cells is explained **in chapter 4,** where MRI as an imaging modality was used as an alternative method for non-invasive imaging in vivo. The efficacy of targeting Tumor-Associated Macrophages (TAMs) was assessed by an active nano-targeting method. Since activated TAMs over-express the mannose receptor on their cell-membrane, mannose-PLGA nanoparticles loaded with MR contrast agent were designed, synthesized and characterized to image TAMs in a breast cancer tumor model. The significant contribution to visualize TAMs as function of tumor growth and therapeutic interventions in vivo will be highlighted further.

REFERENCES

1. Iafrate, M. & Fruhwirth, G. O. How Non-invasive in vivo Cell Tracking Supports the Development and Translation of Cancer Immunotherapies . *Frontiers in Physiology* vol. 11 154 (2020).
2. Pollard, J. W. Tumour-educated macrophages promote tumour progression and metastasis. *Nature reviews. Cancer* vol. 4 71–78 (2004).
3. Gajewski, T. F., Schreiber, H. & Fu, Y.-X. Innate and adaptive immune cells in the tumor microenvironment. *Nat. Immunol.* **14**, 1014–1022 (2013).
4. Chaudhary, B. & Elkord, E. Regulatory T Cells in the Tumor Microenvironment and Cancer Progression: Role and Therapeutic Targeting. *Vaccines* **4**, (2016).
5. McCarthy, C. E., White, J. M., Viola, N. T. & Gibson, H. M. In vivo Imaging Technologies to Monitor the Immune System. *Front. Immunol.* **11**, 1067 (2020).
6. Mezzanotte, L., van 't Root, M., Karatas, H., Goun, E. A. & Löwik, C. W. G. M. In Vivo Molecular Bioluminescence Imaging: New Tools and Applications. *Trends Biotechnol.* **35**, 640–652 (2017).
7. Strack, R. Building up bioluminescence. *Nat. Methods* **16**, 20 (2019).
8. Kaskova, Z. M., Tsarkova, A. S. & Yampolsky, I. V. 1001 lights: luciferins, luciferases, their mechanisms of action and applications in chemical analysis, biology and medicine. *Chem. Soc. Rev.* **45**, 6048–6077 (2016).
9. Wilson, T. & Hastings, J. W. BIOLUMINESCENCE. *Annu. Rev. Cell Dev. Biol.* **14**, 197–230 (1998).
10. Kotlobay, A. A., Kaskova, Z. M. & Yampolsky, I. V. Palette of Luciferases: Natural Biotools for New Applications in Biomedicine. *Acta Naturae* **12**, 15–27 (2020).
11. Paley, M. A., Prescher, J. A. & Edu, J. Bioluminescence: a versatile technique for imaging cellular and molecular features. doi:10.1039/C3MD00288H.
12. Zambito, G., Chawda, C. & Mezzanotte, L. Emerging tools for bioluminescence imaging. *Curr. Opin. Chem. Biol.* **63**, 86–94.
13. Xu, T. *et al.* The Expanding Toolbox of In Vivo Bioluminescent Imaging. *Front. Oncol.* **6**, 150 (2016).
14. Endo, M. & Ozawa, T. Advanced Bioluminescence System for In Vivo Imaging with Brighter and Red-Shifted Light Emission. *Int. J. Mol. Sci.* **21**, (2020).
15. Kotlobay, A. A. *et al.* Genetically encodable bioluminescent system from fungi. *Proc. Natl. Acad. Sci.* **115**, 12728 LP – 12732 (2018).
16. Gregor, C., Gwosch, K. C., Sahl, S. J. & Hell, S. W. Strongly enhanced bacterial bioluminescence with the ilux operon for single-cell imaging. *Proc. Natl. Acad. Sci.* **115**, 962 LP – 967 (2018).
17. Su Y, Walker JR, Park Y, Smith TP, Liu LX, Hall MP, Labanieh L, Hurst R, Wang DC, Encell LP, Kim N, Zhang F, Kay MA, Casey KM, Majzner RG, Cochran JR, Mackall CL, Kirkland TA, L. M. Novel NanoLuc substrates enable bright two-population bioluminescence imaging in animals. *Nat. Methods* **17**, 852–860 (2020).
18. Yao, Z., Zhang, B. S. & Prescher, J. A. Advances in bioluminescence imaging: new probes from old recipes. *Curr. Opin. Chem. Biol.* **45**, 148–156 (2018).
19. Friebel, M., Helfmann, J., Netz, U. J. & Meinke, M. C. Influence of oxygen saturation on the optical scattering properties of human red blood cells in the spectral range 250 to 2000 nm. *J. Biomed. Opt.* **14**, 1–6 (2009).
20. Jathoul, A. P., Grounds, H., Anderson, J. C. & Pule, M. A. A dual-color far-red to near-infrared firefly luciferin analogue designed for multiparametric bioluminescence imaging. *Angew. Chem. Int. Ed. Engl.* **53**, 13059—13063 (2014).

21. Smith, A. M., Mancini, M. C. & Nie, S. Bioimaging: second window for in vivo imaging. *Nat. Nanotechnol.* **4**, 710–711 (2009).
22. Iwano, S. *et al.* Single-cell bioluminescence imaging of deep tissue in freely moving animals. *Science (80-.).* **359**, 935 LP – 939 (2018).
23. Gaspar, N. *et al.* Evaluation of NanoLuc substrates for bioluminescence imaging of transferred cells in mice. *J. Photochem. Photobiol. B Biol.* **216**, 112128 (2021).
24. Chu, J. *et al.* A bright cyan-excitable orange fluorescent protein facilitates dual-emission microscopy and enhances bioluminescence imaging in vivo. *Nat. Biotechnol.* **34**, 760–767 (2016).
25. Takai, A. *et al.* Expanded palette of Nano-lanterns for real-time multicolor luminescence imaging. *Proc. Natl. Acad. Sci.* **112**, 4352 LP – 4356 (2015).
26. Taylor, A., Sharkey, J., Plagge, A., Wilm, B. & Murray, P. Multicolour In Vivo Bioluminescence Imaging Using a NanoLuc-Based BRET Reporter in Combination with Firefly Luciferase. *Contrast Media Mol. Imaging* **2018**, 2514796 (2018).
27. Mezzanotte L, van 't R. M. & Karatas H, Goun EA, L. C. In Vivo Molecular Bioluminescence Imaging: New Tools and Applications. *Trends Biotechnol.* **35**, 640–652 (2017).
28. Aswendt, M. *et al.* Quantitative in vivo dual-color bioluminescence imaging in the mouse brain. *Neurophotonics* **6**, 1–11 (2019).
29. Gammon, S. T., Leevy, W. M., Gross, S., Gokel, G. W. & Piwnica-Worms, D. Spectral unmixing of multicolored bioluminescence emitted from heterogeneous biological sources. *Anal. Chem.* **78**, 1520–1527 (2006).
30. Mezzanotte, L. *et al.* Evaluating reporter genes of different luciferases for optimized in vivo bioluminescence imaging of transplanted neural stem cells in the brain. *Contrast Media Mol. Imaging* **8**, 505–513 (2013).
31. Branchini, B. R. *et al.* Red-emitting luciferases for bioluminescence reporter and imaging applications. *Anal. Biochem.* **396**, 290–297 (2010).
32. Hall, M. P. *et al.* Click beetle luciferase mutant and near infrared naphthyl-luciferins for improved bioluminescence imaging. *Nat. Commun.* **9**, 132 (2018).
33. Nakajima Y, Yamazaki T, Nishii S, Noguchi T, Hoshino H, Niwa K, et al. Enhanced Beetle Luciferase for High-Resolution Bioluminescence Imaging. *PLoS One* **5(4): e100**,.
34. Maguire, C. A. *et al.* Triple bioluminescence imaging for in vivo monitoring of cellular processes. *Mol. Ther. Nucleic Acids* **2**, e99 (2013).
35. Kim, I. S. & Zhang, X. H.-F. One microenvironment does not fit all: heterogeneity beyond cancer cells. *Cancer Metastasis Rev.* **35**, 601–629 (2016).
36. Yang, M., McKay, D., Pollard, J. W. & Lewis, C. E. Diverse Functions of Macrophages in Different Tumor Microenvironments. *Cancer Res.* **78**, 5492–5503 (2018).
37. Yang, Q. *et al.* The role of tumor-associated macrophages (TAMs) in tumor progression and relevant advance in targeted therapy. *Acta Pharm. Sin. B* **10**, 2156–2170 (2020).
38. Mantovani, A., Marchesi, F., Malesci, A., Laghi, L. & Allavena, P. Tumour-associated macrophages as treatment targets in oncology. *Nat. Rev. Clin. Oncol.* **14**, 399–416 (2017).
39. Schulz, M., Salamero-Boix, A., Niesel, K., Alekseeva, T. & Sevenich, L. Microenvironmental Regulation of Tumor Progression and Therapeutic Response in Brain Metastasis. *Front. Immunol.* **10**, 1713 (2019).
40. Kessenbrock, K., Plaks, V. & Werb, Z. Matrix metalloproteinases: regulators of the tumor microenvironment. *Cell* **141**, 52–67 (2010).
41. Chen, J. J. W. *et al.* Tumor-associated macrophages: the double-edged sword in cancer progression. *J. Clin. Oncol. Off. J. Am. Soc. Clin. Oncol.* **23**, 953–964 (2005).

42. Casazza, A. *et al.* Impeding macrophage entry into hypoxic tumor areas by Sema3A/Nrp1 signaling blockade inhibits angiogenesis and restores antitumor immunity. *Cancer Cell* **24**, 695–709 (2013).
43. Zhang, M. *et al.* Adipocyte-Derived Lipids Mediate Melanoma Progression via FATP Proteins. *Cancer Discov.* **8**, 1006–1025 (2018).
44. Vitale, I., Manic, G., Coussens, L. M., Kroemer, G. & Galluzzi, L. Macrophages and Metabolism in the Tumor Microenvironment. *Cell Metab.* **30**, 36–50 (2019).
45. Andón, F. T. *et al.* Targeting tumor associated macrophages: The new challenge for nanomedicine. *Semin. Immunol.* **34**, 103–113 (2017).
46. Ahrens, E. T., Flores, R., Xu, H. & Morel, P. A. In vivo imaging platform for tracking immunotherapeutic cells. *Nat. Biotechnol.* **23**, 983–987 (2005).
47. Attia, M. F., Anton, N., Wallyn, J., Omran, Z. & Vandamme, T. F. An overview of active and passive targeting strategies to improve the nanocarriers efficiency to tumour sites. *J. Pharm. Pharmacol.* **71**, 1185–1198 (2019).
48. Wilhelm, S. *et al.* Analysis of nanoparticle delivery to tumours. *Nat. Rev. Mater.* **1**, 16014 (2016).
49. Adair, J. H., Parette, M. P., Altınoğlu, E. İ. & Kester, M. Nanoparticulate Alternatives for Drug Delivery. *ACS Nano* **4**, 4967–4970 (2010).
50. Seth, A., Park, H. S. & Hong, K. S. Current Perspective on In Vivo Molecular Imaging of Immune Cells. *Molecules* vol. 22 (2017).
51. Serkova, N. J. Nanoparticle-Based Magnetic Resonance Imaging on Tumor-Associated Macrophages and Inflammation. *Front. Immunol.* **8**, 590 (2017).
52. Tang, Y. *et al.* Overcoming the Reticuloendothelial System Barrier to Drug Delivery with a 'Don't-Eat-Us' Strategy. *ACS Nano* **13**, 13015–13026 (2019).
53. Srinivas, M. *et al.* Customizable, multi-functional fluorocarbon nanoparticles for quantitative in vivo imaging using 19F MRI and optical imaging. *Biomaterials* **31**, 7070–7077 (2010).
54. Suk, J. S., Xu, Q., Kim, N., Hanes, J. & Ensign, L. M. PEGylation as a strategy for improving nanoparticle-based drug and gene delivery. *Adv. Drug Deliv. Rev.* **99**, 28–51 (2016).
55. Wang, E. C. & Wang, A. Z. Nanoparticles and their applications in cell and molecular biology. *Integr. Biol.* **6**, 9–26 (2014).
56. Dalzon, B. *et al.* Influences of Nanoparticles Characteristics on the Cellular Responses: The Example of Iron Oxide and Macrophages. *Nanomater. (Basel, Switzerland)* **10**, (2020).
57. Binnemars-Postma, K., Storm, G. & Prakash, J. Nanomedicine Strategies to Target Tumor-Associated Macrophages. *International Journal of Molecular Sciences* vol. 18 (2017).
58. Hasebroock, K. M. & Serkova, N. J. Toxicity of MRI and CT contrast agents. *Expert Opin. Drug Metab. Toxicol.* **5**, 403–416 (2009).
59. Wáng, Y. X. J. & Idée, J.-M. A comprehensive literatures update of clinical researches of superparamagnetic resonance iron oxide nanoparticles for magnetic resonance imaging. *Quant. Imaging Med. Surg.* **7**, 88–122 (2017).
60. Makela, A. V *et al.* Magnetic Particle Imaging of Macrophages Associated with Cancer: Filling the Voids Left by Iron-Based Magnetic Resonance Imaging. *Mol. imaging Biol.* **22**, 958–968 (2020).
61. Wang, G., Serkova, N. J., Groman, E. V, Scheinman, R. I. & Simberg, D. Feraheme (Ferumoxytol) Is Recognized by Proinflammatory and Anti-inflammatory Macrophages via Scavenger Receptor Type AI/II. *Mol. Pharm.* **16**, 4274–4281 (2019).
62. Daldrup-Link, H. E. *et al.* MRI of tumor-associated macrophages with clinically applicable iron oxide nanoparticles. *Clin. cancer Res. an Off. J. Am. Assoc. Cancer Res.* **17**, 5695–5704 (2011).

63. Zanganeh, S. *et al.* Iron oxide nanoparticles inhibit tumour growth by inducing pro-inflammatory macrophage polarization in tumour tissues. *Nat. Nanotechnol.* **11**, 986–994 (2016).
64. Blanco, E., Shen, H. & Ferrari, M. Principles of nanoparticle design for overcoming biological barriers to drug delivery. *Nat. Biotechnol.* **33**, 941–951 (2015).
65. Yang R, Fu C, Fang J, Xu X, Wei X, Tang W, Jiang X, Z. L. Hyaluronan-modified superparamagnetic iron oxide nanoparticles for bimodal breast cancer imaging and photothermal therapy. *Int J Nanomedicine.* **12**, 197–206 (2017).
66. Nabil, G. *et al.* Nano-engineered delivery systems for cancer imaging and therapy: Recent advances, future direction and patent evaluation. *Drug Discov. Today* **24**, 462–491 (2019).
67. Lee, G. Y. *et al.* Theranostic nanoparticles with controlled release of gemcitabine for targeted therapy and MRI of pancreatic cancer. *ACS Nano* **7**, 2078–2089 (2013).
68. Kamaly, N., Xiao, Z., Valencia, P. M., Radovic-Moreno, A. F. & Farokhzad, O. C. Targeted polymeric therapeutic nanoparticles: design, development and clinical translation. *Chem. Soc. Rev.* **41**, 2971–3010 (2012).
69. Wang, X. *et al.* The development of site-specific drug delivery nanocarriers based on receptor mediation. *J. Control. Release* **193**, 139–153 (2014).
70. Jiang, W. *et al.* Conjugation of functionalized SPIONs with transferrin for targeting and imaging brain glial tumors in rat model. *PLoS One* **7**, e37376 (2012).
71. Ahrens, E. T. & Zhong, J. In vivo MRI cell tracking using perfluorocarbon probes and fluorine-19 detection. *NMR Biomed.* **26**, 860–871 (2013).
72. Ahrens, E. T. & Bulte, J. W. M. Tracking immune cells in vivo using magnetic resonance imaging. *Nat. Rev. Immunol.* **13**, 755–763 (2013).
73. Chapelin, F., Capitini, C. M. & Ahrens, E. T. Fluorine-19 MRI for detection and quantification of immune cell therapy for cancer. *J. Immunother. Cancer* **6**, 105 (2018).
74. Makela, A. V, Gaudet, J. M. & Foster, P. J. Quantifying tumor associated macrophages in breast cancer: a comparison of iron and fluorine-based MRI cell tracking. *Sci. Rep.* **7**, 42109 (2017).
75. Srinivas, M., Heerschap, A., Ahrens, E. T., Figdor, C. G. & de Vries, I. J. M. (19)F MRI for quantitative in vivo cell tracking. *Trends Biotechnol.* **28**, 363–370 (2010).
76. Rho, J. *et al.* Paramagnetic Fluorinated Nanoemulsions for in vivo F-19 MRI. *Mol. Imaging Biol.* **22**, 665–674 (2020).
77. Hu, H. Recent Advances of Bioresponsive Nano-Sized Contrast Agents for Ultra-High-Field Magnetic Resonance Imaging. *Front. Chem.* **8**, 203 (2020).
78. Kim, E.-J. *et al.* In Vivo Tracking of Phagocytic Immune Cells Using a Dual Imaging Probe with Gadolinium-Enhanced MRI and Near-Infrared Fluorescence. *ACS Appl. Mater. Interfaces* **8**, 10266–10273 (2016).

2

Emerging Tools for Bioluminescence Imaging

Giorgia Zambito [1,2,3], Chintan Chawda [1, 2], Laura Mezzanotte[1,2*]

[1]Department of Radiology and Nuclear Medicine, Erasmus MC Rotterdam, The Netherlands.
[2]Department of Molecular Genetics, Erasmus MC Rotterdam, The Netherlands.
[3]Medres medical research GmBH, Cologne, Germany.
*Correspondence:
Laura Mezzanotte, Ph.D.
E-mail: l.mezzanotte@erasmusmc.nl

Current Opinion in Chemical Biology
Volume 63, 2021, Pages 86-94

ABSTRACT

Bioluminescence (BL) relies on the enzymatic reaction between luciferase, a substrate conventionally named luciferin and various cofactors. Bioluminescence imaging has become a widely used technique to interrogate gene expression and cell fate, both in small and large animal models of research. Recent developments include the generation of improved luciferase/luciferin systems for deeper and more sensitive imaging but as well as new caged luciferins to report on enzymatic activity and other intracellular functions. Here, we critically evaluate the emerging tools for bioluminescence imaging, aiming to provide the reader with an updated compendium of the latest developments (2018-2020) and their notable applications.

Keywords: Bioluminescence imaging, luciferase, luciferin, caged luciferin, photo-uncaging.

INTRODUCTION

Bioluminescence, the natural phenomenon of light emitting organisms, is caused by an enzymatic reaction between luciferase and a substrate conventionally named luciferin. The application of bioluminescence to the imaging of cells, plants and animals using a sensitive CCD camera and a dark box, started in the 1990s and flourished in the new millennium [1,2]. Currently, bioluminescence imaging (BLI), defined as a molecular imaging technique based on the use of luciferase and their substrates, especially for in vivo imaging, has become a common practice in research laboratories. This is because BLI is easy to perform, is relatively cheap and, most importantly, is characterized by a high detection sensitivity that allows refining of experiments and consequently for a reduction in the number of animals needed for research. In recent years, a range of novel red and near infrared-shifted bioluminescent systems has emerged, along with a plethora of novel luciferin analogues, which together are aimed at expanding the palette of colors available or for measuring enzymatic activities.

Novel Luciferase/Luciferin systems

Imaging cellular processes or molecular reactions within the deep tissue of animals are optimal when the BL enzymatic reaction has a high quantum yield and when emitted bioluminescence falls under the so-called optical window for *in vivo* imaging (wavelengths above 650 nm)[1,2]. Conversely, photons associated with wavelengths below 650nm are readily scattered or absorbed by components of the tissue. This is why the latest research in bioluminescence concentrates on the development of brighter and red-shifted BL systems with the aim of generating BL systems that can be combined for multicolor applications, as is the case for fluorescent proteins and dyes [3-6] (Figure 1). Amongst the terrestrial luciferases, mutated red-emitting click beetles (CBRs) offer the additional benefit of achieving greater brightness for imaging in deep tissue. In particular, CBR2 luciferase has improved the sensitivity in deep tissue giving a bright, near-infrared, signal (λ_{max} 730 nm) with NH_2-NpLH2 luciferin substrate [7,8].

The last few years has also witnessed the emergence of synthetic luciferase enzymes: one example being Akaluc luciferase [9]. Differing from firefly luciferin (Fluc) in 28 amino acids, Akaluc enables more sensitive imaging than Fluc in preclinical models when paired with AkaLumine-HCl. Akaluc/AkaLumine-HCl pairing has been named AkaBLI system (λ_{max} 650 nm). Interestingly, this system was used to transduce the right striatum of a marmoset brain and to visualize the BLI for over a year (Figure 1).

Further improvements were also reported with optimized marine luciferases yielding brighter bioluminescence. Starting from Nanoluc luciferase [10], Yeh et. al re-engineered

Nanoluc to react with a coelenterazine (CTZ) analogue named diphenylterazine (DTZ) (λ_{max} 502 nm). The novel teLuc luciferase with DTZ achieved greater brightness and sensitivity subcutaneously when compared to Fluc/D-Luc and Nanoluc/furimazine (FRZ) [11]. In an analogy to the Antares luciferase, teLuc was fused in between the two domains of the fluorescent protein CYoFP to achieve intramolecular bioluminescence resonance energy transfer (BRET). This fusion created Antares 2 luciferase which emits more photons above 600 nm compared to Antares and leads to improved performances compared to simple teLuc/DTZ for liver imaging.

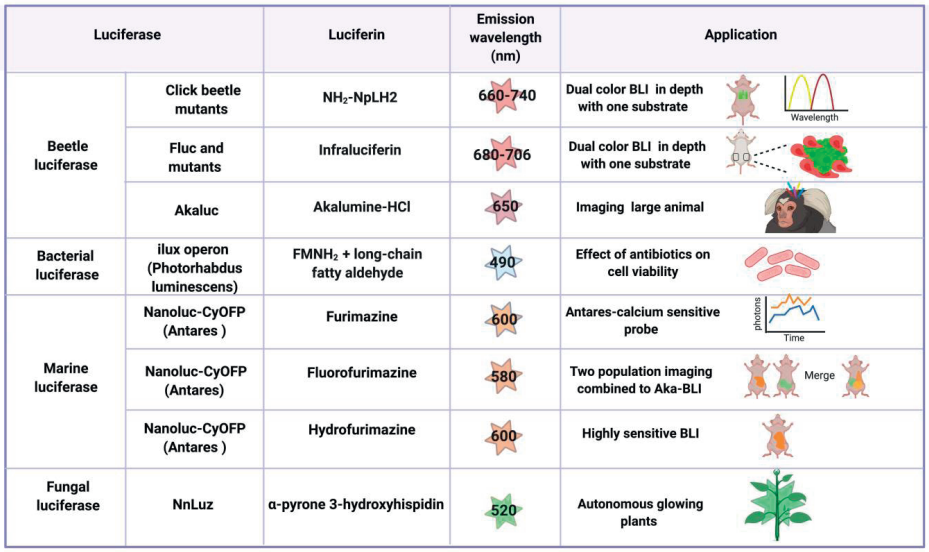

Figure 1. Schematic illustration of emerging tools in bioluminescence imaging.

More recently, 8pyDTZ, a pyridine analog of Diphenylterazine (DTZ) with Lumiluc, a mutant version of teLuc, exhibited a significant red-shift bioluminescence [12]. Furthermore, to enhance signal emission, LumiScarlet, a fused product of mScarlet-1 and LumiLuc luciferase was generated (d max >600nm). In the presence of 8pyDTZ, LumiScarlet exhibited a ~3-fold higher signal emission over LumiLuc/8pyDTZ and Akaluc/AkaLumine-HCl reporters, demonstrating its superior deep-tissue imaging potency [12]. The biochemical pathway leading to the synthesis of D-luciferin and CTZ in bioluminescent organisms is largely unknown while the bacterial BL system is entirely encoded by the lux operon and has been known for decades [13]. Bacterial luciferases emit blue photons (λ_{max} ~ 490 nm), like marine luciferases, and the operon can be entirely inserted in the genome of the heterologous organism. Although the photon yield of such a system is low, the independence from the exogenous administration of luciferin makes their use particularly interesting. A recent advancement in bacterial luciferases was the design of the ilux

operon by Gregor and colleagues, enabling single-cell imaging [14-15]. A breakthrough in the bioluminescence field was the discovery of the entire biochemical pathway involved in generating bioluminescence in fungi. In particular, the wild-type *Neonothopanus nambi* luciferase (nnLuz) utilizes a α-pyrone 3-hydroxyhispidin substrate and emits green light (~ 520 nm) in the presence of O_2 [16]. Interestingly, this system was engineered into plants to produce glowing plants without exogenous administration of a substrate [17-18] (Figure 1).

Novel luciferin analogs

Recent years have also seen remarkable advancements in the generation of luciferin analogues in order to improve the brightness of the BL system; cell permeability; blood brain barrier penetration; as well as modulate color emission. Several modifications have been introduced on D-luciferin (D-Luc) to achieve these goals (e.g. π–extended luciferins 19). In that direction, Wu and colleagues developed a series of Fluc substrates, namely N-cycloalkylaminoluciferins (cybLucs) [20]. To enhance cellular uptake, lipophilic N-cycloalkyl group was introduced in aminoluciferin. The intravenous injection of cybLuc in luciferase-expressing transgenic mice revealed a four-fold extended circulatory half-life and brighter bioluminescent signal intensity relative to D-Luc. In terms of signal stability within the brain hippocampus, where the bioluminescence emission from dLuc was found to fade within 5 minutes, cybLucs emission persisted for more than 30 minutes, making it a preferred substrate for brain imaging (Figure 2).

Pyridone luciferins have been generated with the aim of developing novel orthologous bioluminescent systems for multicolor application. Zhang BS. and colleagues, developed luciferin analogs that had their original dLuc scaffold modified at pyridone cores [21]. For many of them Km values were >100-fold higher than that of dLuc when using firefly luciferase. To overcome that, Fluc mutants, namely 24 and 166, were generated. Nevertheless in *in vitro* studies, pyridine analogs (oxy4) with mutant luciferase 24, and especially 166, attained the near to equivalent binding affinity seen in native Fluc, the reason being F295l mutation. Secondly, in live cells authors found the emission spectra of oxy4 with Fluc (λmax = 530 nm) was close to that of Fluc/DLuc.

Other interesting developments are the furimazine (FRZ) analogues described in the work of Su and colleagues by targeting polar substitutions on phenyl rings [22]. Hydrofurimazine (Hfz) (3'hydrozxy substitution), under its saturation dose, gave a four-fold higher bioluminescence than that generated from FRZ. Furthermore, with fluorine substitutions on analogs' phenyl rings, the authors designed Fluorofurimazine (Ffz). These analogues were formulated in Poloxamer-407 (solubilizing formulation) which enabled intraperitoneal injection of higher doses of the substrate and ensured good

biodistribution in animals. Antares/FFz and AkaBLI systems were employed to achieve dual color population imaging *in vivo* by using Antares expressing tumor cells and Car-T cells expressing Akaluc [22]. Other interesting novel coelenterazine analogues include Hikarazines which are O-acetylated luciferins that are highly stable at room temperature for up to two years. Hikarazines can react with Nanoluc luciferases. However, their performance for *in vivo* imaging still needs to be further evaluated [23].

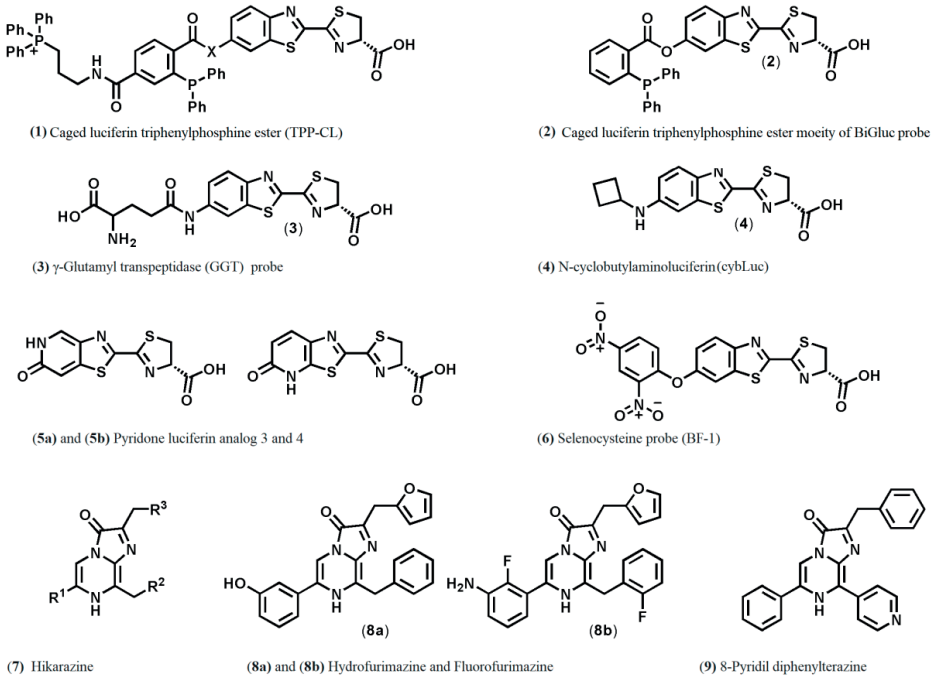

Figure 2. Chemical structure of novel bioluminescent substrates. (1) Mitochondrial-activated luciferin (MAL)- Bazhin et al. 2020. (2) Bioluminescent glucose-uptake probe (BiGluc)- Maric et al. 2019. (3) ɣ-Glutamyl transpeptidase (GGT) probe- Lin et al. 2 2017. (4) N-cyclobutylaminoluciferin (cybLuc), a cycloaminoluciferin analog- Wu et al. 2017. (5a) and (5b) Pyridone luciferin analog 3 and 4- Zhang et al. 2018. (6) Selenocysteine probe (BF-1)- Zhang et al. 2019. (7) Hikarazine, a coelenterazine analogue- Coutant et al. 2020. (8a) and (8b) Hydrofurimazine and Fluorofurimazine, Furimazine analogs- Su et al. 2020. (9) 8-Pyridil diphenylterazine (8pyDTZ), a diphenylterazine analog- Yeh et al. 2019A)

Caged luciferins

Caged luciferin substrates are used to monitor enzymatic activities and other molecular events upon the release of D-Luc. Making use of this phenomenon is a sensor for detecting *in vivo* fibroblast activation protein-α (FAP) activity which, was designed by Lin and colleagues [24]. Here, N-carbobenzyoloxy-Gly-Pro-OH (Probe-1) was used to mask the substrate recognition site on aminoluciferin, making it inaccessible to the firefly luciferase (Fluc). The peptidase activity of membrane bound FAP allows it to cleave the

amide bond after proline within Probe-1, making animoluciferin available. In a tumor xenograft mice model involving U87MG-Fluc cells, injecting 5mg/kg of SP-13786 inhibitor led to 4-fold decrease in bioluminescence from the test group relative to the control group with the vehicle (saline+Probe-1). Other similar recent developments are a caged luciferin to monitor peptide uptake [25], in order to detect Biothiols [26] for real-time *in vivo* detection of Selenocysteine (Sec) [27] and ɣ-glutamyl transpeptidase (GGT) [28] but also photoactivable substrates [29] (Figure 2). A bioluminescent glucose uptake reporter (BiGluc) [30] and mitochondrial membrane potential ($\Delta\alpha_m$) sensor (MAL) [31] were designed by harnessing the reaction efficiency of Staudingers' ligation to report molecules' bioavailability through bioluminescence. Both the reporters utilized caged luciferin triphenylphosphine (CLP) and an azide or azido linked molecule of interest. TPP, being a lipophilic cation caging luciferin could be passively taken up through the lipid bilayer. In the MAL sensor, both its components, luciferin and organic azide were linked to TPP for permitting mitochondrial matrix accumulation. In proximity, the reaction of chemical moieties results in the uncaging of luciferin and bioluminescence emission when reacting with cytosolic luciferase. For example, in FVB-luc$^+$ mice (ubiquitous luciferase expression under β-actin promoter), testing of MAL3 reporter (superior variant) in presence/absence of Butylated Hydroxytoluene (BHT) and Nigericin, aided successful visualization of mitochondrial membrane potential depolarization and hyperpolarization [31] (Figure 3).

Emerging bioluminescence technologies

Bioluminescent nanoparticles

The formulation of bioluminescent nanoparticles (bio-Nps) has emerged as an attractive application to combine bioimaging and nanomedicine. Usually BL-quantum dots (QDs), relying on BRET, are applied for imaging purposes [32, 33]. Recently, D-luciferin has been linked via a disulfide bond to the surface of ferritin conjugated nanoparticles, with the aim of monitoring the delivery of drugs, with high sensitivity, into the tumor site [34]. In fact, the presence of a high concentration of glutathione inside the cells leads to the release of D-Luc, making the BL remission dependent on nanoparticle uptake. Another interesting application is the development of biocompatible near-infrared-II (NIR-II) bioluminescent probes (NIR-II-BPs). These probes integrate a BRET process with a two-step fluorescence resonance energy transfer (FRET) process, in order to image blood vessels and lymphatics with a high signal-to-noise ratio at NIR-II wavelengths (1000-1700nm). The nanoparticle-based probe consists of Nanoluc luciferase and three fluorescent acceptors for sequential energy transfer (BRET-FRET-FRET) [35] (Figure 4).

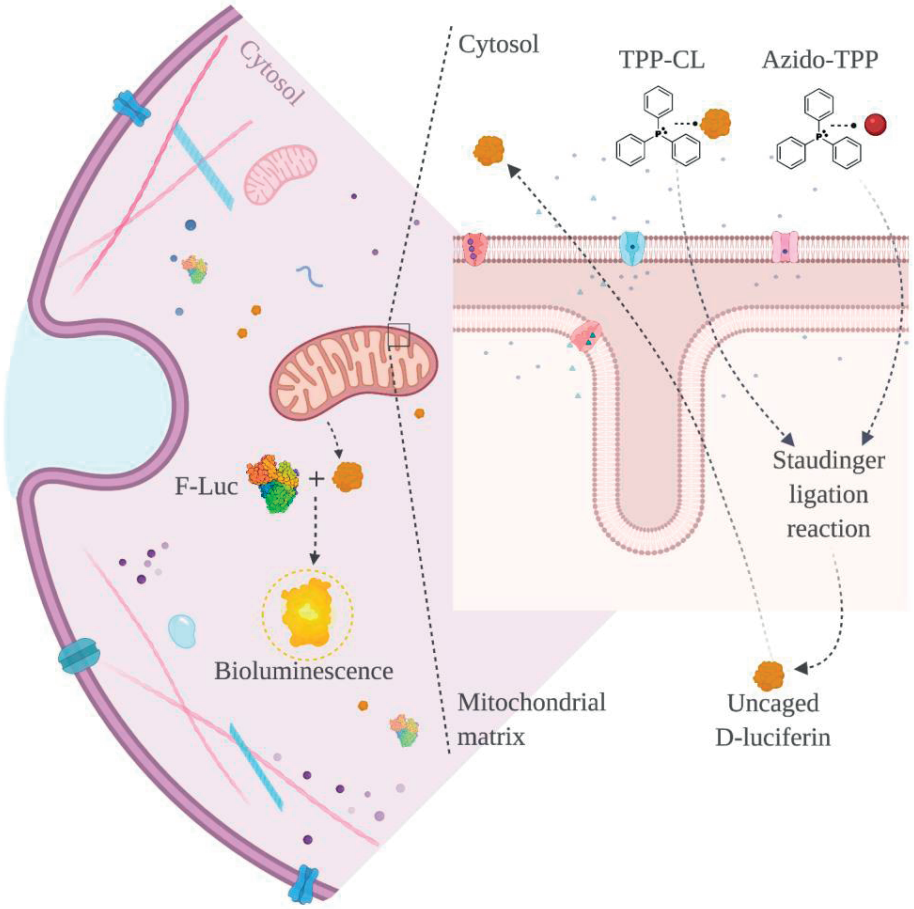

Figure 3. Molecular mechanism of Mitochondrial activable luciferin (MAL) probe. Active components of MAL reporter are D-Luc and azido moiety, each of which are linked with triphenylphosphine; Triphenylphosphine caged luciferin (TPP-CL) and Triphenylphosphine linked azido (Azido-TPP). Within mitochondrial matrix, Staudinger ligation reaction is triggered whenever TPP-CL and Azido-TPP are in proximity, uncaging DLuc. Free luciferin is then exported out to the cytoplasm where cell-expressed firefly luciferase (F-Luc) is present. Lastly, reaction between F-Luc and D-Luc, in presence of ATP and Mg2+, gives out bioluminescence thus, reflecting kinetics of mitochondrial membrane potential.

Automated image processing and analysis

BL images are usually analyzed by manually selecting and drawing Region of Interests (ROIs) on bioluminescent areas. Therefore, the robustness of the measurements might be compromised by multiple factors such as the operator; the animal positioning relative to the camera; the spatial location of the reporter; and the imaging view. In an interesting work [36], Klose et al. successfully developed an automated image processing tool: a body-fitting animal shuttle and a statistical mouse atlas conjugated by a multispectral

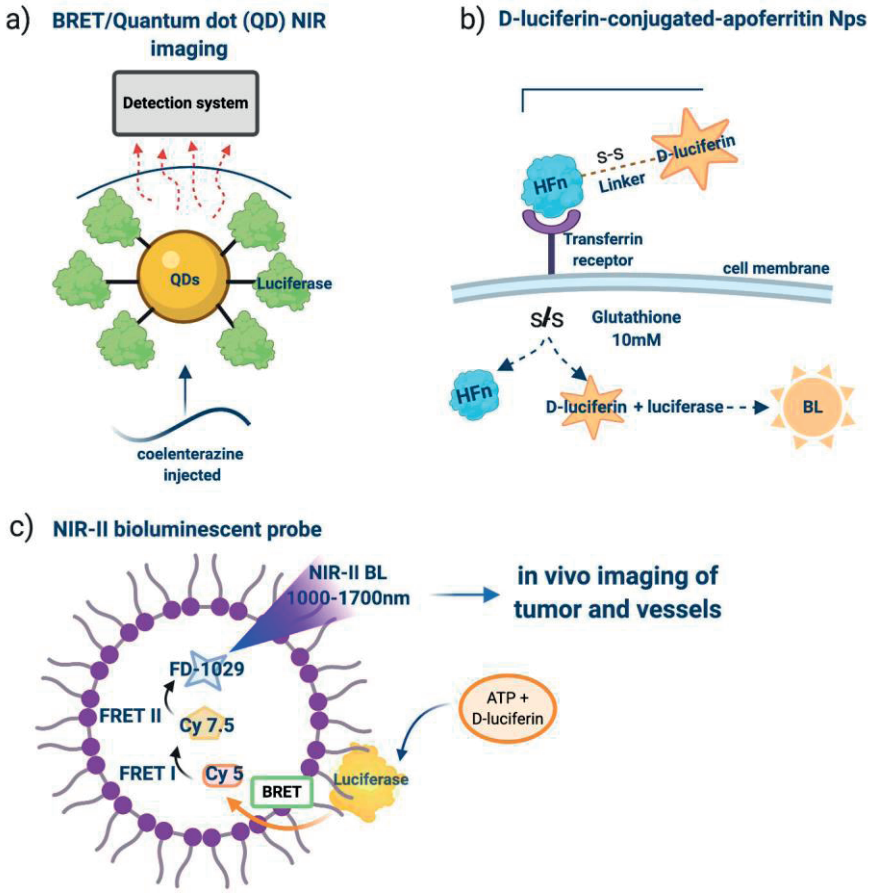

Figure 4. Illustration of different types of bioluminescent nanoparticles. a) Bioluminescent quantum dots (QDs. **b)** D-Luc conjugated apoferritin nanoparticles for in vivo imaging **c)** Bioluminescent probe for in vivo NIR-II imaging of tumors and vessels.

bioluminescence tomography technique, which aided the quantification of an *in vivo* distributed bioluminescent reporter. This tool will help to collect more throughput data and being consistent with measurements *in vivo* [36].

Multiplexing in deep tissue

Another example for BLI applications is to combine luciferases with different emission properties to visualize multiple molecular events. This can be done by combining orthogonal luciferase/luciferin pairs. The selectivity of the substrate for each luciferase guarantees specificity and distinct bioluminescent signals [37]. The most common combination uses D-Luc substrate analogs paired with terrestrial luciferases such as Fluc and CTZ analogs paired with marine derived luciferases [38]. However, multiple substrate

injections and longer imaging sessions can be stressful for the animals. Additionally, errors in data analysis can also be introduced due to differences in the solubility, biodistribution and clearance of the substrates used [39]. These issues can be resolved using a single substrate that activates two luciferases and results in spectrally-separated emissions. Recently, Stowe et al. attempted to perform an *in vivo* single-substrate, dual-color, BLI application. The far red-shifted color of luciferase mutants using infraluciferin *in vivo* measurements allowed for dual color imaging in deep tissues [40].

CRISPR/CAS knock-in

CRISPR/Cas based gene editing has revolutionized biotechnology. The knock-in of genes up to 2Kb can now be performed with high specificity and efficiency as well as enabling the monitoring of protein expression at the endogenous level [41-43]. For example, researchers successfully attempted to use HiBiT peptide as a luminescent reporter tag of endogenous proteins on a cellular level[44]. More recently, in a mouse model affected by Duchene muscular dystrophy (DMD), the Luc gene was inserted in frame with the C-terminus of the dystrophin gene. In the model disruption of the dystrophin gene extinguishes the luciferase expression. After gene therapy, the group could monitor the restoration of the dystrophin gene in deficient mice via BLI imaging [45].

Recent BRET-based systems: biosensors and bioluminolysis

To monitor the efficacy of monoclonal antibodies (mAbs) in vivo and non-invasively, fluorescent-mAbs has been developed to recognize and bind Nanoluc-receptors and producing BRET [46]. BRET-based systems are also used to study intracellular signaling molecules in vivo. Interestingly, FRET biosensors can be converted in BRET-biosensors (hyBRET) allowing sensitive cell imaging in vivo [47]. BRET can also be used to turn on functions in living cells. Changs, Lindberg and colleagues demonstrated that an excited state of coumarin compound can trigger hydrolysis to uncage a target molecule (bioluminolysis) [48,49]. The excitation of coumarin is achieved with an efficient BRET from Nanoluc-Halotag chimera protein to a coumarin substrate. This application of BLI opens up the possibility to image and control the delivery of bioactive small molecules *in vivo*.

CONCLUSION AND OUTLOOK

The emerging luciferase/luciferin pairs have expanded the bioluminescent palette enabling the imaging of deeper tissues as well as the detection of a low number of cells with more reliability *in vivo*. The discovery of new bioluminescent systems [50,51] and the design and optimization of synthetic ones using computational models [52], will produce tools for more challenging applications *in vivo*. We expect, in the near future, to be able

to visualize single cells unequivocally in deep tissues, especially if novel, more sensitive detection systems are produced. Moreover, the function of small molecules and the control and release of drugs can now be imaged *in vivo* with a high level of sensitivity. Such innovations and tools, especially if disseminated widely in the scientific community, will accelerate the advancement of the bioluminescence imaging field.

Acknowledgments The authors acknowledge Marc C.M. Stroet for help with the drawing of figure 2. The authors created the illustrations using Biorender.com. The authors thanks Roisin McMorrow for English language editing.

Conflict of Interest The authors have nothing to disclose. **Author contributions** G.Z. conceptualization, writing-original draft; C.C. conceptualization, writing-original draft; LM conceptualization, writing-review and editing, supervision.

REFERENCES

1. Contag CH, Bachmann MH: **Advances in in vivo bioluminescence imaging of gene expression**. *Annu Rev Biomed Eng* 2002, **4**: 235-260.
2. Mezzanotte L, van 't Root M, Karatas H, Goun EA, Löwik CWGM: **In Vivo Molecular Bioluminescence Imaging: New Tools and Applications**. *Trends Biotechnol* 2017, **35**: 640-652.
3. Love AC, Prescher JA: **Seeing (and Using) the Light: Recent Developments in Bioluminescence Technology**. *Cell Chem Biol* 2020, **27**:904-920.
4. Yao Z, Zhang BS, Prescher JA: **Advances in bioluminescence imaging: new probes from old recipes**. *Curr Opin Chem Biol* 2018, **45**: 148-156.
5. Ikeda Y, Nomoto T, Hiruta Y, Nishiyama N, Citterio D: **Ring-Fused Firefly Luciferins: Expanded Palette of Near-Infrared Emitting Bioluminescent Substrates**. *Anal Chem* 2020, **92**: 4235-4243.
6. Kitada N, Saito R, Obata R, Iwano S, Karube K, Miyawaki A, Hirano T, Maki SA: **Development of near-infrared firefly luciferin analogue reacted with wild-type and mutant luciferases**. *Chirality* 2020, **32**: 922-931.
7. Hall MP, Woodroofe CC, Wood MG, Que I, Van't Root M, Ridwan Y, Shi C, Kirkland TA, Encell LP, Wood KV, et al.: **Click beetle luciferase mutant and near infrared naphthyl-luciferins for improved bioluminescence imaging.** *Nat Commun* 2018, **9**: 132. *****

Authors develop a codon optimized mutant of click beetle luciferase functionally adapted to two naphthyl-luciferin substrates. This bioluminescent system is capable of generating near infrared emission (730 and 743nm) and a higher bioluminescence flux in-vivo relative to firefly luciferase.

8. Zambito G, Gaspar N, Ridwan Y, Hall MP, Shi C, Kirkland TA, Encell LP, Löwik C, Mezzanotte L: **Evaluating Brightness and Spectral Properties of Click Beetle and Firefly Luciferases Using Luciferin Analogues: Identification of Preferred Pairings of Luciferase and Substrate for In Vivo Bioluminescence Imaging**. *Mol Imaging Biol* 2020, **22**: 1523–1531.
9. Iwano S, Sugiyama M, Hama H, Watakabe A, Hasegawa N, Kuchimaru T, Tanaka KZ, Takahashi M, Ishida Y, Hata J, et al.: **Single-cell bioluminescence imaging of deep tissue in freely moving animals**. *Science* 2018, **359**: 935-939. ******

Using Akaluc with AkaLumine-HCl, authors could successfully visualize single tumorigenic cells in mouse lung vasculature. Similarly, using AkaBLI system as a neural activity sensor, long-term visualization of hippocampal neurons was made possible under stimulating environments.

10. Hall MP, Unch J, Binkowski BF, Valley MP, Butler BL, Wood MG, Otto P, Zimmerman K, Vidugiris G, Machleidt T, et al.: **Engineered luciferase reporter from a deep sea shrimp utilizing a novel imidazopyrazinone substrate.** *ACS Chem Biol* 2012, **7**: 1848-1857.
11. Yeh HW, Karmach O, Ji A, Carter D, Martins-Green MM, Ai HW: **Red-shifted luciferase-luciferin pairs for enhanced bioluminescence imaging.** *Nat Methods* 2017, **14**: 971-974. *****

Here, a red-shift bioluminescent system was developed, comprising of synthetic coelenterazine analogs diphenylterazine with teLuc. Their combination proves to be superior in terms of in-vitro, in cellulo and in-vivo bioluminescence. For deep tissue imaging, fusion of teLuc with CyOFP was made generating Antares2 reporter.

12. Yeh HW, Xiong Y, Wu T, Chen M, Ji A, Li X, Ai HW: **ATP-Independent Bioluminescent Reporter Variants To Improve in Vivo Imaging**. *ACS Chem Biol* 2019, **14**: 959-965.
13. Brodl E, Winkler A, Macheroux P: **Molecular Mechanisms of Bacterial Bioluminescence**. *Comput Struct Biotechnol J* 2018, **16**: 551-564.
14. Gregor C, Gwosch KC, Sahl SJ, Hell SW: **Strongly enhanced bacterial bioluminescence with the ilux operon for single-cell imaging**. *Proc Natl Acad Sci U S A* 2018, **115**: 962-967.

15. Gregor C, Pape JK, Gwosch KC, Gilat T, Sahl SJ, Hell SW: **Autonomous bioluminescence imaging of single mammalian cells with the bacterial bioluminescence system**. *Proc Natl Acad Sci U S A* 2019, **52**: 26491-26496. *****

Authors co-expressed codon optimized form of bacterial *luxCDABE* and frp genes in mammalian cells via multiple plasmids. Using the optimized bacterial bioluminescent system, it was possible to attain autonomous bioluminescence in single mammalian cell.

16. Kotlobay AA, Sarkisyan KS, Mokrushina YA, Marcet-Houben M, Serebrovskaya EO, Markina NM, Gonzalez Somermeyer L, Gorokhovatsky AY, Vvedensky A, Purtov KV, et al.: **Genetically encodable bioluminescent system from fungi.** *Proc Natl Acad Sci U S A* 2018, **115**: 12728-12732. ******

Authors report the identification of the fungal luciferase along with key biosynthetic enzymes involved in generating luciferin from caffeic acid. As a poof of study, when genes from this fungal bioluminescent system were introduced into the genome of *Pichia pastoris*, auto luminescent colonies were found growing on standard media.

17. Mitiouchkina T, Mishin AS, Somermeyer LG, Markina NM, Chepurnyh TV, Guglya EB, Karataeva TA, Palkina KA, Shakhova ES, Fakhranurova LI, et al.: **Plants with genetically encoded autoluminescence**. *Nat Biotechnol* 2020, **38**: 944-946.
18. Khakhar A, Starker CG, Chamness JC, Lee N, Stokke S, Wang C, Swanson R, Rizvi F, Imaizumi T, Voytas DF: **Building customizable auto-luminescent luciferase-based reporters in plants**. *Elife* 2020, **9**.
19. Yao Z, Zhang BS, Steinhardt RC, Mills JH, Prescher JA: **Multicomponent Bioluminescence Imaging with a π-Extended Luciferin**. *J Am Chem Soc* 2020, **142**: 14080-14089. *****

Authors synthesized set of π-extended luciferins and complementary luciferases using Rosetta-guided enzyme design. The luciferins being rotationally labile were designed to interact in presence of luciferase enforcing planarity. The intramolecular lock thus formed generates red-shift bioluminescence.

20. Wu W, Su J, Tang C, Bai H, Ma Z, Zhang T, Yuan Z, Li Z, Zhou W, Zhang H, et al.: **cybLuc: An Effective Aminoluciferin Derivative for Deep Bioluminescence Imaging**. *Anal Chem* 2017, **89**: 4808-4816.
21. Zhang BS, Jones KA, McCutcheon DC, Prescher JA: **Pyridone Luciferins and Mutant Luciferases for Bioluminescence Imaging.** *Chembiochem* 2018, **19**: 470-477.
22. Su Y, Walker JR, Park Y, Smith TP, Liu LX, Hall MP, Labanieh L, Hurst R, Wang DC, Encell LP, et al.: **Novel NanoLuc substrates enable bright two-population bioluminescence imaging in animals**. *Nat Methods* 2020, **17**: 852-860. *****

New substrates, hydrofurimazine followed by fluorofurimazine both possessing an enhanced in-vivo solubility and bioavailability were developed. In-vivo, the emitted brightness from hydrofurimazine /antares was comparable to that from Akaluc/ AkaLumine-HCl reporter and allowed imaging of tumor and T cells in the same mice.

23. Coutant EP, Gagnot G, Hervin V, Baatallah R, Goyard S, Jacob Y, Rose T, Janin YL: **Bioluminescence Profiling of NanoKAZ/NanoLuc Luciferase Using a Chemical Library of Coelenterazine Analogues**. *Chemistry* 2020, **26**: 948-958.
24. Lin Y, Ma Z, Li Z, Gao Y, Qin X, Zhang Z, Wang G, Du L, Li M: **Bioluminescent Probe for Monitoring Endogenous Fibroblast Activation Protein-Alpha.** *Anal Chem* 2019, **91**: 14873-14878. *****

Here, membrane bound glycoprotein FAP acted as an uncaging agent for N-carbobenzyloxy-Gly-Pro-OH caged aminoluciferin. Uncaged aminoluciferin in the presence of luciferase emits bioluminescence reflecting the abundance and activity of endogenous FAP protein

25. Karatas H, Maric T, D'Alessandro PL, Yevtodiyenko A, Vorherr T, Hollingworth GJ, Goun EA: **Real-Time Imaging and Quantification of Peptide Uptake**. *ACS Chem Biol* 2019, **14**: 2197-2205.
26. Zhang L, Shi Y, Sheng Z, Zhang Y, Kai X, Li M, Yin X: **Bioluminescence Imaging of Selenocysteine in Vivo with a Highly Sensitive Probe**. *ACS Sens* 2019, **4**: 3147-3155.
27. Lin Y, Gao Y, Ma Z, Jiang T, Zhou X, Li Z, Qin X, Huang Y, Du L, Li M: **Bioluminescence probe for γ-glutamyl transpeptidase detection in vivo**. *Bioorg Med Chem* 2018, **26**: 134-140.
28. Nomura N, Nishihara R, Nakajima T, Kim SB, Iwasawa N, Hiruta Y, Nishiyama S, Sato M, Citterio D, Suzuki K: **Biothiol-Activatable Bioluminescent Coelenterazine Derivative for Molecular Imaging in Vitro and in Vivo**. *Anal Chem* 2019, **91**: 9546-9553.
29. Zhang C, Cheng L, Dong G, Han G, Yang X, Tang C, Li X, Zhou Y, Du L, Li M: **Novel photoactivatable substrates for Renilla luciferase imaging in vitro and in vivo**. *Org Biomol Chem* 2018, **16**: 4789-4792.
30. Maric T, Mikhaylov G, Khodakivskyi P, Bazhin A, Sinisi R, Bonhoure N, Yevtodiyenko A, Jones A, Muhunthan V, Abdelhady G, et al.: **Bioluminescent-based imaging and quantification of glucose uptake in vivo**. *Nat Methods* 2019, **16**: 526-532.
31. Bazhin AA, Sinisi R, De Marchi U, Hermant A, Sambiagio N, Maric T, Budin G, Goun EA: **A bioluminescent probe for longitudinal monitoring of mitochondrial membrane potential**. *Nat Chem Biol* 2020, **12**: 1385-1393. ******

In-vivo mitochondrial membrane potential (ΔΨm) could be visualized using mitochondrial activable luciferin (MAL) reporter. It consisted of triphenylphosphine-caged luciferin and azido moiety. Within mitochondrial matrix, biorthogonal reaction leads to luciferin uncaging and bioluminescence emission with luciferase. In FVB-luc+ mice, MAL reporter in presence/absence of ΔΨm effectors allowed visualization of ΔΨm depolarization and hyperpolarization.

32. Derfus AM, Chan WCW, Bhatia SN: **Probing the Cytotoxicity Of Semiconductor Quantum Dots**. *Nano Lett* 2004, **4**:11-18.
33. So MK, Loening AM, Gambhir SS, Rao J: **Creating self-illuminating quantum dot conjugates**. *Nat Protoc* 2006, **1**:1160-1164.
34. Bellini M, Riva B, Tinelli V, Rizzuto MA, Salvioni L, Colombo M, Mingozzi F, Visioli A, Marongiu L, Frascotti G, et al.: **Engineered Ferritin Nanoparticles for the Bioluminescence Tracking of Nanodrug Delivery in Cancer**. *Small* 2020: e2001450.
35. Lu L, Li B, Ding S, Fan Y, Wang S, Sun C, Zhao M, Zhao CX, Zhang F: **NIR-II bioluminescence for in vivo high contrast imaging and in situ ATP-mediated metastases tracing**. *Nat Commun* 2020, **11**: 4192. *****

Utilizing BRET and two step fluorescence resonance energy transfer in the presence of cyanine dye FD-1029, authors designed bioluminescent probes possessing emission wavelength in second near infrared (1029 nm) region.

36. Klose AD, Paragas N: **Automated quantification of bioluminescence images.** *Nat Commun* 2018, **9**: 4262.*

Authors develop a computer-aided analysis tool for quantitively estimating biodistribution of bioluminescent reporter in-vivo. A body-fitting animal shuttle and a statistical mouse atlas conjugated with multispectral bioluminescence tomography technique aid the calculation of in-vivo distributed bioluminescent reporter.

37. Kleinovink JW, Mezzanotte L, Zambito G, Fransen MF, Cruz LJ, Verbeek JS, Chan A, Ossendorp F, Löwik C: **A Dual-Color Bioluminescence Reporter Mouse for Simultaneous**. *Front Immunol* 2018, **9**: 3097.

38. Taylor A, Sharkey J, Plagge A, Wilm B, Murray P: **Multicolour In Vivo Bioluminescence Imaging Using a NanoLuc-Based BRET Reporter in Combination with Firefly Luciferase**. *Contrast Media Mol Imaging* 2018, **2018**: 2514796.
39. Yeh HW, Wu T, Chen M, Ai HW: **Identification of Factors Complicating Bioluminescence Imaging**. *Biochemistry* 2019, **58**: 1689-1697.
40. Stowe CL, Burley TA, Allan H, Vinci M, Kramer-Marek G, Ciobota DM, Parkinson GN, Southworth TL, Agliardi G, Hotblack A, et al.: **Near-infrared dual bioluminescence imaging in mouse models of cancer using infraluciferin.** *Elife* 2019, **8**. *****

In vivo reaction of stabilized color mutants of firefly luciferase with luciferin analog infraluciferin shows bioluminescence emission in near-infrared spectrum. In addition, emitted bioluminescent signals from infraluciferin show a superior spectral unmixing over that from luciferin.

41. Jore MM, Lundgren M, van Duijn E, Bultema JB, Westra ER, Waghmare SP, Wiedenheft B, Pul U, Wurm R, Wagner R, et al.: **Structural basis for CRISPR RNA-guided DNA recognition by Cascade**. *Nat Struct Mol Biol* 2011, **18**: 529-536.
42. Jinek M, Chylinski K, Fonfara I, Hauer M, Doudna JA, Charpentier E: **A programmable dual-RNA-guided DNA endonuclease in adaptive bacterial immunity**. *Science* 2012, **337**: 816-821.
43. Pickar-Oliver A, Gersbach CA: **The next generation of CRISPR-Cas technologies and applications**. *Nat Rev Mol Cell Biol* 2019, **20**: 490-507.
44. Schwinn MK, Machleidt T, Zimmerman K, Eggers CT, Dixon AS, Hurst R, Hall MP, Encell LP, Binkowski BF, Wood KV: **CRISPR-Mediated Tagging of Endogenous Proteins with a Luminescent Peptide**. *ACS Chem Biol* 2018, **13**: 467-474.
45. Amoasii L, Li H, Zhang Y, Min YL, Sanchez-Ortiz E, Shelton JM, Long C, Mireault AA, Bhattacharyya S, McAnally JR, et al.: **In vivo non-invasive monitoring of dystrophin correction in a new Duchenne muscular dystrophy reporter mouse.** *Nat Commun* 2019, **10**: 4537. *****

For in-vivo gene correction strategy, authors inserted Luc gene in frame with C-terminus of dystrophin gene. This insertion of Luc disrupts DMD gene. Gene therapy for correction DMD gene orientation, restore expression of luciferase and bioluminescence emission reflects correction specificity.

46. Tang Y, Parag-Sharma K, Amelio AL, Cao Y. **A Bioluminescence Resonance Energy Transfer-Based Approach for Determining Antibody-Receptor Occupancy In Vivo**. iScience. 2019, **15**: 439-451.
47. Komatsu N, Terai K, Imanishi A, Kamioka Y, Sumiyama K, Jin T, Okada Y, Nagai T, Matsuda M: **A platform of BRET-FRET hybrid biosensors for optogenetics, chemical screening, and in vivo imaging.** Sci Rep 2018, **8 (1)**: 8984
48. Chang D, Lindberg E, Feng S, Angerani S, Riezman H, Winssinger N: **Luciferase-Induced Photouncaging: Bioluminolysis.** Angew *Chem Int Ed Engl* 2019, **58**: 16033-16037. ******

Authors developed first kind of BRET induced photolysis system. Here, BRET induced energy transfer from Nanoluc Halo tag chimera protein to DEAC450-based coumerin triggers coumerin excitation. This in turn leads to hydrolysis and release of small molecules.

49. Lindberg E, Angerani S, Anzola M, Winssinger N: **Luciferase-induced photoreductive uncaging of small-molecule effectors**. *Nat Commun* 2018, **9**: 3539.
50. Viviani VR, Silva JR, Amaral DT, Bevilaqua VR, Abdalla FC, Branchini BR, Johnson CH: **A new brilliantly blue-emitting luciferin-luciferase system from Orfelia fultoni and Keroplatinae (Diptera)**. *Sci Rep* 2020, **10**: 9608.
51. Kotlobay AA, Dubinnyi MA, Purtov KV, Guglya EB, Rodionova NS, Petushkov VN, Bolt YV, Kublitski VS, Kaskova ZM, Ziganshin RH, Nelyubina YV, Dorovatovskii PV, Eliseev IE, Branchini BR, Bouren-

kov G, Ivanov IA, Oba Y, Yampolsky IV, Tsarkova AS.: **Bioluminescence chemistry of fireworm Odontosyllis**. *Proc of the Nat Ac of Sci* 2019, **116 (38)**: 18911-18916.

52. Vreven T, Miller SC. **Computational investigation into the fluorescence of luciferin analogues.** *J Comput Chem*. 2019, **40 (2)**: 527-531.

3

Evaluating brightness and spectral properties of click beetle and firefly luciferases using luciferin analogues: identification of preferred pairings of luciferase and substrate for *in vivo* bioluminescence imaging

Giorgia Zambito[1,2,3], Natasa Gaspar[1,2,4], Yanto Ridwan[1,2], Mary P. Hall[5], Ce Shi[6], Thomas A. Kirkland[6], Lance P. Encell[5], Clemens Löwik[1,2,7], Laura Mezzanotte[1,2]

[1]Erasmus Medical Center, Optical Molecular Imaging, Radiology, Rotterdam, The Netherlands
[2]Erasmus Medical Center, Molecular Genetics, Rotterdam, The Netherlands
[3]Medres medical research GmbH, Cologne, Germany
[4]Percuros B.V., Leiden, The Netherlands
[5]Promega Corporation, Madison, Wisconsin, USA
[6]Promega Biosciences Incorporated, San Luis Obispo, California, USA
[7]CHUV Department of Oncology, University of Lausanne, Switzerland.
Corresponding author:
Dr. Laura Mezzanotte
l.mezzanotte@erasmusmc.nl

Mol Imaging Biol 22, 1523–1531 (2020)

ABSTRACT

Purpose

Currently a variety of red and green beetle luciferase variants are available for bioluminescence imaging (BLI). In addition, new luciferin analogues providing longer wavelength luminescence have been developed that show promise for improved deep tissue imaging. However, a detailed assessment of these analogues (e.g., Akalumine-HCl, CycLuc1 and amino naphthyl luciferin (NH_2-NpLH2) combined with state-of-the-art luciferases has not been performed. The aim of this study was to evaluate for the first time the *in vivo* brightness and spectral characteristics of firefly (Luc2), click beetle green (CBG99), click beetle red 2 (CBR2) and Akaluc luciferases when paired with different D-luciferin (D-LH2) analogues *in vivo*.

Procedures

Transduced human embryonic kidney (HEK 293T) cells expressing individual luciferases were analyzed both *in vitro* and in mice (via subcutaneous injection). Following introduction of the luciferins to cells or animals, the resulting bioluminescence signal and photon emission spectrum was acquired using a sensitive charge-coupled device (CCD) camera equipped with a series of band pass filters and spectral unmixing software.

Results

Our *in vivo* analysis resulted in four primary findings: 1. The best substrate for Luc2, CBG99 and CBR2 in terms of signal strength was D-luciferin; 2. The spectra for Luc2 and CBR2 were shifted to a longer wavelength when Akalumine-HCl was the substrate; 3. CBR2 gave the brightest signal with the near-infrared substrate, NH_2-NpLH2; and 4. Akaluc was brighter when paired with either CycLuc1 or Akalumine-HCl when paired with D-LH2.

Conclusion

We believe that the experimental results described here should provide valuable guidance to end users for choosing the correct luciferin/luciferase pairs for a variety of BLI applications.

Keywords: bioluminescence; *in vivo* imaging; luciferase; emission spectrum; luciferin;

INTRODUCTION

Bioluminescence imaging (BLI) is a well-known, non-invasive technique employed during preclinical studies to track cells and monitor biological processes in living animals [1-3]. BLI is performed by capturing the light generated by a luciferase upon exogenous substrate (e.g., D-luciferin (D-LH2)) addition to report real-time, cellular and molecular events [4].

Over the last decade the bioluminescence toolbox has greatly expanded [1,5-6]. Novel luciferin analogues have been introduced that enhance light emission *in vivo* and increase detection sensitivity in deeper tissues [7]. Cycluc1 has been shown to enhance emission of codon optimized firefly luciferase (Luc2), especially in brain. Furthermore, this system provides slightly red-shifted emission resulting in deeper light penetration and less scattering of the bioluminescence signal [8-9]. Likewise, Akalumine-HCl has a spectral peak in the near infrared (NIR) (677 nm) as well as enhanced emission with Luc2 when administered at low concentration [10]. Akalumine-HCl paired with the recently engineered Akaluc luciferase is even brighter, although the spectral peak is blue-shifted to 650 nm [11]. Amino naphthyl luciferin (NH_2-NpLH2) represents another new substrate with potential for deeper tissue BLI [12]. This substrate was shown to emit in the NIR with a peak of 740 nm when reacting with an engineered version of click-beetle luciferase (CBR2). CBR2 can also utilize D-LH2 and this combination was shown to improve imaging in black fur mice compared to Luc2/D-LH2.

Research into the development of improved BLI reagents has generally focused on bioluminescence systems comprised of compatible luciferase/luciferin pairings [13-18]. Most comparative studies have been performed using D-LH2. For example, Miloud *et al.* compared firefly (Luc2) and click beetle luciferases *in vivo* with D-LH2 as substrate and concluded that click beetle green (CBG99) has sensitivity and total photon yield comparable to click beetle red [15]. In other studies, Luc2 was shown to have improved performance compared to a red-shifted firefly mutant (PpyRE9) and CBG99 for brain imaging [16-17], but D-LH2 was the only substrate examined. A direct comparison (either *in vitro* or *in vivo*) of emission spectra and relative brightness of bioluminescence systems comprised of different luciferase enzymes in combination with novel luciferins has, to date, not been reported.

Here, we provide a detailed *in vitro* and *in vivo* analysis of brightness and emission spectra for four luciferases when combined with four different substrates using a CCD camera equipped with a series of band pass filters and spectral unmixing software. We anticipate that the results of this comparative analysis will help enable researchers

to choose the best enzyme/substrate pairs for different BLI applications. In addition, our findings revealed that depending on the luciferase/luciferin pair, a wide range of spectral emission peaks (i.e., multicolored luciferases) is available that could broaden the BLI toolbox in the future for multiplex analysis both *in vitro* and *in vivo.*

MATERIALS AND METHODS

Animals

Animal experiments were approved by the Bioethics Committee of Erasmus MC, Rotterdam, The Netherlands and performed in accordance with national guidelines and regulations established by the Dutch Experiments on Animal Act (WoD) and by the European Directive on the Protection of Animals used for scientific purpose (2010/63/EU). BALB/C nude (females) were obtained from Charles River Laboratory (The Netherlands). All mice aged 6–8 weeks were provided access to food and water *ad libitum* and were hosted in the animal facility at the Erasmus MC, Rotterdam, The Netherlands.

Cell line

Human embryonic kidney cells (HEK-293T) were cultured in Dulbecco's Modified Eagle's Medium (DMEM) (Sigma, St. Louis, Mo, USA) supplemented with 10% of FBS and 1% Penicillin-Streptomycin. The culture was incubated at 37 °C with 5% CO_2.

Lentivirus production

Virus production and cell transduction were performed under appropriate biosafety level conditions (ML-II) in accordance with the National Biosafety Guidelines and Regulations for Research on Genetically Modified Organisms. Procedures and protocols were reviewed and approved by the EMC Biosafety Committee (GMO permit 99-163). The lentiviral plasmids pCDH-EF1-CBG99-T2A-copGFP, pCDH-EF1-Luc2-T2A-copGFP, pCDH-EF1-CBR2-T2A-copGFP were previously described [12,15]. The plasmid pCDH-EF1-Akaluc-T2A-copGFP was produced by inserting the sequence of Akaluc (amplified with specific primers from pcDNA3 Venus-Akaluc plasmid from RIKEN BRC repository) without stop codon using BamHi and NotI sites in pCDH-EF1-MCS -T2A-copGFP vector. Lentiviruses were produced by transfection of HEK-293T packaging cells with three packaging plasmids (pCMV-VSVG, pMDLg-RRE, pRSV-REV; Addgene, Cambridge, MA, USA) and the lentiviral vector plasmids as previously described in details [16].The supernatant containing lentiviral particles were collected after 48 and 72 h. Subsequent quantification of the virus was performed using a standard antigen-capture HIV p24 ELISA (ZeptoMetrix Corporation, NY, USA).

Cell transduction and transfection

Cell transduction was performed by culturing HEK293T cells in DMEM supplemented with 10% of FBS and 1% of Penicillin-Streptomycin at the density of 200,000 cells in a T25-flask with 5 ml of medium. Expression in the lentiviral plasmid is driven by house-keeping elongation factor 1α (EF1) promoter. Cells were transduced with MOI 1 of either pCDH-EF1-Luc2-T2A-copGFP, pCDH-EF1-CBG99-T2A-copGFP, pCDH-EF1-CBR2-T2A-copGFP or pCDH-EF1-Akaluc-T2A-copGFP lentivirus plus with polybrine (hexametride bromide, Sigma-Aldrich) at the final concentration of 8 µg/ml. Transgene expression was confirmed by the presence of the super bright green fluorescent protein copGFP from the copepod *Potenilla plumata* (excitation/emission maximum = 482/502 nm).

Flow cytometry to sort stable cell lines

Positive stable clones were sorted for comparable levels of copGFP expression by cell sorting (BD-FACS ARIA III, BD Biosciences). Forward and side scatters were also drawn to eliminate cellular debris from the analysis and to select highly positive cells for GFP.

In vitro BLI

Transduced cells were plated at a density of 2 x 10^4 cells per well in a black 96-well plate (Greiner Cell Star®) and imaged in 100 µl of D-PBS. Bioluminescence signal from wells was measured with IVIS® spectrum system (PerkinElmer, Boston, MA, USA) every 5 min after substrate addition (final concentration of each substrate was 0.1 mM). All *in vitro* measurements were acquired after 1 min at 37 °C using a 30 s acquisition time with an open filter or using a series of band pass filters ranging from 520 nm to 800 nm. Data were analyzed by Living Image software version 4.3 (PerkinElmer). Data in every well were normalized for fluorescence emission detected using a Glomax®-Multi plate reader.

In vivo BLI

Each stable expressing cell line was injected subcutaneously 1 x 10^5 cells/50 µl. The number of animals was chosen according to power analysis (p value at least <0.05 and power 95%) considering that we expected from the data generated *in vitro* that the brightest BL system would differ by 1–2 orders of magnitude *in vivo*. Mice (N=3 per group) received two different cell lines, one in each flank. Animals were then imaged after intra-peritoneal injection of D-LH2 substrate (150 mg/kg), NH_2-NpLH2 substrate (220 mg/kg), CycLuc1 (7.6 mg/kg) and Akalumine-HCl substrate (50 mg/kg). These doses were chosen based on maximum solubility (for CycLuc1 and Akalumine-HCl), tolerability in mice and maximum attainable signal based on previous findings. Mice were randomly assigned and anaesthetized by isoflurane inhalation prior to performing BLI imaging. The person performing the subcutaneous injections was blind as to the cells being injected. Images were acquired with the IVIS® spectrum small animal imager system (PerkinElmer). Light

was measured using open filter and a series of 20 nm wavelength band filters from 520 nm to 800 nm with acquisition time of 30 s during a time of about 30 min after substrate injection (kinetic analysis). Emission signals were measured with Living Image software® version 4.3 (Perkin Elmer).

Statistical analysis

All statistical analyses were performed using Graphpad Prism 6 software and ONE-WayAnova followed by Tukey's post-test. P-values <0.05 were considered statistically significant.

RESULTS

In vitro evaluation of emission properties for different combinations of luciferase variant and luciferin analogue.

The aim of this study was to evaluate *in vitro* and *in vivo* light emission and spectral differences between four luciferases (Luc2, CBG99, CBR2 and Akaluc) when combined with D-LH2 or three luciferin analogs (NH_2-NpLH2, Akalumine-HCl or CycLuc1) for bioluminescence imaging (BLI). To compare the different emissions, HEK293T cells stably expressing each of the four luciferases were treated with substrates (0.1 mM) and imaged at 37 °C. Equimolar expression of each luciferase was achieved by selecting cells for GFP emission.

We found that the luciferase/luciferin pairs yielding the highest photon emission (p value <0.001) were Luc2/D-LH2 and Akaluc/CycLuc1 when the substrate was added at a concentration of 0.1 mM. The combinations of Luc2/CycLuc1, Akaluc/Akalumine-HCl, CBG99/D-LH2 and CBR2/D-LH2 produced ~2-fold fewer photons (Fig. 1a), while cells expressing CBG99 were much less efficient (~100-fold dimmer with NH_2-NpLH2/Akalumine-HCl; 10-fold dimmer with CycLuc1) (Fig. 1a). CBR2-expressing cells were more promiscuous compared to CBG99 cells. However, they generated 10-fold less luminescence (compared to Luc2/D-LH2) with Akalumine-HCl and NH_2-NpLH2. The CBR2-expressing cells gave a signal comparable to Luc2/D-LH2 with CycLuc1. Finally, Akaluc produced similar luminescence intensity when either Akalumine-HCl or CycLuc1 were used as substrate (Fig. 1a). Akaluc also showed nearly 100-fold lower signal with D-LH2 or NH_2-NpLH2 compared to Akalumine-HCl and CycLuc1.

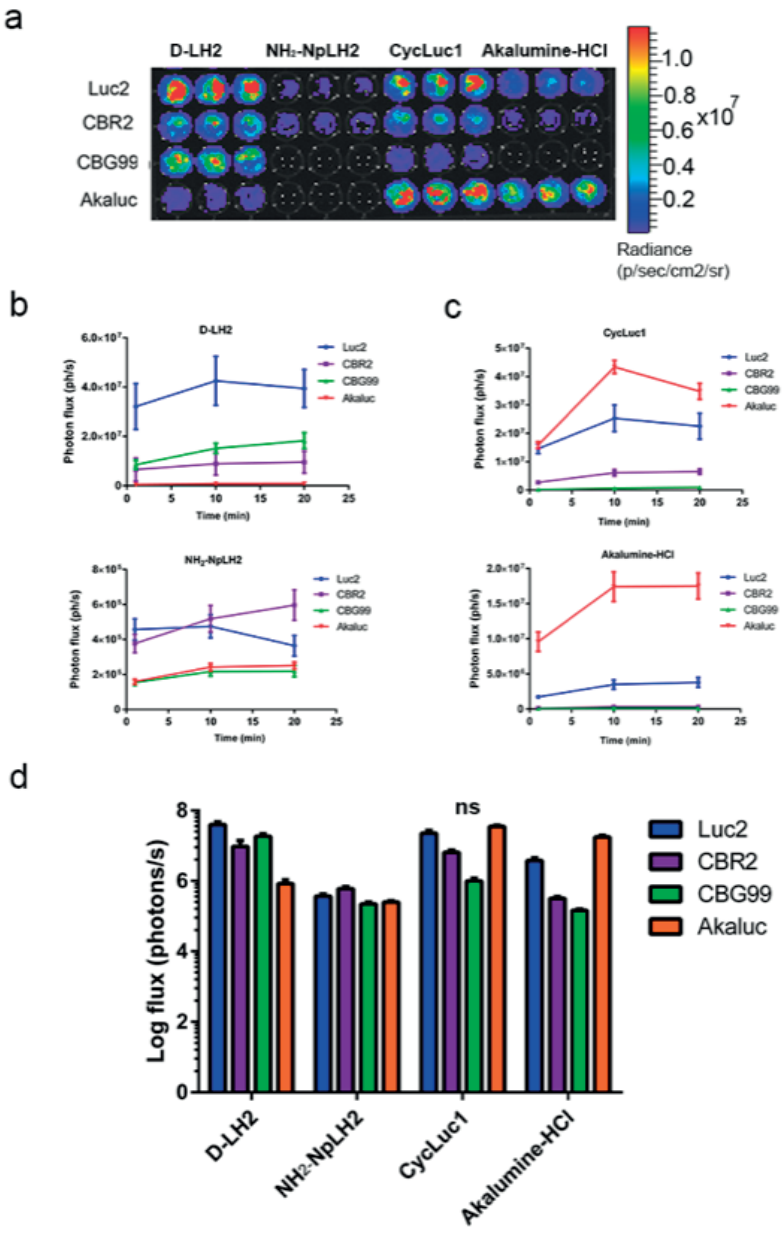

Figure 1. Bioluminescence profiles for Luc2, CBR2, CBG99 and Akaluc luciferases combined with four different luciferin analogues in live cells. Photon flux (ph/s) in HEK293T cells expressing individual luciferases upon addition of substrates (0.1 mM) was quantified using an exposure time of 30 s. Statistical analysis (N=3) was performed using ONE-Way Anova followed by Tukey's T test (*p<0.01 for Luc2/D-LH2 compared to all combinations with the exception of Akaluc/Cycluc1 which was not significantly different).

In vivo emission spectrum of luciferases detected using a series of 20 nm band pass filters

The day of injection, HEK293T cells (expressing the various luciferases) were prepared at a concentration of $1x10^6$ cells/ml in PBS and fluorescence emission measured at IVIS, confirming the comparable average expression of GFP (Supplementary Fig. 1). Following subcutaneous injection of $1x\ 10^5$ HEK293T cells (expressing the various luciferases) into both flanks of mice, images were acquired after injection of D-LH2 (150 mg/kg), NH_2-NpLH2 (220 mg/kg), Akalumine-HCl (50 mg/kg) or CycLuc1 (7.6 mg/kg). We used the optimal concentration for each given substrate based on previous literature [8,10,12,19]. For D-LH2 this was 150 mg/kg [19]. Because of poor aqueous solubility, CycLuc1 and Akalumine-HCl were injected at 7.6 mg/kg (5 mM in saline) and 50 mg/kg (33 mM in saline), respectively [8,10]. We previously demonstrated that the solubility of NH_2-NpLH2 allows injection of a maximal dose of 220 mg/kg (60 mM in saline) and that it produces significantly higher photon fluxes than a dose of 150 mg/kg [12]. Multiple acquisitions using a series of 20 nm band pass filters were performed with an exposure time of 30 s. The BLI measurements were performed at the time of peak of emission after injection of the luciferins into sedated animals.

In terms of emission spectra, Luc2/D-LH2, CBG99/D-LH2, CBR2/D-LH2 and Akaluc/D-LH2 produced peaks at 610 nm, 540 nm, 620 nm and 640 nm, respectively (Fig. 2a). NH_2-NpLH2 caused a red shift of the peak of emission with all the luciferases (Luc2, 700 nm; Akaluc, 720 nm; CBR, 730 nm; and CBG99, 620 nm) (Fig. 2b). In contrast, when CycLuc1 was used as a substrate, the emission peak for each luciferase was in the range of 620 nm (Luc2 and Akaluc were green shifted towards 600 nm and CBG99 and CBR2 were red shifted towards 640 nm) (Fig. 2c). Akaluc/Akalumine-HCl, also referred to as the AkaBLI system [11], produced a peak of emission at 660 nm while the other luciferases peaked in the NIR (~680 nm) when paired with Akalumine-HCl (Fig. 2d).

In vivo comparison of brightness of luciferase/luciferin pairing

Next, we compared the total emission of each luciferase *in vivo* with D-LH2 or the luciferin analogues. Figure 3 shows the representative bioluminescent images of nude mice where CBG99, Luc2, CBR2 and Aka-Luc expressing cells were implanted and each of the different substrates was injected intraperitoneally. The data in Figure 4 represents signals at peak of emission (which differs slightly between BLI systems (Supplementary Fig. 2). Luc2, CBG99 and CBR2 paired with D-LH2 produced the highest signals which were 20-fold higher compared to Akaluc/D-LH2 (p value < 0.001) (Fig. 4a). When NH_2-NpLH2 was used as a substrate, Luc2 and CBR2 produced approximately 10-fold higher signal output (p value, 0.001) compared to both CBG99 and Akaluc (Fig. 4b). When CycLuc1 was used as a substrate, the strongest signal was detected for Luc2/Cycluc1. AkaLuc,

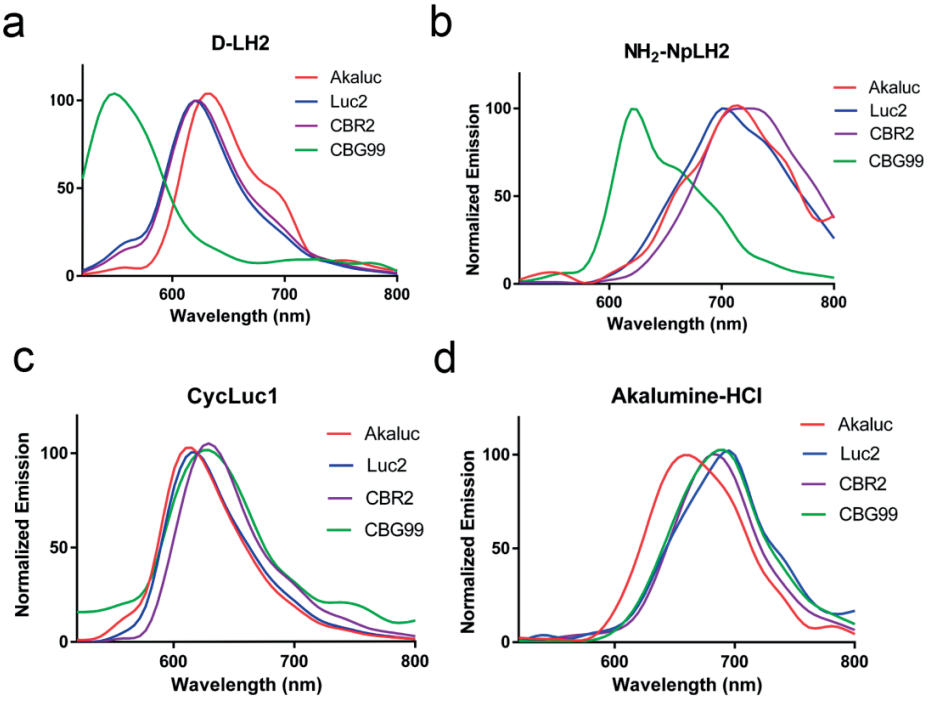

Figure 2. ***In vivo*** **(BALB/C) emission spectra for different combinations of luciferase (Luc2, CBG99, CBR2 or Akaluc expressed in HEK-293T cells implanted subcutaneously in the flanks) and luciferin or luciferin analogue**. Panel a: D-LH2 (150 mg/Kg), panel b: NH_2-NpLH2 (220 mg/Kg), panel c: CycLuc1 (7.6 mg/Kg) and panel d: Akalumine-HCl (50 mg/Kg); substrates were injected intraperitoneally. Spectral data were acquired 15–20 min after injection.

CBR2, and CBG99 paired with Cycluc1 produced ~5, 16, and 70-fold lower signal output, respectively (Fig. 4c). When Akalumine-HCl was used as a substrate, Luc2 and Akaluc produced ~2-fold higher signal compared to CBR2, and there was no detectable signal for CBG99 (Fig. 4d).

The luciferase/luciferin pairs that gave the highest photon yields *in vivo* were Luc2/D-LH2, Luc2/CycLuc1, CBG99/D-LH2 and CBR2/D-LH2 (1–2 x 10^7 ph/s). The following luciferin/luciferase pairs produced approximately 10-fold fewer photons: Akaluc/Cycluc1, Akaluc/Akalumine-HCl, Luc2/Akalumine-HCl, Luc2/NH_2-NpLH2 and CBR2/NH2-NpLH2. Finally, the following pairs produced nearly 100-fold fewer photons: CBR2/CycLuc1, CBR2/Akalumine-HCl, CBG99/Cycluc1, CBG99/NH_2-NpLH2 and Akaluc/NH_2-NpLH2 (Fig. 4e, Table 1).

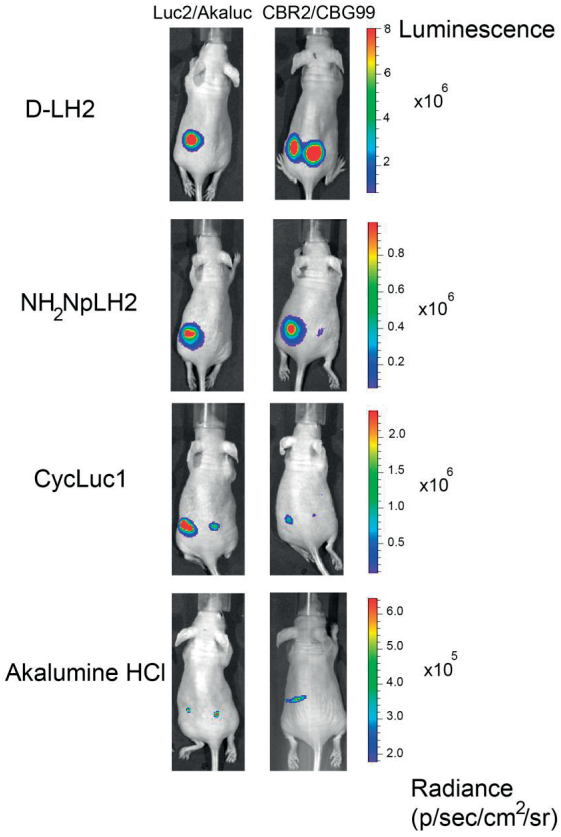

Figure 3. Superficial bioluminescence imaging of BALB/C mice in which 1 x 10^5 HEK293T cells transduced with Luc2 and Akaluc or CBR2 and CBG99. Cells were implanted subcutaneously into the left and right flanks of mice, respectively, and treated (intraperitoneally) with **a)** D-LH2 (150 mg/kg), **b)** NH_2-NpLH2 (220 mg/kg) **c)** CycLuc1 (7.6 mg/Kg) and **d)** Akalumine-HCl (50 mg/kg). Imaging data were collected using open filters and with an exposure time of 30 s. Average luminescence is reported as photons/s/cm^2/sr.

Table 1
In vivo intensity relative to Luc2/D-LH2.

	D-LH2		NH2-NpLH2		CycLuc1		Akalumine-HCl	
Luciferase	Spectral peak [nm]	Normalized intensity	Spectral peak [nm]	Normalized intensity	Spectral peak [nm]	Normalized intensity	Spectral peak [nm]	Normalized intensity
Luc2	620	**1**	700	**0.1**	620	**0.5**	700	**0.8**
CBR2	620	**0.98**	720	**0.1**	620	**0.03**	680	**0.03**
CBG99	540	**1**	620	**0.01**	620	**0.01**	680	**0**
Akaluc	640	**0.05**	720	**0.01**	620	**0.1**	660	**0.06**

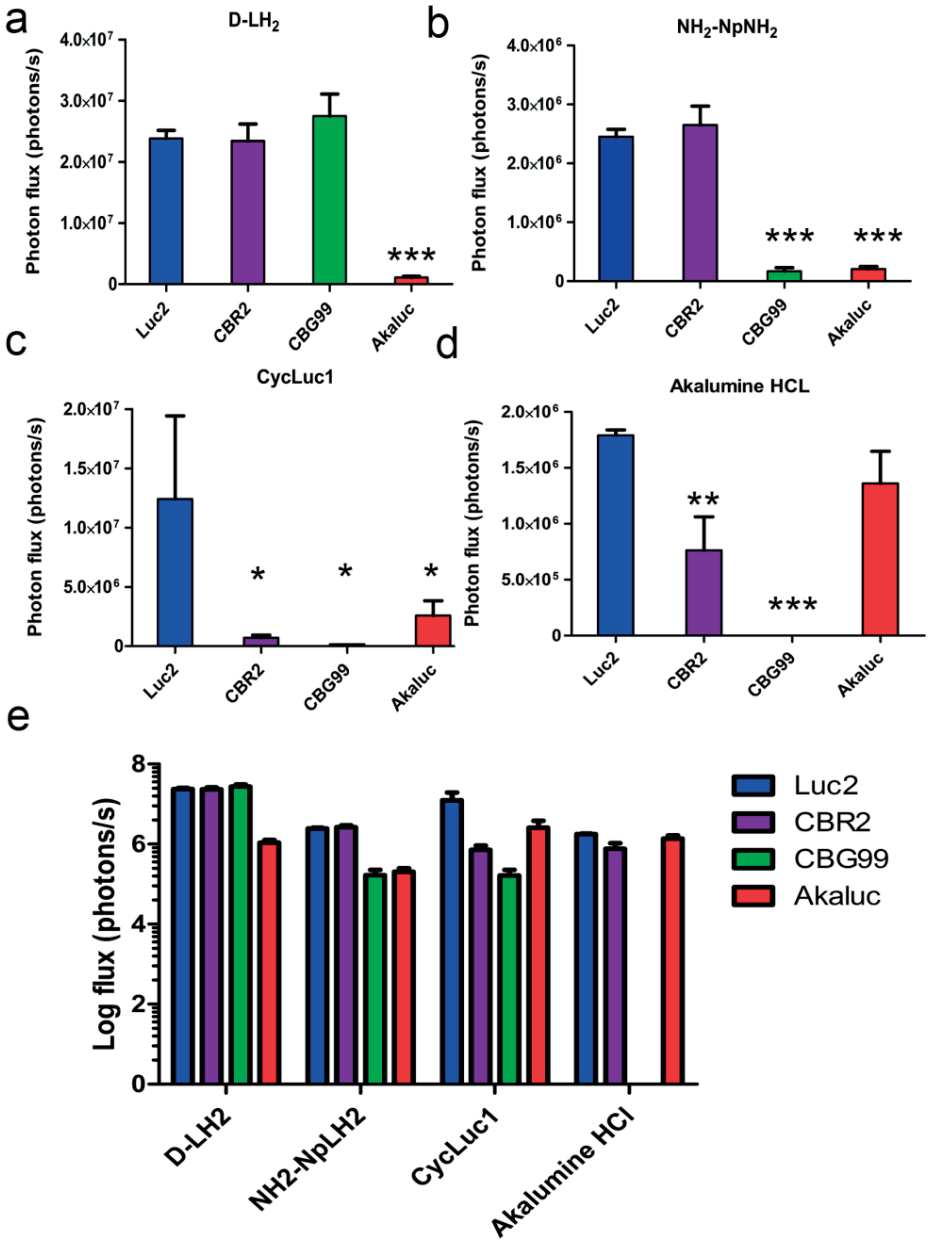

Figure 4. Quantification of photon flux (ph/s) measured in vivo for all combinations of luciferase and substrate (D-LH2 (panel a), Akalumine-HCl (panel b), CycLuc1 (panel c) and (d) NH2-NpLH2 (panel d). Combined data is also presented in logarithmic scale (panel e). Statistical analysis of data was performed using ONE-Way Anova followed by Tukey's post-test (**p<0.0019; ***p<0.001; ****p<0.0001).

DISCUSSION

A variety of new luciferase enzymes and novel substrate analogues emerging in recent years has resulted in better tools for *in vivo* BLI. One example is CBR2/NH_2-NpLH2, which was engineered specifically for enhanced NIR emission to improve imaging resolution in deeper tissues [12]. Another example is Akaluc/Akalumine-HCl [11], an engineered pair offering improved *in vivo* sensitivity. Another relatively new substrate, Cycluc1, has shown *in vivo* utility (including more efficient crossing of the blood brain barrier compared to D-LH2) when used in combination with the already well-established Luc2 [8]. With the emergence of these and other new bioluminescence systems we felt it would be of interest and potential benefit for the *in vivo* BLI community, particularly for those interested in dual color readouts, to analyze different pairings of luciferase/substrate using a common set of test parameters. Here, we report on the photon yields and spectral characterization of Luc2, CBG99, CBR2 and Akaluc luciferases combined with four different substrates (D-LH2, NH_2-NpLH2, Cycluc1 and Akalumine-HCl) both *in vitro* and *in vivo*. Our goal was to use these parameters to compare the various luciferase/substrate combinations in a standard subcutaneous *in vivo* BLI model, with the intention to provide guidance for the *in vivo* BLI community when choosing appropriate systems for specific applications involving dual color detection. Note the longer emission wavelengths for CBR2/NH_2-NpLH2 and Akaluc/Akalumine-HCl provide a sensitivity advantage in deeper tissue (refs) that will not be fully realized in a subcutaneous model. However, we postulated that the peak emissions in the NIR for these systems would provide excellent spectral separation from shorter wavelength signals nonetheless.

We have demonstrated *in vitro* that at a relatively low, but biologically relevant (*in vivo*) substrate concentration (0.1 mM), three of the four luciferases give maximum signal when combined with D-LH2. The exception was Akaluc, which produced more photons when using either Cycluc1 or Akalumine-HCl as substrate. We observed the same trend in a low-depth, superficial *in vivo* tissue model. Though we did not examine deeper tissues in this study, we predict based on our results that the red-shifted NIR systems (CBR2/NH_2-NpLH2, Akaluc/Akalumine-HCl and Luc2/Akalumine-HCl) would perform best.

To evaluate spectral properties *in vivo* as a way to determine the potential for multiplexing, we used the same superficial, subcutaneous model where different luciferase expressing cell lines were injected into the backs of mice. This minimally invasive model allowed us to determine the light emission characteristics for different BLI systems using a small cohort of animals. Based on the analysis we are able to recommend new combinations of luciferases with distinct colors having potential for multiplexing with a single substrate in superficial tissue e.g., CBG99/D-LH2 (540 nm) and CBR2/D-LH2 (620 nm)

(examples of spectral unmixing showed in Supplementary Fig. 3) ; CBG99/D-LH2 (540 nm) and Luc2/D-LH2 (610 nm); Luc2/Akalumine (680 nm) and Akaluc/Akalumine (650 nm). Such an approach could be useful for analyzing multiple parameters or biological processes in animals using either engrafted cells or transgenes expressed in particular tissues or organs, and as part of a single imaging session requiring fewer animals.

Successful multiplexing of luminescence systems with different emission spectra relies on the acquisition of images using multiple filters followed by accurate, algorithm-based spectral unmixing to resolve the contributions from each luciferase to total light output. This can be a challenge with shorter wavelength systems (e.g., CBG99/D-LH2), as they tend to shift their apparent emission peak to significantly longer wavelengths when imaged in deeper tissues or even in superficial tissue when using mice with dark fur [20-22]. For these more challenging imaging targets it is therefore desirable to use bioluminescence pairs that emit in the NIR (>650 nm), as emission peaks are essentially constant in this range of the spectrum [22,23]. In this regard, we found that click beetle luciferases have high photon emission with NH_2-NpLH2 [12] and that there is a broad spectral separation between CBG99 (620 nm) and CBR2 (720 nm) (spectral unmixing is shown in Supplementary Fig. 2). However, before giving serious consideration to this pair with NH_2-NpLH2 as a multiplexing opportunity for deep tissue imaging in mice it will likely be necessary to improve the photon yield for CBG99/NH_2-NpLH2.

Acknowledgements
We acknowledge the funding for this work provided by the European Commission under the H2020-MSCA-RISE award grant number 777682 (CANCER) and under the H2020-MSCA-ITN award, grant number 675743 (ISPIC) and the Applied Molecular Imaging Erasmus MC (AMIE) facility.

Conflict of interest
The authors declare that they have no conflict of interest.

REFERENCES

1. Contag CH, Bachmann M (2002) Advances in In Vivo bioluminescence imaging of gene expression. AnnuRev Biomed Eng 4:235-260.
2. Brader P, Serganova I and Blasberg RG, (2013) Noninvasive Molecular Imaging Using Reporter Genes. J Nucl Med 54:167-172.
3. Close DM, Xu T, Sayler GS, Ripp S (2010) In vivo bioluminescent imaging (BLI): noninvasive visualization and interrogation of biological processes in living animals. Sensors (Basel, Switzerland) 11:180-206.
4. Wilson TA, Hastings JW (1998) Bioluminescence Annual Review of Cell and Developmental Biology 14:197-230.
5. Mezzanotte L, vant Root M, Karatas H et al. (2017) In Vivo molecular bioluminescence imaging: new tools and applications Trends in Biotechnology 35:640-652.
6. Xu T CD, Handagama W, Marr E, et al. (2016) The expanding Toolbox of In Vivo Bioluminescent imaging. Frontiers in Oncology 6:150.
7. Adams ST, Miller SC (2014) Beyond D-luciferin: expanding the scope of bioluminescence imaging in vivo. Current Opinion in Chemical Biology 21:112-120.
8. Evans MS, Chaurette JP, Adams ST et al. (2014) A synthetic luciferin improves bioluminescence imaging in live mice. Nat Methods 11:393-395.
9. Simonyan H, Hurr C, Young CN (2016) A synthetic luciferin improves in vivo bioluminescence imaging of gene expression in cardiovascular brain regions. Physiological Genomics 48(10): 762–770.
10. Kuchimaru T, Iwano S, Kiyama M, et al. (2016) A luciferin analogue generating near-infrared bioluminescence achieves highly sensitive deep-tissue imaging. Nat Commun 7:11856.
11. Iwano S, Sugiyama M, Hama H et al. (2018) Single-cell bioluminescence imaging of deep tissue in freely moving animals. Science 359:935-939.
12. Hall MP, Woodroofe CC, Wood MG, et al. (2018) Click beetle luciferase mutant and near infrared naphthyl-luciferins for improved bioluminescence imaging. Nature Communications 9:132.
13. Ohmiya Y (2015) Simultaneous multicolor luciferase reporter assays for monitoring of multiple genes expressions. Combinatorial Chemistry & High Throughput Screening 18: :937.
14. Branchini BR, Southworth TL, Fontaine DM, Kohrt D, Florentine CM, Grossel MJ (2018) A Firefly Luciferase Dual Color Bioluminescence Reporter Assay Using Two Substrates To Simultaneously Monitor Two Gene Expression Events. Scientific Reports 8:5990.
15. Miloud T, Gunter CH, Hammerling J, Quantitative comparison of click beetle and firefly luciferases for in vivo bioluminescence imaging. J Biomed Opt 12(5).
16. Mezzanotte L, Aswendt M, Tennstaedt A, et al. (2013) Evaluating reporter genes of different luciferases for optimized in vivo bioluminescence imaging of transplanted neural stem cells in the brain. Contrast Media Mol Imaging 8:505-513.
17. Branchini BR, Ablamsky DM, Davis AL, et al. (2010) Red-emitting luciferases for bioluminescence reporter and imaging applications. Analytical Biochemistry 396:290-297.
18. Kaskova ZM, Tsarkova AS, Yampolsky IV (2016) 1001 lights: luciferins, luciferases, their mechanisms of action and applications in chemical analysis, biology and medicine. Chemical Society Reviews 45:6048-6077.
19. Contag CH, Spilman SD, Contag PR et al. (1997) Visualizing gene expression in living mammals using a bioluminescent reporter. Photochem Photobiol. 66(4):523-31.

20. Mezzanotte L, Que I, Kaijzel E et al. (2011) Sensitive dual color in vivo bioluminescence imaging using a new red codon optimized firefly luciferase and a green click beetle luciferase. PloS One: 10.1371/journal.pone.0019277.
21. Aswendt M, Vogel S, Schäfer C et al. (2019) Quantitative in vivo dual-color bioluminescence imaging in the mouse brain. Neurophotonics. 6(2):025006.
22. Stowe CL, Burley TA, Allan H, et al (2019) Near-infrared dual bioluminescence imaging in mouse models of cancer using infraluciferin. Elife: 10.7554/eLife.45801.
23. Jathoul A, Grounds E, Anderson JC, Pule M (2015) A Dual-Color Far-Red to Near-Infrared Firefly Luciferin Analogue Designed for Multiparametric Bioluminescence Imaging. Angew Chem Int Ed Engl. 54(6): 1698.

Supplementary Figures

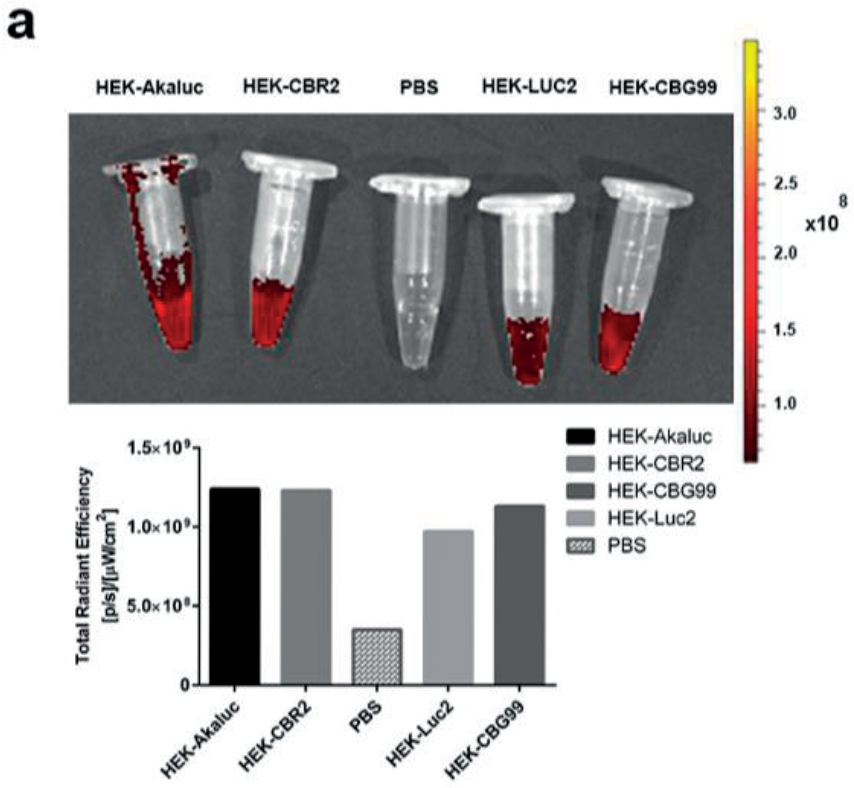

Supplemental figure 1. a) Representative fluorescent image of the cell solutions before injection. b) Quantification of the average fluorescent signals from 0.5 ml solution containing $2x10^6$ cells/ml. Experiment was done in triplicate.

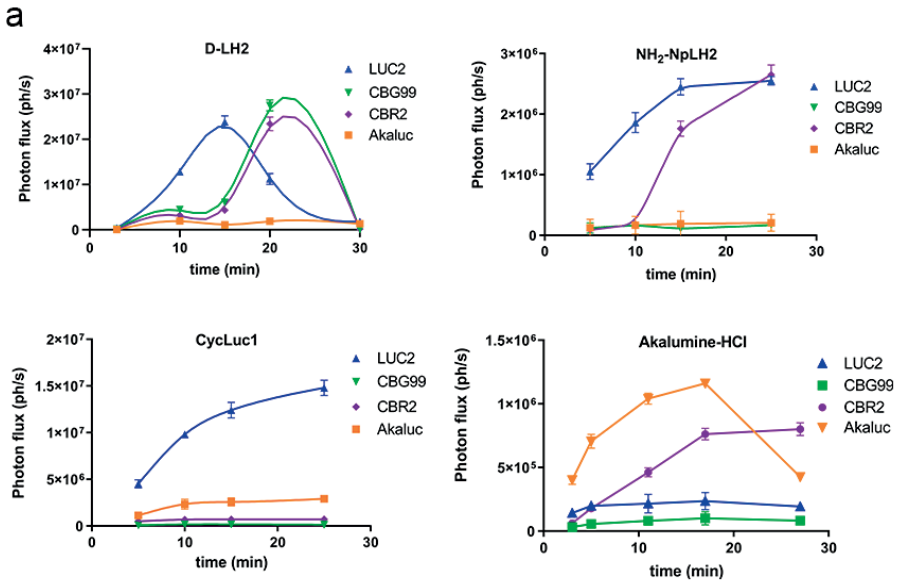

Supplemental figure 2. *In vivo* kinetics of D-LH2, NH_2-NpLH2, CycLuc1 and Akalumine-HCl at various time points ranged between 5 and 30 minutes after injection of substrates. Data are presented as means (n=3) and SD and curves are generated using lowess smoothing function.

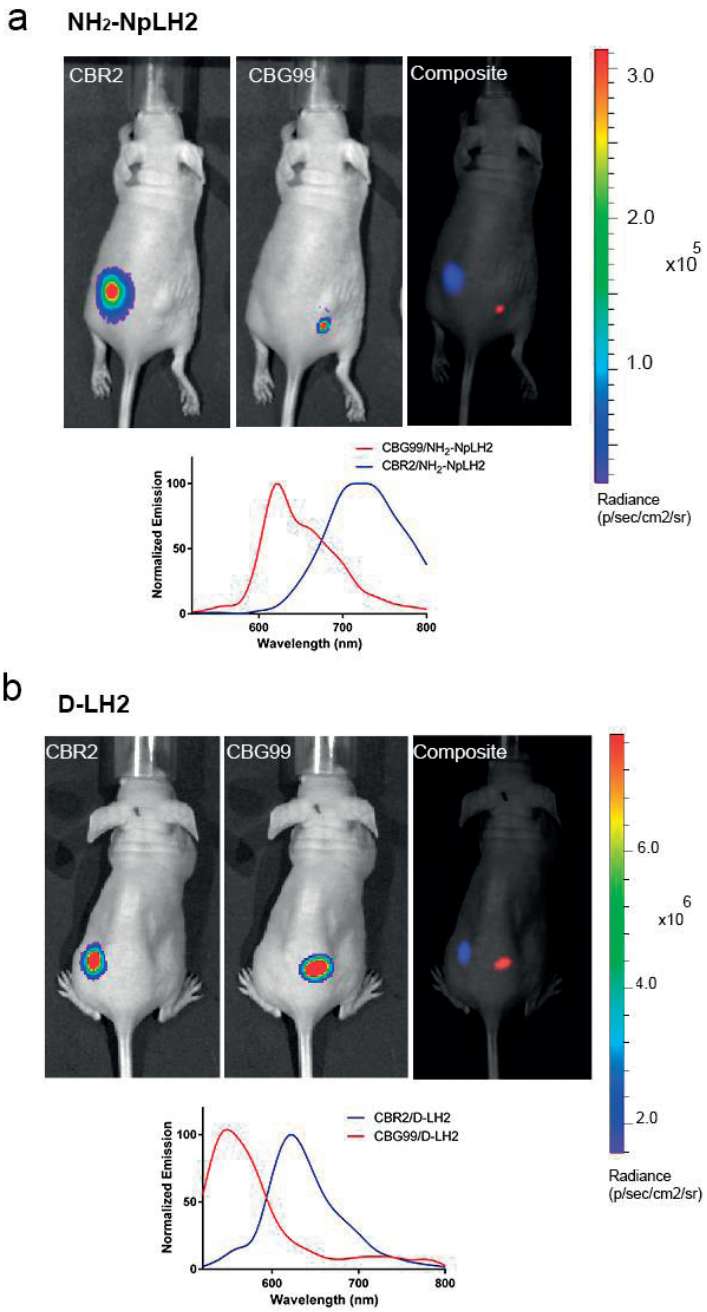

Supplemental Figure 3. Representative spectral unmixing images of CBR2 and CBG99 luciferases. Mice were imaged after administration of NH_2-NpLH2 (a) or of D-LH2 (b) substrates using a series of band pass filters at IVIS spectrum (Perkin Elmer). A spectral unmixing algorithm applied to the images extracted and measured each luciferase contribution and generated the two reported spectra of emission.

4

Red-shifted click beetle luciferase mutant expands the multicolor bioluminescent palette for deep tissue imaging

Giorgia Zambito[1,2,3], Mary P. Hall[4], Monika Wood[4], Natasa Gaspar[1,2,5], Yanto Ridwan[1,2], Fabio F. Stellari[6], Ce Shi[7] Thomas A. Kirkland[7], Lance P. Encell[4], Clemens Löwik[1,2,8], Laura Mezzanotte[1,2,9,*]

[1]Erasmus Medical Center, Radiology and Nuclear Medicine, Rotterdam, 3015 CE, The Netherlands
[2]Erasmus Medical Center, Molecular Genetics, Rotterdam, 3015 CE, The Netherlands
[3]Medres medical research GmBH, Cologne, 50931, Germany
[4]Promega Corporation, Madison, Wisconsin 53711, USA
[5]Percuros B.V., Leiden, 1333 CL, The Netherlands
[6]Chiesi Farmaceutici, Parma, 43122, Italy
[7]Promega Biosciences Incorporated, San Luis Obispo, California 93401, USA
[8]CHUV Department of Oncology, University of Lausanne, 461011, Lausanne, Switzerland.
[9] Lead Contact
*Corresponding author:
Dr. Laura Mezzanotte**:** l.mezzanotte@erasmusmc.nl

iScience, Volume 24, Issue 1, 2021

SUMMARY

For in vivo multicolor bioluminescence applications, red and near-infrared signals are desirable over shorter wavelength signals because they are not as susceptible to light attenuation by blood and tissue. Herein, we describe the development of a new click beetle luciferase mutant, CBG2, with a red-shifted color emission. When paired with NH_2-NpLH2 luciferin, CBG2 (λ=660 nm) and CBR2 (λ=730 nm) luciferases can be used for simultaneous dual-color bioluminescence imaging in deep tissue. Using a spectral unmixing algorithm tool it is possible to distinguish each spectral contribution. Ultimately, this enzyme pair can expand the near-infrared bioluminescent toolbox to enable rapid visualization of multiple biological processes in deep tissue using a single substrate.

Subject Areas dual-color bioluminescence, luciferase, optical imaging, mutagenesis, near-infrared emission.

INTRODUCTION

Bioluminescence imaging (BLI) has become a highly adopted technique for preclinical and non-invasive study of biological events in vivo (Kaskova et al., 2016; Mezzanotte et al., 2017). The production of bioluminescence depends on luciferase enzyme catalyzed oxidation of a luciferin substrate (Wilson et al., 1998). The use of luciferases emitting photons in the "bio-optical window" (λ=600 nm to 800 nm) is highly recommended to limit light absorption by tissue components in vivo (Jathoul et al., 2014; Smith et al., 2009). Thus, red-shifted luciferase mutants improve the sensitivity of BLI and allow tracking of single cells over time in deep tissue (Branchini et al., 2010; Iwano et al., 2018). However, it is still challenging to visualize multiple biological processes over time in deep tissue because current BLI offerings are limited. In many of the systems currently used, sequential administration of multiple substrates is required, making interpretation of data challenging (Maguire et al., 2013; Taylor et al., 2018). Previously, we attempted dual-color BLI using green click beetle (CBG99) and red firefly (PpyRe8) luciferases with D-LH2. However, the signal for CBG99 was attenuated in deep tissue resulting in acquisition of predominantly the red contribution (Mezzanotte et al., 2011). An ideal approach for deep tissue multicolor BLI would be to utilize a single substrate with two luciferases emitting spectrally separated signals in the near-IR bio-optical window. Notably, the recent development of infra-luciferin (iLH2) proved to shift the FLuc mutants to the far-red and near-infrared region of spectrum (FLuc_green ~680 nm and FLuc_red ~720 nm) (Jathoul et al., 2014; Branchini et al., 2007). Stowe et al., demonstrated that engrafted red-CAR T cells can expand and reach the green-Raji B lymphoma when iLH2 is used in vivo (Stowe et al., 2019). Green and red signals were acquired with a sensitive CCD camera and quantified using a validated spectral unmixing algorithm as part of the instrument software (Aswendt et al., 2019; Gammon et al., 2006).

Herein, we introduce a novel click beetle mutant named CBG2. CBG2 paired with NH_2-NpLH2 substrate (λ=660 nm) can be integrated with the near-infrared system CBR2/NH_2-NpLH2 (λ=730 nm) (Hall et al., 2018) for dual-color near-infrared (NIR) BLI in vivo. We demonstrate that it is possible to spectrally resolve and quantify the bright emissions of CBG2 and CBR2 using a spectral unmixing algorithm. The high solubility and low toxicity associated with the salt form of NH_2-NpLH2 luciferin make the system amenable to in vivo injection, thus expanding the BLI toolbox for measuring multiple biological processes in a single imaging session using a single luciferase substrate.

RESULTS

Rational design of CBG2 luciferase and spectral characterization

Color variation in click beetle luciferases can be influenced at the protein level by a small number of amino acid positions. The best characterized mutants, CBG99, CBR, and CBR2, differ at only 9 positions. To create a luciferase that can produce NIR emission suitable for multiplexing with CBR2 and efficiently utilize NH_2-NpLH2, we chose CBG99 as our starting point. CBG99 was preferred over CBR primarily because of its narrower spectrum (Figure S1a). We first codon optimized CBG99 luciferase (CBG99opt) to improve gene expression and protein levels in mammalian cells. CBG99opt has identical codons to CBR2 except at sites where there are amino acid differences. We confirmed that CBG99opt produces a spectral peak at 540 nm when combined with D-LH2 (Xu et al., 2016; Miloud et al., 2007) and a peak at 545 nm when used with NH_2-NpLH2 (Table 1).

Purified Mutant Enzyme	*D-LH2 lytic*	*Spectral Peak D-LH2 (nm)*	*NH_2-NpLH2 lytic*	*Spectral Peak NH_2-NpLH2 (nm)*
CBR	0.96	620	26.72	660
CBR2	1.97	620	26.34	730
CBG99	0.83	540	0.58	545
CBG99opt	1.00	550	1.00	545
CBG2	4.38	585	14.72	660

Table 1. Relative light unit (RLU) of CBR2, CBG99 and CBG2 measured with D-LH2 and NH2-NpLH2 in transiently transfected and lytic HEK293T cells. Spectral peak data were acquired using purified enzymes.

Next, we designed a panel of mutants based on the 9 amino acid differences between CBG99 and CBR2. The set included amino acid substitutions in the active site known to red-shift emission of beetle luciferases (Viviani et al., 2016). The mutant of highest interest that emerged from this analysis, CBG2, differs by six residues compared to CBG99 and by three residues compared to CBR2. CBG2 was red-shifted by 75 nm with NH_2-NpLH2 (660 nm), when compared to the wild type CBG99/NH_2-NpLH2 (545 nm) (Table 1). A summary of the spectral characterization and brightness for the purified luciferase mutants is presented in Table 1. Residues that differ between CBR2 and CBG2 are highlighted in the structure model shown in Figure 1a. These residues are mainly located in the luciferin binding pocket of the enzymes and contribute to substrate affinity and color-shift (Woodroofe et al., 2008). We employed D-LH2 and its analogs NH_2-NpLH2 and Akalumine-HCl (depicted in Figure 1b) to evaluate the function of the novel mutant in this study.

Luminescence signals for CBR2 and CBG2 with D-LH2 and NH_2-NpLH2 (100 µM) were measured in live cells and lysates (Figure 1c). With D-LH2 as substrate, CBG2 was ~5-fold brighter and red-shifted ~40 nm (to 585 nm) relative to both CBG99 and CBG99opt. Interestingly, the specificity of CBG2 in live cells is significantly higher than both CBG99 and CBG99opt with NH_2-NpLH2, producing a 25-fold increase in light output with a ~115 nm red-shift (660 nm). CBR2 luciferase yielded the brightest photon emission when used with NH_2-NpLH2 and a near-infrared peak at 720 nm (Figure 1c). The CBR variant (also giving a peak at 660 nm) was considered for multiplex BLI, but further investigations in live cells revealed a broad, more intense spectral profile that significantly overlapped with the CBR2 spectrum (Figure S1a). Kinetic properties for the mutant luciferases were tested in HEK293T live cells with 1.85 µM of NH_2-NpLH2 (Figure 1d). After an initial loss (~10-fold) in signal, CBG2 reached steady state after 10 min. The signal strength for CBR2 was higher compared to CBG2, but its signal duration was longer (Figure 1d). V_{max} and Km parameters of the enzymes with titrated D-LH2 or NH_2-NpLH2 can be found in Figure S1b. Luminescence photon fluxes of HEK cells stably expressing CBG2, Luc2, CBR2 or Akaluc luciferases and their respective brightness with D-LH2, NH_2-NpLH2 and Akalumine-HCl are highlighted in Figure S2a. We attempted to unmix (i.e., resolve) the spectra of CBG2 and CBR2 with D-LH2 or NH_2-NpLH2 using transfected HEK293T cells. When treated with D-LH2, CBG2 cells produced nearly 2-fold higher photon flux compared to CBR2. Emission peaks for the two systems were separated by 35 nm. This modest separation, combined with the broad emission spectrum for CBR2, prevented efficient resolution of signals (Figure 1e). In contrast, CBG2 cells treated with NH_2-NpLH2 showed a consistent, red-shifted bioluminescent spectrum peaking at ~660 nm and with a photon emission of $1.2x10^6$ ph s^{-1}. This allowed enough spectral separation from the 730 nm peak for CBR2 (Figure 1f). Moreover, we confirmed sufficient spectral separation when CBR2 and CBG2 were co-transfected HEK cells. Use of the spectral unmixing tool allowed us to calculate the respective unmixed photon fluxes from cells expressing both luciferases (Figure S2b).

In vitro kinetics and spectral unmixing of CBG2 and CBR2 luciferases

Kinetic profiles for CBG2 and CBR2 were measured in stably luciferase-expressing HEK cells in vitro (Figure 2a). To validate the spectral unmixing of HEK-CBG2 and HEK-CBR2 signals, cells expressing either CBG2 or CBR2 were plated in various ratios (ranging from 100% to 0%) in 96-well black plates (Figure 2b). Spectral imaging and unmixing were performed by selecting 14 band pass filters ranging from 540 to 800 nm on the IVIS Spectrum using NH_2-NpLH2 as substrate (1 mM). Interestingly, the algorithm was able to measure pure green signals (100% CBG2) and pure red signals (100% CBR2) making it possible to build a specific library for each luciferase contribution. The library was then applied to spectral unmixing. Figure 2c shows the successful unmixing of each spectrum

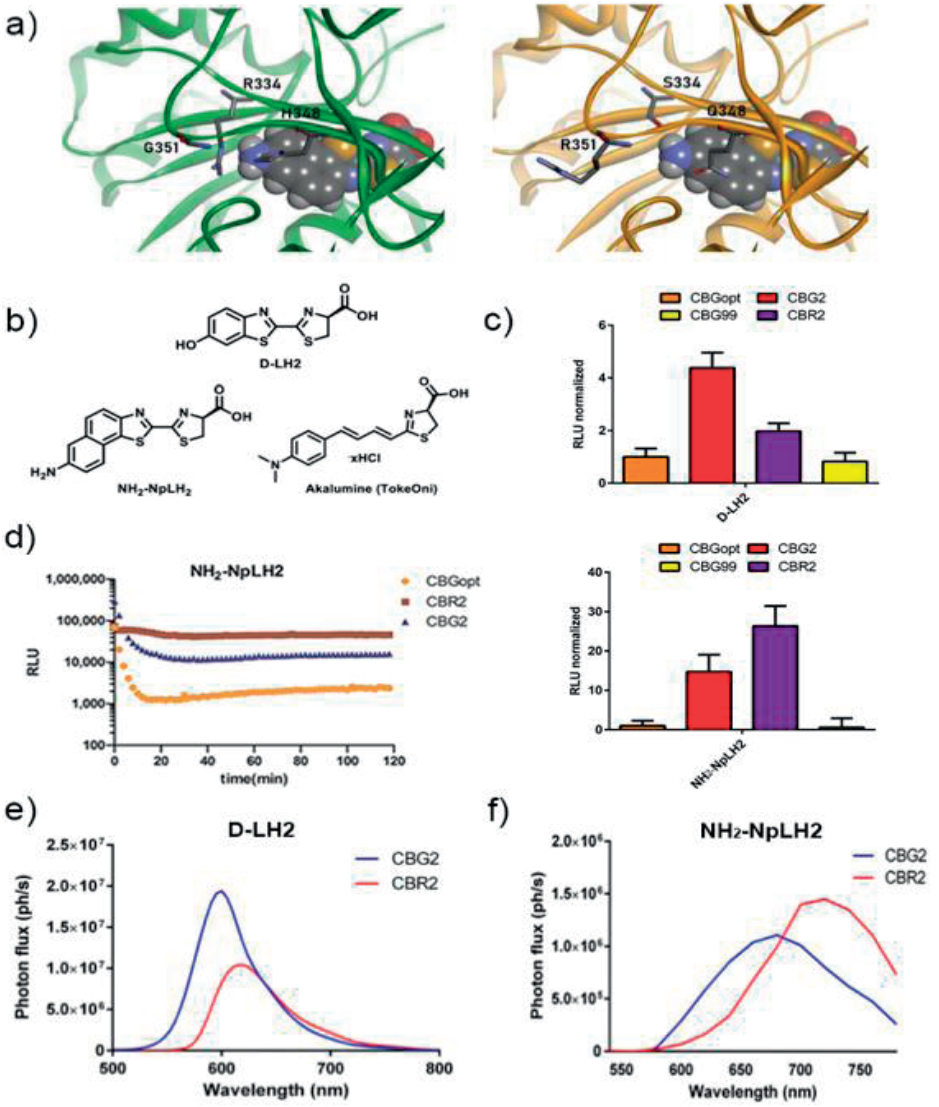

Figure 1. Rational design of CBG2 luciferase and spectral characterization. a) Homology models of CBG2 (left) and CBR2 (right) luciferases with NH_2-NpLH2, based on firefly luciferase X-ray structure templates (PDB accession codes 2D1S, 4G36, and 5KYT). Residues that differ between CBG2 and CBR2 (334, 348, 351) are indicated. Modeling and rendering were performed using Discovery Studio software (BIOVIA). **(b)** Chemical structures of D-LH2, NH_2-NpLH2 and Akalumine-HCl. **(c)** Bioluminescence intensity (RLU_{max}) of CBG99, CBG99opt, CBR2 and CBG2 (cell lysates) combined with D-LH2 or NH_2-NpLH2 (N=3). The spectra of CBG2/D-LH2 and CBG2/NH_2-NpLH2 are presented as reference points. A summary of spectral peaks of the different combinations is reported in Table 1. **(d)** Kinetics (HEK293T lysates) of CBG99opt, CBG2 and CBR2 with NH_2-NpLH2. **(e)** and **(f)** Bioluminescence emission spectra for CBG2 and CBR2 lysates with D-LH2 and NH_2-NpLH2.

which then allowed us to plot the normalized and partially overlapped spectra of CBG2 (blue line) and CBR2 (red line). The same library was also used to quantify the photon flux of mixed green and red cell populations at different percentages between 100% and 0% (Figure 2d).

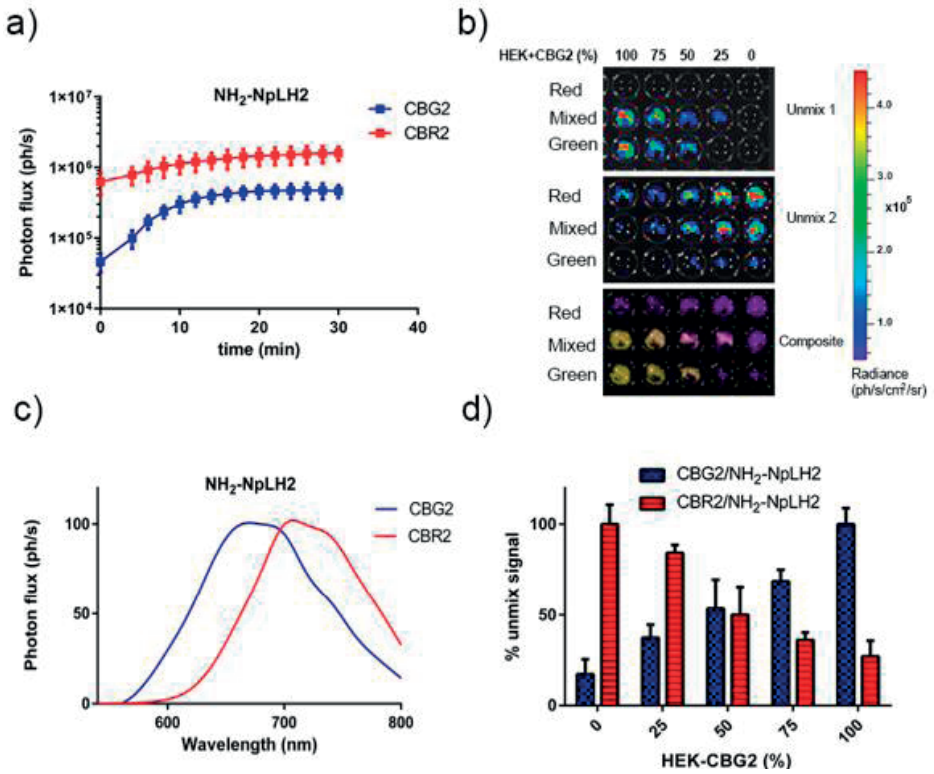

Figure 2. In vitro kinetics and spectral unmixing of CBG2 and CBR2 luciferases. (a) Live cell Kinetic reported for HEK-CBG2 and HEK-CBR2 with NH_2-NpLH2. **(b)** Spectral unmixing of HEK cell expressing CBG2 or CBR2 and mixed in various proportions ranging from 100% to 0% of the total population. Plate was spectrally imaged using IVIS system. Spectral unmix was produced building a specific library for each pure luciferase/luciferin BLI and then applied to the mixture**. (c)** Normalized bioluminescence spectra generated by the spectral unmixing and revealing the feasibility to efficiently separate green and red spectra. Spectra were normalized to the peak emission for each Click beetle mutants with each substrate. **(d)** Quantification of the percentage unmixed signals of HEK-CBG2 and HEK-CBR2 with NH_2-NpLH2. Unmixed signals were normalized to 100% cell ratios with $p< 0.0001$ and F-ratio 30.26 for mean values of HEK-CBG2 group and 31.82 for mean values of HEK-CBR2, calculated by ONE-way ANOVA.

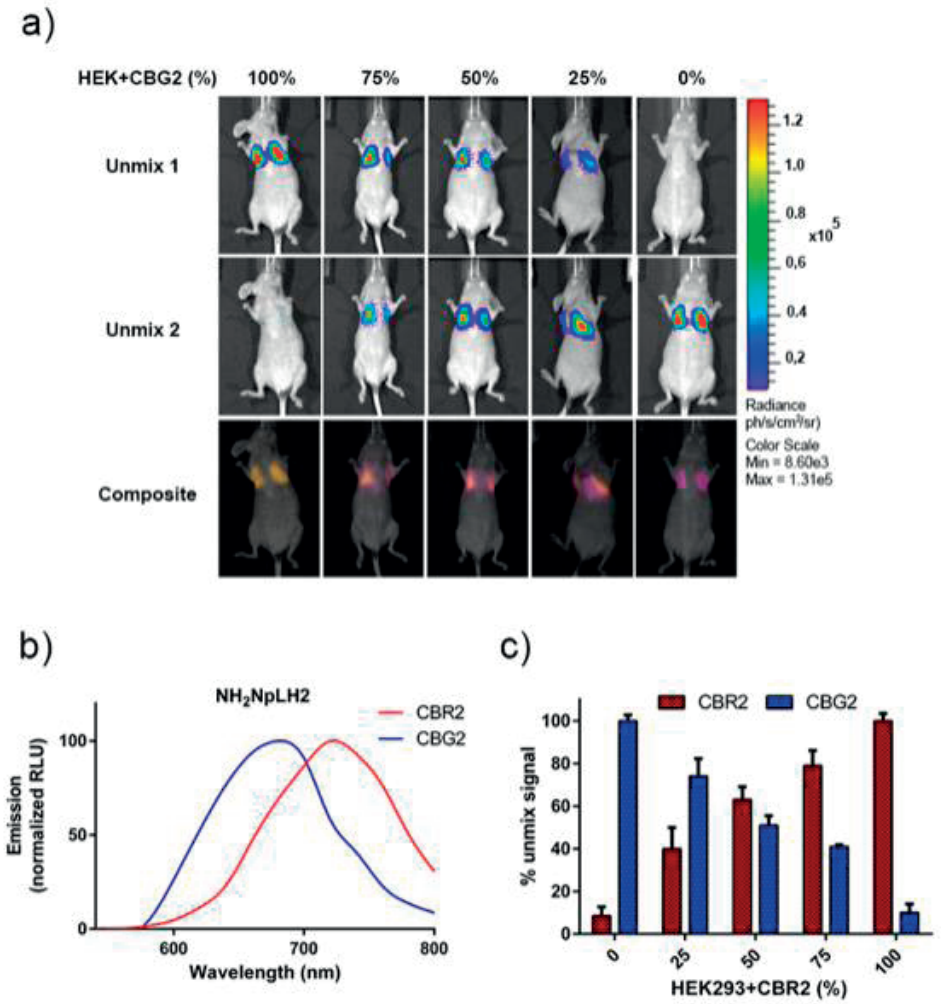

Figure 3. In vivo characterization of CBG2 and CBR2 mutants and spectral unmixing. (a) Representative unmixed bioluminescence images of CBG2 and CBR2 with NH_2-NpLH2 in deep tissue. Representative images of mice injected with different cell ratios of HEK-CBG2 and HEK-CBR2 with NH_2-NpLH2 in a lung model (n=3 samples). HEK-CBG2 or HEK-CBR2 cells were injected i.v. at the different proportions and NH_2-NpLH2 substrate was injected i.p. Images were acquired 15 min after substrate injection. Acquisition time for each filter was of 30 s. Band pass filters selected were between 540 nm and 800 nm. Filters selected for the green spectral unmixing is at 680 nm and for the red spectral unmixing is at 720 nm. Images were recorded 15 min after substrate injection considering the enzyme kinetics. Composite images indicate the linearity between the percentage of cells and the photons emitted. **(b)** Spectral proprieties HEK-CBG2 and HEK-CBR2 with NH_2-NpLH2. **(c)** Quantification of the photon fluxes of the different percentages of HEK-CBG2/NH_2-NpLH2 and HEK-CBR2/NH_2-NpLH2 ranged from 100% to 0% as shown in Figure 3a. Bioluminescent unmixed signals were normalized to 100% cell ratios (n=3 samples) with $p < 0.05$, F-ratio 4.064 for mean values of HEK-CBG2 group and 16.33 for mean values of HEK-CBR2, calculated by ONE-way ANOVA.

In vivo characterization of CBG2 and CBR2 mutants and spectral unmixing

To validate the potentiality of the dual-color BLI system in deep tissue, we first injected HEK-CBG2 or HEK-CBR2 to build a guided library for pure green or red signals. Images were captured using an IVIS imager with 15 band pass filters ranging from 540 to 800 nm. Pure HEK-CBG2 and HEK-CBR2 or a mixture of the two cell types was injected following the schema: 100–0%; 75–25%; 50–50% of green–red and then the same for red-green. NH_2-NpLH2 substrate was injected intraperitoneally and photons flux was recorded 10 min after substrate injection. The spectral unmixing algorithm efficiently extracted green or red contributions at the different percentages (Figure 3a). Notably, unmixing was also successful when 25% of the total population of the unmixed green was injected. Quantitative analysis for the unmixed green and red photon flux for each percentage (0% -25% -50% -75% -100%) was performed using Living Image software. Figure 3b-c reveals a linear correlation between the percentage of cells injected and photons recorded for both HEK-CBG2 and HEK-CBR2.

Versatility of CBG2 luciferase combined with AkaBLI system for dual color imaging.

We further explored whether CBG2/NH_2-NpLH2 could be combined with Akaluc/Akalumine-HCl (Iwano et al., 2018) for dual-color BLI. We selected two filters: 700 nm for CBG2/NH_2-NpLH2 and 660 nm for Akaluc/Akalumine-HCl. Akaluc yielded the brightest photon emission with Akalumine-HCl (~20-fold higher than CBG2/Akalumine-HCl, Figure 4a). When the filter was set at 700 nm, CBG2/NH_2-NpLH2 was ~40-fold higher than Akaluc/NH_2-NpLH2. Interestingly, the pairings CBG2/Akalumine-HCl and Akaluc/NH_2-NpLH2 both recorded a dim signal, suggesting low enzyme activity for these combinations (Figure 4a). Thus, for dual-color BLI application the use of a single substrate where the enzymes have comparable expression was not feasible. Spectral curves and respective photon fluxes are depicted in Figure 4b. Next, we investigated whether a mixture of CBG2 or Akaluc cells could be measured using Akalumine-HCl and NH_2-NpLH2 for dual-color BLI. First, the original spectrum libraries were efficiently built with 100% CBG2-cells or 100% Akaluc-cells using Living Image software (Perkin Elmer). Each luciferase contribution was effectively separated and quantified Figure 4c (left). Separation could be achieved when the luciferase contributions were equal (50% HEK-CBG2 and 50% HEK-Akaluc). The spectral curves and quantification of luminescence signals at different cell ratios are depicted in Figure 4c (right).

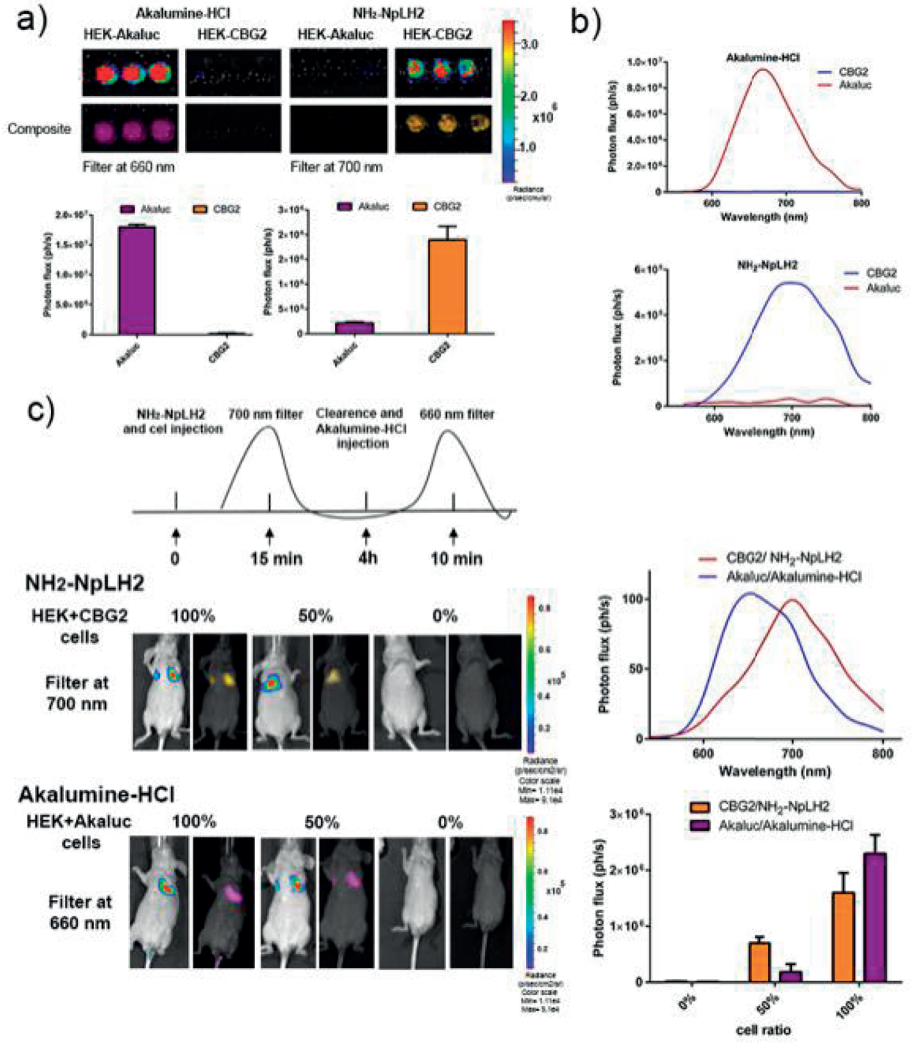

Figure 4. Versatility of CBG2 luciferase combined with AkaBLI system for dual color imaging. (a) Representative live cell images of HEK-cells expressing Akaluc and CBG2 and tested with Akalumine-HCl and NH_2-NpLH2. Filters for the spectral unmixing were set at 660 nm for Akaluc/Akalumine-HCl and at 700 nm for CBG2/NH_2-NpLH2. Plots indicate photon fluxes for in vivo measurements. **(b)** Spectral properties of HEK-Akaluc and HEK-CBG2 treated with Akalumine-HCl and NH_2-NpLH2 (0.1 mM). **(c)** Representative spectral unmixing in vivo (n=3 samples) for 100%, 50% or 0% of HEK-CBG2 or HEK-Akaluc with Akalumine-HCl or NH_2-NpLH2. Cells were injected intravenously and substrates were injected intraperitoneally. Images were acquired first 15 min after NH_2-NpLH2 injection. Then, when pre-scan confirmed the clearance of NH_2-NpLH2, Akalumine-HCl was injected and images acquired 5 min after substrate injection. Guided libraries were generated to identify each signal by Living image software (Perkin Elmer). Normalized spectra generated confirmed the feasibility to separate CBG2 and Akaluc signals in vivo by selecting filters at 660 nm for Akaluc/Akalumine-HCl and 700 nm for CBG2/NH_2-NpLH2. Acquisition time for each filter was 30 s. Quantification of the photon flux at the different cell percentages (100%-50%-0%) for HEK-CBG2 or HEK-Akaluc with NH_2-NpLH2 and for HEK-CBG2 or HEK-Akaluc with Akalumine-HCl are plotted (right-bottom), $p<0.05$, N=3 samples.

DISCUSSION

We report here on a novel dual NIR click beetle luciferase system that can record semi-quantitative data from deep-tissue and whole-body imaging by reducing light attenuation caused by hemoglobin, melanin and water. Importantly, the administration of NH_2-NpLH2 as single substrate provides high sensitivity, reduces the number of animals required and minimizes animal discomfort during the study (Cool et al., 2013). In comparison to previously published method (Stowe et al., 2019) the brightness of our system allowed for a substantial reduction in imaging time to 6 min or less (acquisition time per filter of 30 s instead of 120 s). Similar to previous reports using green luciferases, we observed some attenuation of CBG2 light emission due to the partial absorbance of the emitted green photons and a shift of the spectral peak to ~680–700 nm in deep tissue (Rumyantsev et al., 2016). However, the spectra of CBG2 and CBR2 maintained adequate spectral separation in the lungs which allowed us to distinguish each luciferase contribution.

We also compared the versatility of the new CBG2/NH_2-NpLH2 system with the recently developed AKA-BLI system (650 nm) (Iwano et al., 2018). This method can be exploited for multiplexed bioluminescence applications where Akaluc/Akalumine-HCl and CBG2/NH_2-NpLH2 can give distinct signals. Indeed, this setup will effectively probe more than one cellular process, each producing specific BL signals upon sequential administration of each substrate in vivo. However, this multiplex application will be less specific with CBR2/NH_2-NpLH2 (730 nm) due to the bioluminescence recorded when Akalumine-HCl is used (Hall et al., 2018; Zambito et al., 2020). Another limitation is that sequential substrate administration requires longer imaging sessions (Kleinovink et al., 2019; Yeh et al., 2019). Indeed, injection of two substrates requires the clearance of the first substrate but provides maximal light emission for each luciferase thereby reducing spectral interference from each luciferase. Finally, we envision a highly sensitive triple color BLI application with CBG2/CBR2 with NH_2-NpLH2 (680 nm and 720 nm respectively) coupled with the novel optimized NanoLuc/hydrofurimazine (460 nm) in the same animal model. (Su et al., 2020). This system (i.e., tri-plex BLI) could be used to visualize localization, activation, and functional state of immune cells. In conclusion, a novel dual-color BLI in the NIR window can be accessed using CBG2 and CBR2 cells treated with a single substrate, NH_2-NpLH2. This represents a promising approach for simultaneous visualization and quantification of two cell populations in deep tissue and in the same animal model. Collectively, this work will contribute to expand the toolset for in vivo multicolor bioluminescence imaging.

LIMITATIONS OF THE STUDY

The size and the photon flux of the signal area in deep tissue represent a potential limitation in the ability to efficiently separate and quantify the contribution of each luciferase. Although we demonstrated feasibility for lung imaging, we expect the method to be more accurate for dual color imaging of small areas (e.g., lymph nodes and depots of injected cells in deep organs) as demonstrated previously (Branchini et al., 2007). The kinetics of light emission after i.p. administration of NH_2-NpLH2 is slow (BL signals peaking at ~20 min), so repeated administration of substrate and imaging must be delayed by approximately 3 h. When CBG2/NH_2-NpLH2 and Akaluc/Akalumine-HCl are used for multiplex imaging, sequential administration of the two substrates is needed. This may require longer imaging sessions depending on substrate properties as solubility, enzyme affinity, different bio-distribution and serum stability (Yeh et al., 2019).

RESOURCE AVAILABILITY

Lead Contact

Further information and requests should be directed to the Lead Contact, Dr. Laura Mezzanotte (l.mezzanotte@erasmusmc.nl)

Materials Availability. Materials are available from the corresponding author on request.

Data and Code Availability. This study did not generate computer code. All data and analytical methods are available in the main text or in Supplemental Information.

Acknowledgments. We acknowledge the funding for this work provided by the European Commission under the H2020-MSCA-RISE award grant number 777682 (CANCER) and under the H2020-MSCA-ITN award, grant number 675743 (ISPIC).

Author contributions. Conceived and performed experiments G.Z. and M.P.H., F.S.; Writing original draft, G.Z. and M.P.H.; Review & editing, N.G., M.P.H., T.K., L.P.E., C.L., L.M.; Provided expertise and feedback Y.R., L.M., M.P.H., F.S., M.W.; Funding Acquisition L.M. and C.L.; Supervision L.M.

Declaration of Interests. Authors have no financial interests/commercial Conflict of Interest.

REFERENCES

Kaskova, Z.M., Tsarkova, A.S., Yampolsky, I.V. (2016). 1001 lights: luciferins, luciferases, their mechanisms of and applications in chemical analysis, biology and medicine. Chem Soc Rev. 45(21):6048-6077

Mezzanotte, L., van 't Root, M., Karatas, H., Goun, E.A., Löwik, C. (2017). In Vivo Molecular Bioluminescence Imaging: New Tools and Applications. Trends in Biotechnology 35(7):640-652

Wilson, T., Hastings, J.W. BIOLUMINESCENCE. (1998). Annu Rev Cell Dev Biol. 14(1):197-230.

Jathoul, A.P., Grounds, H., Anderson, J.C., Pule, MA. (2014). A dual-color far-red to near-infrared firefly luciferin analogue designed for multiparametric bioluminescence imaging. Angew Chem Int Ed Engl. 53(48):13059—13063.

Smith, A. M., Mancini, M. C., Nie, S. (2009). Bioimaging: second window for in vivo imaging. *Nat. Nanotechnol.* **4**, 710–711.

Branchini, B.R., Southworth, T.L., Fontaine, D.M., Kohrt, D., Florentine, C.M., Grossel, M.J. (2010). Red-emitting luciferases for bioluminescence reporter and imaging applications. Anal Biochem. 396(2):290-297.

Iwano, S., Sugiyama, M., Hama, H., Watakabe, A., Hasegawa, N., Kuchimaru, T., Tanaka, K.Z., Takahashi, M., Ishida, Y., Hata, J., Shimozono, S., Namiki, K., Fukano, T., Kiyama, M., Okano, H., Kizaka-Kondoh, S., McHugh, T.J., Yamamori, T., Hioki, H., Maki, S., Miyawaki, A. (2018). A Single-cell bioluminescence imaging of deep tissue in freely moving animals. Science 359(6378):935 LP - 939.

Maguire, C.A., Bovenberg, M.S., Crommentuijn, M.H., Niers, J.M., Kerami, M., Teng, J., Sena-Esteves, M., Badr, C.E., Tannous, B.A. (2013). Triple bioluminescence imaging for in vivo monitoring of cellular processes. Mol Ther Nucleic Acids 2(6):e99.

Taylor, A., Sharkey, J., Plagge, A., Wilm, B. & Murray, P. (2018). Multicolour In Vivo Bioluminescence Imaging Using a NanoLuc-Based BRET Reporter in Combination with Firefly Luciferase. *Contrast Media Mol. Imaging* 2514796.

Mezzanotte, L., Que, I., Kaijzel, E., Branchini, B., Roda, A., Löwik, C. (2011) Sensitive dual color in vivo bioluminescence imaging using a new red codon optimized firefly luciferase and a green click beetle luciferase. PLoS One 6(4).

Branchini, B.R., Ablamsky, D.M., Murtiashaw, M.H., Uzasci, L., Fraga, H., Southworth, T.L. (2007). Thermostable red and green light-producing firefly luciferase mutants for bioluminescent reporter applications. Anal Biochem. 361, 2.

Stowe, C.L., Burley, T.A., Allan, H., Vinci, M., Kramer-Marek, G., Ciobota, D.M., Parkinson, G.N., Southworth, T.L., Agliardi, G., Hotblack, A., Lythgoe, M.F., Branchini, B.R., Kalber, T.L., Anderson JC, Pule MA. (2019). Near-infrared dual bioluminescence imaging in mouse models of cancer using infraluciferin. eds. Elife. 8:e45801.

Aswendt, M., Voge,l S., Schäfer, C., Jathoul ,A., Pule, M., Hoehn, M. (2019). Quantitative in vivo dual-color bioluminescence imaging in the mouse brain. Neurophotonics. 6(2):1-11.

Gammon, S. T., Leevy, W. M., Gross, S., Gokel, G. W. & Piwnica-Worms, D. (2006). Spectral unmixing of multicolored bioluminescence emitted from heterogeneous biological sources. *Anal. Chem.* 78, 1520–1527.

Hall, M. P., Woodroofe, C.C., Wood M.G., Que I., van't Root, M., Ridwan, Y., Shi, C., Kirkland, T.A., Encell, L.P., Wood, K.V., Löwik C., Mezzanotte, L. (2018) Click beetle luciferase mutant and near infrared naphthyl-luciferins for improved bioluminescence imaging. Nat Commun. 9(1):132.

Xu, T., Close, D., Handagama, W., Marr, E., Sayler, G., Ripp, S. (2016). The Expanding Toolbox of In Vivo Bioluminescent Imaging. Front Oncol. 6:150.

Miloud, T., Henrich, C. & Hammerling, G. J. (2007). Quantitative comparison of click beetle and firefly luciferases for in vivo bioluminescence imaging. *J. Biomed. Opt.* 12, 1–5.

Viviani, V.R, Simões, A., Bevilaqua, V.R., Gabriel, G.V.M., Arnoldi, F.G.C., Hirano, T. (2016) Glu311 and Arg337 Stabilize a Closed Active-site Conformation and Provide a Critical Catalytic Base and Countercation for Green Bioluminescence in Beetle Luciferases. Biochemistry 55(34):4764-4776.

Woodroofe, C.C., Shultz, J.W., Wood, M.G., Osterman, J., Cali, J.J, Daily, W.J., Meisenheimer, P.L., Klaubert, D.H. (2008). N-Alkylated 6′-aminoluciferins are bioluminescent substrates for Ultra-Glo and QuantiLum luciferase: new potential scaffolds for bioluminescent assays. Biochemistry 47, 10383–10393.

Cool, S. K., Breyne, K., Meyer, E., De Smedt, S. C. & Sanders, N. N. (2013) Comparison of In Vivo Optical Systems for Bioluminescence and Fluorescence Imaging. *J. Fluoresc.* 23, 909–920.

Rumyantsev, K. A., Turoverov, K. K., Verkhusha, V.V.(2016). Near-infrared bioluminescent proteins for two-color multimodal imaging. Scientific Reports 6, 36588.

Zambito, G., Natasa, G., Ridwan, Y., Hall M.P., Shi, C., Kirkland, T.A., Encell, L. P., Löwik, C., Mezzanotte, L. (2020). Evaluating brightness and spectral properties of click beetle and firefly luciferases using luciferin analogues: identification of preferred pairings of luciferase and substrate for in vivo bioluminescence imaging. Molecular Imaging and Biology volume 22, 1523–1531.

Kleinovink, J.W., Mezzanotte, L., Zambito, G., Fransen, M.F., Cruz, L.J., Verbeek, J.S., Chan, A., Ossendorp, F., Löwik, C. (2019). A Dual-Color Bioluminescence Reporter Mouse for Simultaneous in vivo Imaging of T Cell Localization and Function. Front Immunol. 9:3097.

Yeh, H-W., Wu, T., Chen, M., Ai, H-W. (2019). Identification of Factors Complicating Bioluminescence Imaging. Biochemistry 58(12):1689-1697.

Su, Y., Walker, J.R., Park, Y., Smith, T.P., Liu, L.X., Hall, M.P., Labanieh, L., Hurst, R., Wang, D.C., Encell, L.P., Kim, N., Zhang, F., Kay, M.A., Casey, K.M., Majzner, R.G., Cochran, J.R., Mackall, C.L., Kirkland, T.A., Lin, M.Z. (2020) Novel NanoLuc substrates enable bright two-population bioluminescence imaging in animals. Nature Methods 17(8):852-860.

Supplemental figures

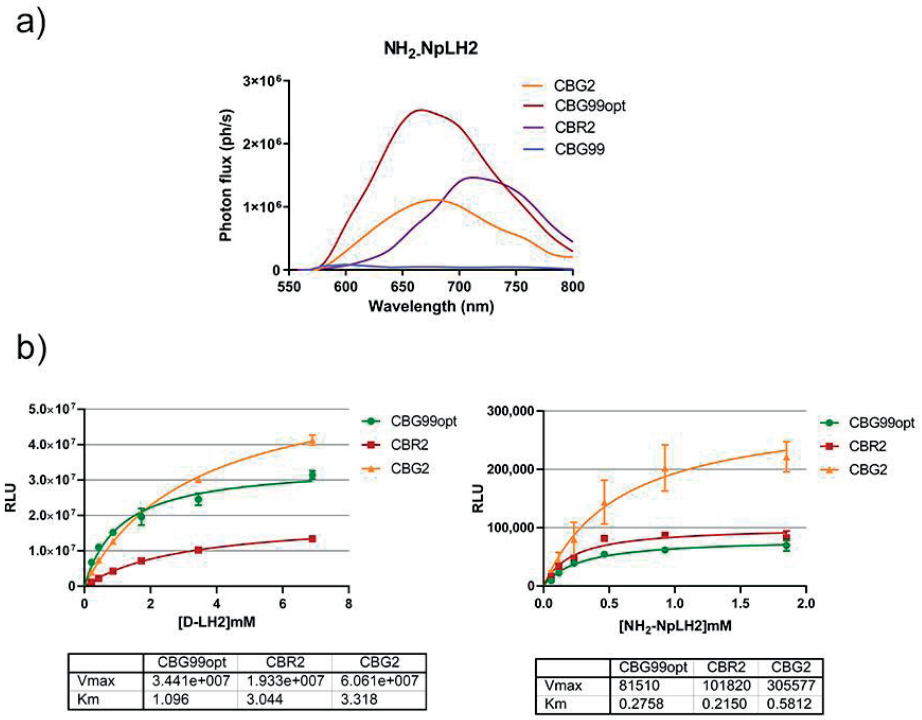

	CBG99opt	CBR2	CBG2
Vmax	3.441e+007	1.933e+007	6.061e+007
Km	1.096	3.044	3.318

	CBG99opt	CBR2	CBG2
Vmax	81510	101820	305577
Km	0.2758	0.2150	0.5812

Figure S1. In vitro characterization of click beetle luciferase variants, related to Figure 1. (a) Live HEK293T cell lines were transfected with plasmids expressing CBR2, CBG2, CBG99 or CBG99opt luciferase genes. Photon fluxes were quantified after treatment with NH2-NpLH2 substrate (1mM) by the IVIS imager. Spectral curves were built by Living image software 4.5 (Perkin Elmer). (b) Vmax and Km parameters of the CBG99opt, CBG2 and CBR2 enzymes with titrated DLH2 or NH2-NpLH2. Km and RLU-max values were calculated using GraphPad Prism (Michaelis–Menten regression).

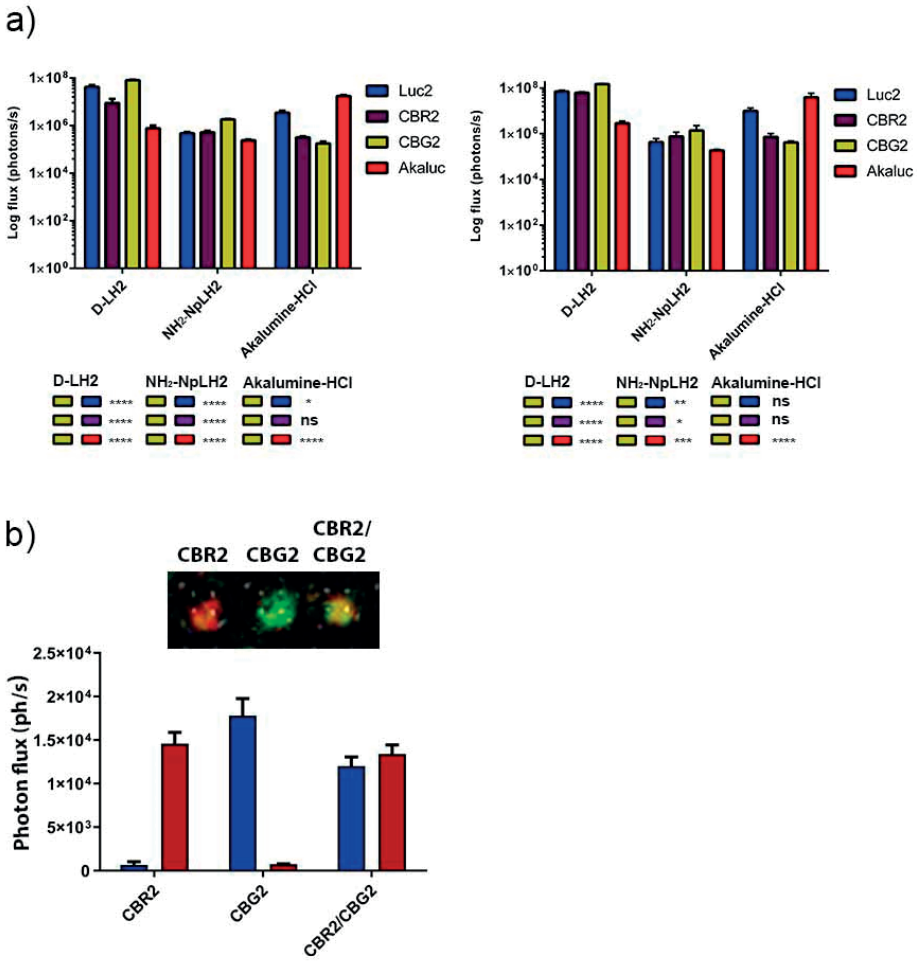

Figure S2. In vitro measurements of the photon fluxes and two-population luciferase brightness test. Related to Figure 2. (a) Live HEK293T cells stably expressing Luc2, CBR2, CBG2 and Akaluc luciferases, were tested for their brightness after addition of 0.1 mM (left panel) and 1 mM (right panel) of D-LH2 or analogues. Quantifications were performed 10 min after substrate addition. BL signals were compared to the brightness of CBG2 and statistical analysis was performed by One-way ANOVA, p<000.1. Experiment was performed in triplicate (n=3 samples). Error bars represent ±SD. b) In vitro two-population dual-color imaging of transfected HEK293T cells expressing CBR2 or/and CBG2 and respective quantification of the unmixed photon fluxes by spectral unmixing algorithm (n=3 samples).

5

Near-infrared bioluminescence imaging of two cell populations in living mice

Giorgia Zambito [1,2,3], Laura Mezzanotte [1,2,4,*]

[1] Erasmus Medical Center, Dept. of Radiology and Nuclear Medicine, Rotterdam, 3015 CE, The Netherlands
[2] Erasmus Medical Center, Dept. of Molecular Genetics, Rotterdam, 3015CE, The Netherlands
[3] Technical contact
[4] Lead contact
*Correspondence: l.mezzanotte@eramsusmc.nl

Manuscript accepted in STAR protocols, Cell Press

SUMMARY

Multicolor bioluminescence imaging using near-infrared emitting luciferases is an attractive application to detect two cell populations within one animal model. Herein, we describe how to distinguish dual color bioluminescent signals co-localized in the same compartment. We tested CBG2 click beetle (λ=660 nm) and CBR2 click beetle (λ=730 nm) luciferases paired with NH_2-NpLH2 luciferin. Following spectral unmixing algorithm, single spectral contributions can be resolved and quantified enabling the visualization of multiple cell types in deep-tissue by injection of a single substrate.

For complete details on the use and execution of this protocol, please refer to Zambito G. et al. (2020).

GRAPHICAL ABSTRACT

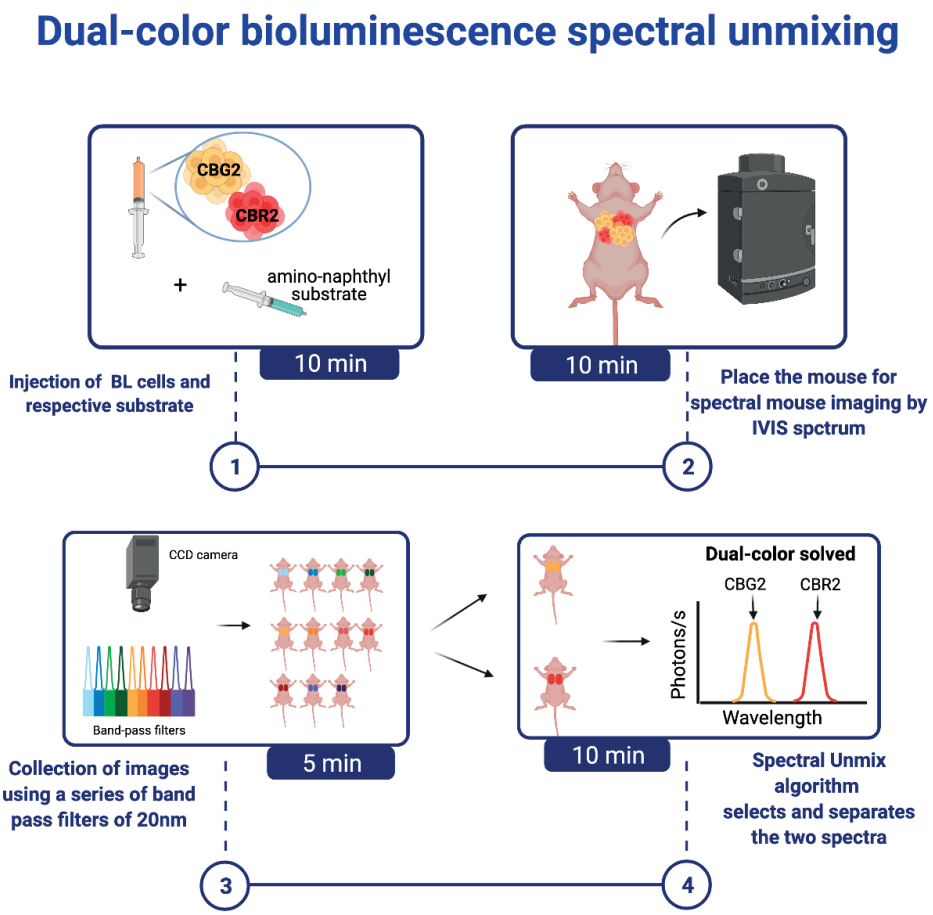

BEFORE YOU BEGIN

Experimental design considerations

Luciferase reporter genes provide a well-studied application for bioluminescence imaging of various biological molecular events both *in vitro* and *in vivo*. The production of bioluminescence (BL) light relies on the luciferase enzyme that catalyzes the oxidation of a luciferin substrate. Besides the traditional Fluc firefly luciferase reporter gene, new mutant red-shifted luciferases derived from fireflies or click beetles have been designed and developed recently (Zambito G. et al., 2021). Indeed, the signal attenuation due to absorption and scattering by tissues is reduced when red or near-infra-red luciferases are employed. Thus, the use of luciferases emitting in the so called “bio-optical window”

(λ= 600 nm to 800 nm) is highly desirable to improve imaging sensitivity (Mezzanotte et al., 2013 and Aswendt et al., 2019).

For multicolor BLI *in vivo*, the selection of luciferase pairs becomes crucial. Moreover, the administration of multiple substrates will require longer imaging sessions and challenging interpretation of data. The application of a single substrate that has affinity with multiple luciferases might be ideal (Stowe C. et al., 2019). The use of a cooled charged-coupled device (CCD) camera to acquire light emission and an adequate software to quantify light outputs is necessary to perform multicolor near-infrared BLI as described in this protocol.

Herein, we generated HEK-293T cells expressing equimolar amount of either CBG2 or CBR2 luciferase following the standard protocol for lentiviral transduction described in Knol-Blankevoort V.T. et al. 2016. HEK-CBG2 and HEK-CBR2 cells were tested with NH_2-NpLH2 substrate as D-luciferin analog (Figure 1) (Hall M.P. et al., 2018). *In vitro* evaluations were performed to confirm efficiency of transduction and to calculate the expression rate of luciferase reporter genes (Zambito G. et al., 2021). For *in vivo* evaluations, HEK-CBG2 and HEK-CBR2 were injected intravenously and NH_2-NpLH2 luciferin was injected intraperitoneally.

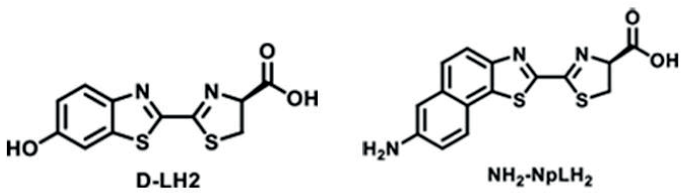

Figure 1 Chemical structures of D-LH$_2$ luciferin and its analog NH$_2$-NpLH2.

Colocalized bioluminescent light outputs from HEK-CBG2 and HEK-CBR2 are detected in the lungs. Separation of the two different spectra of emission and quantification of photon fluxes were performed by spectral unmixing algorithm tool, part of the Living Image software of the IVIS imaging Spectrum system (Perkin Elmer).

Key Resources Table

REAGENT or RESOURCE	SOURCE	IDENTIFIER
Bacterial and virus strains		
Lentivirus carrying EF1-CBR2opt-T2A-copGFP	Addgene	Plasmid #108713
Lentivirus carrying EF1-CBG2-T2A-copGFP	Mezzanotte lab	N/A
Chemicals, peptides, and recombinant proteins		
NH_2-NpLH2 substrate	Promega/ Synthesis reported in [5].	N/A
Isoflurane Isoflutek 1000 mg/g	Laboratorios Karizoo	710004
Dulbecco's Phosphate Buffered Saline (1X), (DPBS)	Lonza Bioscience	BE17-513F
Dulbecco's modified Eagle's medium (DMEM)	Gibco	11880028
Experimental models: cell lines		
293T (HEK) cell line	ATCC	ATCC® CRL-3216™
Experimental models: organisms/strains		
Nude Mouse: Balb/C Wild Type	Charles River Laboratory (The Netherlands)	CAnN.Cg-*Foxn1*^{nu}/Crl
Software and algorithms		
Living Image software 4.5 and above	PerkinElmer	Part # 128113
Graphpad prism 7 software	Graphpad	N/A
Other		
IVIS Spectrum Imager	PerkinElmer	124262
BC Insuline 1 ml U-100 29G, 0.33mmx12.7mm 10x 10st, syringe, single use	BD Biosciences	Cat# 309623
Corning® 96 Well Black Polystyrene Microplate	Greiner Bio-one	CLS3601-100EA
T75 EasYFlask, TC Surface, Solid Cap, Pack of 5	ThermoFisher Scientific	156472

Materials and equipment

HEK-CBG2 and HEK-CBR2 have been cultured in complete DMEM medium, stored at 4 °C for up 1 month.

Reagents	Final concentration (%)	Amount
Dulbecco's modified Eagle's medium (DMEM), stored at 4 °C	89 %	445 ml
FBS	10 %	50 ml
Penicillin/streptomycin	1 %	5 ml
Total	100 %	500 ml

Step-by-step method details

In vitro spectral unmixing of two bioluminescent cell populations

Timing: 3 days

1. Plate mixtures of HEK-CBG2 and HEK-CBR2 cells in the following ratios: 100:0, 75:25, 50:50 for HEK-CBG2:HEKCBR2 and vice versa. Plate them in a 96-well black plate with

clear bottom at the density of 1 x 10^4 cells / 100 µl per well and incubated at 37 ℃ for 24 h. For statistical analysis, two triplicates should be considered.

2. The next day, prepare NH_2-NpLH2 substrate at final concentration of 2 mM in PBS.

   CRITICAL: Keep the NH_2-NpLH2 luciferin solution protected from light and store it at -20 ℃. If the color changes, discard and make fresh luciferin solution.

3. Prior to imaging the plate, replace DMEM culture media with PBS and resuspend the cells in 100 µl PBS per well. This will avoid interference by colored media while measuring the photon flux.
4. Add 10 µl NH_2-NpLH2 substrate (2 mM) to each well containing plated cells in 200 µl PBS. Final concentration of NH_2-NpLH2 substrate will be 0.1 mM.
   a. Start Imaging 10 min after substrate addition to collect the maximum number of photons.
5. Set up imaging settings at the IVIS spectrum system with open filter, 30 s exposure time, field of view (FOV) C, f/stop=1, medium binning.
6. Select bandpass filters ranged from 580 nm to 800 nm to measure the spectra of interest (starting from the lowest to the highest filter)
   a. With the guided spectral library tool, create specific libraries for pure HEK-CBG2 cells (100%) and HEK-CBR2 cells (100%).
   b. Use the relevant libraries of HEK-CBG2 cells (100%) and HEK-CBR2 cells (100%) and apply them to perform the spectral unmixing in wells where unknown HEK-CBG2: HEK-CBR2 cell mixtures are plated.
   c. The resolved HEK-CBG2 and HEK-CBR2 emission will appear as separated images where quantification is possible.

Note: A detailed guide on how to perform spectral unmixing is reported as technical note on Perkin Elmer website
(https://resources.perkinelmer.com/labsolutions/resources/docs/TCH_011047_01_Spectral_Unmixing.pdf)
Normalize the emission spectra so that the CBG2 and CBR2 emission peaks can be visualized.

7. For well plate image analysis, calculate light outputs for the HEK-CBG2 and HEK-CBR2 emission by drawing Region Of Interest (ROI) by Living image software 4.5 (Perkin Elmer). Place a ROI over the signal in each well and select “measure”. The software will record the BL outputs in photon flux (photons/sec).
8. Export, data outputs to Excel (Microsoft) sheet to measure the average amongst triplicates and relative standard deviations.

Note: the substrate is photo sensible and must be kept in the dark. We recommend receiving training on using the IVIS Spectrum.

In vivo Spectral unmixing of two-cell populations

Timing: 2 days

9. Culture separately HEK-CBG2 and HEK-CBR2 cells in a T75 flask (cell density ~ 1x 10^6/ml) and incubated at 37 ℃ for 24 h.
10. The next day, prepare NH_2-NpLH2 substrate solubilized in PBS at the final concentration of 44 mg ml^{-1} (4.4 mg NH_2-NpLH2 in 100 µl of PBS per 20 g mouse corresponds to a dose of 220 mg Kg^{-1}).

    CRITICAL: Keep NH2-NpLH2 luciferin solution protected from light and. If the color changes, discard and make fresh luciferin solution.

11. Prior *in vivo* imaging, wash HEK-CBG2 and HEK-CBR2 cells twice with DPBS and resuspend them in sterile DPBS.
    a. Prepare cell aliquots (final concentration 1x10^6 /100 µl sterile DPBS per mouse) for 100% HEK-CBG2, 100% HEK-CBR2 and for various ratios for HEK-CBG2: HEK-CBR2 and vice versa.
12. Set up imaging settings at the IVIS spectrum imager system with open filter, 30 s exposure time, field of view (FOV) C, f/stop=1, medium binning.
    a. Select bandpass filters ranged from 540 nm to 800 nm to measure the spectra of interest (starting from the lowest to the highest filter)
13. Register guided spectral libraries of 100% luciferase-HEK293T (Figure 2):
    a. Anesthetize BALB/C nude mice (females, aged 6-10 weeks) with 1.5-2.0 % isoflurane (flow rate 1 L/min O_2).
    b. Inject 100 µl 100% HEK-CBG2 or 100% HEK-CBR2 cells with intravenous injections (I.V.)
    c. Inject 220 mg Kg^{-1} of NH_2-NpLH2 substrate solubilized in DPBS intraperitoneally (I.P.)

Note: We recommend pre-loading one syringe per mouse. All mice must be injected with luciferin within a few seconds of each other. This also reduces differences in dosage and enhance the accuracy.

    d. Perform the spectral imaging 10 min post I.P. injection to measure the highest light output.

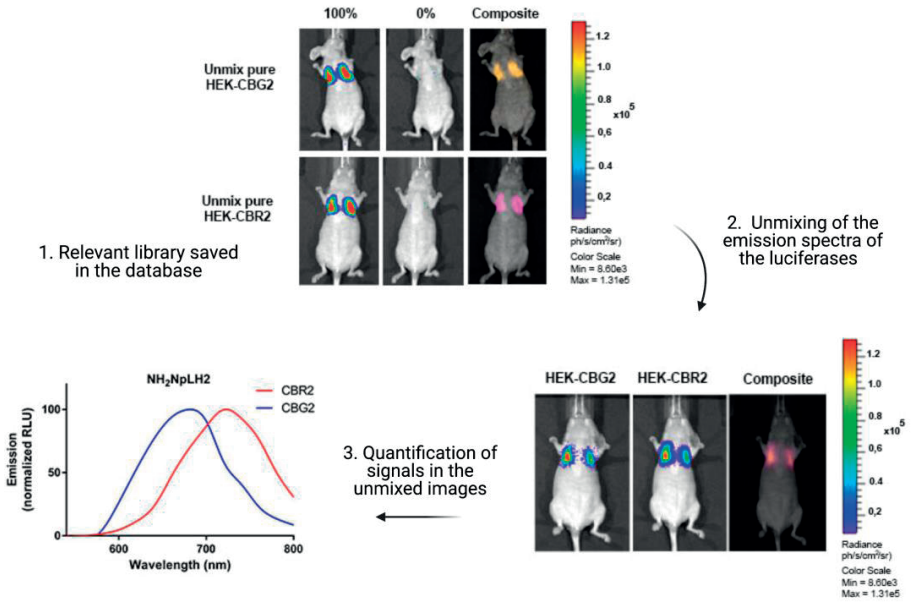

Figure 2. Schematic illustrating the spectral unmixing of co-localized bioluminescent signal *in vivo*.
1) Create and save the specific libraries for pure (100% cell ratio) for HEK-CBG2 and for HEK-CBR2 in the database. 2) Use the relevant libraries to unmix the emission outputs when HEK-CBG2 and HEK-CBR2 are co-injected I.V. in the same mouse. 3) Use the spectral unmix algorithm to separate and quantify the unmixed images. Normalized emission curves can be plotted highlighting the luciferase emission peaks.

e. With the guided spectral library tool (in the ROI menu), create specific libraries for pure *in vivo* signals for HEK-CBG2 injected (100%) and for HEK-CBR2 injected (100%) (Figure 3).

14. Spectral unmixing for unknown HEK-CBG2: HEK-CBR2 cell ratios:
    a. Anesthetize nude mice with 1.5-2.0 % isoflurane (flow rate 1 L/min O_2).
    b. Inject 100 µl HEK-CBG2: HEK-CBR2 and vice versa at different cell ratios with intravenous injections (I.V.)
    c. Perform the spectral imaging 10 min post I.P. injection to let the substrate stabilize and allow the measurement of highest light outputs.
    d. After imaging, the mice can be placed back into their respective cages. They should be awake within 30 second to 1 min.
    e. For spectral imaging, choose a band pass filter between 620-800 nm and select the relevant guided library registered for *in vivo* spectra of HEK-CBG2 cells (100%) or HEK-CBR2 cells (100%) on the ROI menu.

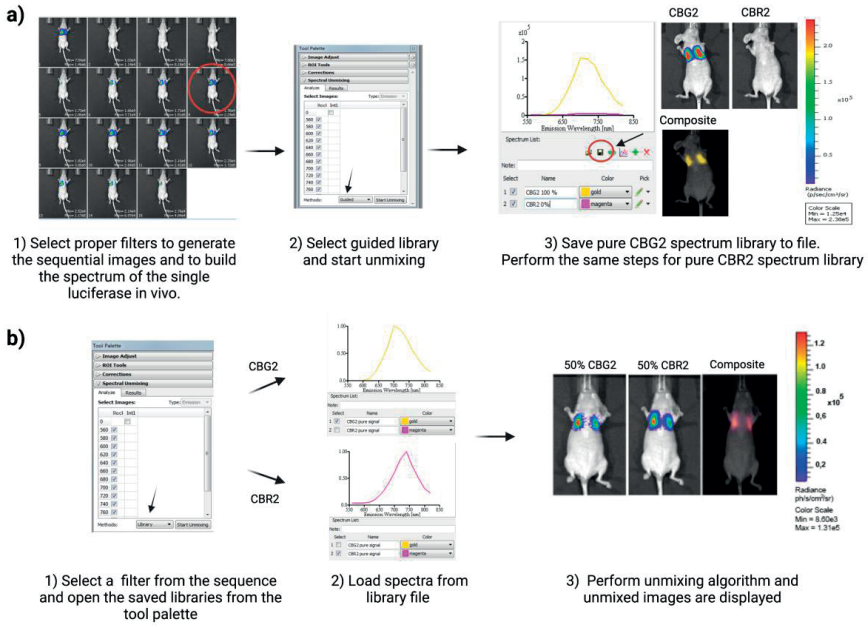

Figure 3. Step-by-step spectral unmixing.
a) Save the specific luciferase spectrum to create a pure (100% cell ratio) HEK-CBG2 or HEK-CBR2 library. **b)** Perform spectral unmixing by loading opportune pure libraries. The algorithm will be able to distinguish each luciferase contribution even if the two luciferases are colocalized in the same area. A detailed guide on spectral unmixing is reported as technical note on Perkin Elmer website.

f. Apply the relevant libraries to perform the spectral unmixing for unknown HEK-CBG2: HEK-CBR2 cell ratios and draw a mask where the cell mixtures are expected to be localized after I.V. injections
g. Proceed with spectral unmixing, the algorithm will separate HEK-CBG2 and HEK-CBR2 cell contributions
h. Two unmixed images will be built each containing the signature of only one of the luciferases of interest.

15. To calculate light outputs for the unmixed images, draw Region Of Interest (ROI) by Living image software 4.5 (Perkin Elmer). Place a ROI over the signal.
16. Export data outputs to Excel (Microsoft) to measure the average amongst triplicates and relative standard deviations. Graph the “total flux” column.
17. Perform the *in vivo* experiment with at least three mice

CRITICAL: Ear tags are necessary to distinguish mice during the luciferin injections.

Note: Up to five mice can be imaged and keep the stage heated to 37 ℃ during the *in vivo* imaging. Total imaging time acquisition is about 6 min.

We recommend receiving training on using the IVIS Spectrum as well as its accompanying isoflurane anesthesia machine.

Expected Outcomes

Simultaneous monitoring of bioluminescent cell populations in the same animal model has the great advantage to visualize cell behavior in their environment. Previously, we have attempted this method by developing CBG2 luciferase that could be used for dual-color BLI *in vivo* and in the lungs as deep tissue model. CBG2 can be paired with CBR2 and both have affinity for NH_2-NpLH2 substrate. HEK-293T cells expressing CBR2 or CBG2 luciferases, can be injected at various percentages *in vivo*. We recommend to use nude mice to enhance the measurement of photon flux *in vivo*.

Spectral unmixing algorithm enables sensitive quantification of bioluminescent signals. We utilized this method to specifically discriminate CBR2 and CBG2 bioluminescent emissions when co-localized in the same area which is the most challenging application. The two BL spectra can be accurately separated and the photon fluxes can be measured for each selected band-pass filter. This technique allows to reduce imaging time sessions and to refine the number of animal models required for the experimental test.

This technique could also be extended to perform *in vivo* multi-color BLI where another luciferase/luciferin system can be added to our proposed protocol for CBG2 and CBR2 with NH_2-NpLH2 substrate. We advise to select an orthogonal system like Nanoluc marine luciferase that has specific affinity for coelenterazine-like substrates but not for D-luciferin-like substrates. This will ensure an enhanced spectral separation for each luciferase used.

However, when the same animal is imaged with two different D-luciferin analogs, selected luciferase enzymes must have low detectable light outputs for one of the substrates employed. This will guarantee a successful spectral unmixing. Indeed, substrates must preserve the color modulation and must prevent color-shift greater than 40 nm *in vivo*. Imaging sessions with two different D-luciferin analogs must be performed at least after 4 h from the first imaging session to allow full clearance of the substrate.

Although we have attempted the spectral unmixing for lung imaging model, we expect the method to be accurate for dual-color imaging of smaller areas (e.g., lymph nodes and cell depots cells in deep organs like brain).

Quantification and Statistical Analysis

In vitro and *in vivo* tests were performed using Graphpad 7 software for ONE-way ANOVA followed by a post-test for column analysis. Results reported as mean ± SD and significance attributed when $p < 0.001$ (*) for *in vitro* experiments or $p < 0.05$ (*) for *in vivo* experiments.

Limitations

It has been noted that a signal limit for spectral unmixing does not exist. However, for accurate quantification we recommend more than 600 counts for all signals in the area to unmix. If the signals are less than 600 counts, background noise will affect the reliability of the quantification. To delineate precise luciferase spectral curve and relative peak of emission, we advise to register also marginal band-pass filters.

Troubleshooting

Problem 1:

The spectral library built *in vitro* has a different spectral peak compared to the spectral library built *in vivo* (In vivo spectral unmixing of two-cell populations, step 14).

Potential solution:

Spectral emission *in vitro* can differ from the spectral emission *in vivo*. This is because tissue components and deep-tissue imaging can alter the detection of photons registered for each band-pass filter. Indeed, we observed a partial shift of the spectral peak for CBG2 luciferase (from 650 to ~ 680–700 nm) due to the partially absorbed green photons when imaging in depth. Please build your spectral library for *in vitro* and *in vivo* separately.

Problem 2:

Spectral library can be built *in vitro* but not *in vivo* (In vivo spectral unmixing of two-cell populations, step 13e)

Potential solution:

Luciferases selected for the dual-color system must have comparable photon yield *in vivo*. It is essential to register first the guided library of pure luciferases *in vivo*. In general, bright and red-shifted luciferases are the best choice for deep tissue imaging. If the spectral emissions are completely overlapping, the spectral unmixing tool will not be able to discriminate each luciferase signature.

Problem 3:

Signal background occurs *in vivo* after NH_2-NpLH2 substrate I.P. injection (In vivo Spectral unmixing of two-cell populations, step 13 d).

Potential solution:

We observed low background derived from NH_2-NpLH2 substrate after I.P. injection in the liver. If this is the case and you need to unmix signal in the liver quantify the background first. If your signals are 10 or 100 times higher than background emission then it can be considered negligible and it will not affect your quantification after unmixing.

Problem 4:

Multiple *in vivo* administration of NH_2-NpLH2 substrate (In vivo Spectral unmixing of two-cell populations, step 13 c).

Potential solution:

NH_2-NpLH2 substrate is not toxic and multiple injections in the same day are possible. Prior imaging, mice should be first checked for BL background and for complete substrate clearance. However, we do not recommend repeated isoflurane anesthesia in a short frame time because this might be toxic and mouse discomfort should be prevented.

Problem 5:

Mice preparation for *in vivo* imaging (In vivo Spectral unmixing of two-cell populations, step 13 a)

Potential solution:

Animal hair can highly affect optical imaging by blocking, absorbing, and scattering the light. The near-infrared spectrum reduces this phenomenon but typically shows minimal scattering and absorbance of light. We recommend removing the fur around the area that needs to be imaged and continuing this practice throughout the study.

Nude mice have the advantage that does not require depilation and they are preferred for optical imaging techniques.

Resource availability

Lead Contact

Further information and requests for resources and reagents should be directed to and will be fulfilled by the lead contact, Laura Mezzanotte, Dr.
l.mezzanotte@erasmusmc.nl

Materials Availability

Lentiviral construct for generation of lentivirus carrying EF1-CBG2-T2A-copGFP or EF1-CBR2-T2A-copGFP are available from the lab upon request. NH_2-NpLH2 substrate is available on request from Promega Corporation.

Data and Code Availability

The protocol does not include all datasets generated or analyzed during this study.

Acknowledgments

We acknowledge the funding for this work provided by the European Commission under the H2020-MSCA-RISE award grant number 777682 (CANCER). The graphical abstract and figures were partially created with BioRender.com.

Author contributions

Conceived protocols and experiments G.Z.; Writing original draft, G.Z.; Review & editing, L.M.; Provided expertise and feedback L.M.; Funding Acquisition L.M.; Supervision L.M.

Declaration of interests

The authors declare no competing interests

References

Zambito, G., Chawda, C., Mezzanotte, L., (2021). Emerging tools in bioluminescence imaging. Curr Opin Chem Biol. 23, 86-94.

Mezzanotte, L., Aswendt, M., Tennstaedt, A., Hoeben, R., Hoehn, M., Löwik, C. (2013) Evaluating reporter genes of different luciferases for optimized in vivo bioluminescence imaging of transplanted neural stem cells in the brain. Contrast Media Mol. Imaging 8, 505–513.

Aswendt, M., Vogel, S., Schäfer, C., Jathoul, A., Pule, M., Hoehn, M. (2019) Quantitative in vivo dual-color bioluminescence imaging in the mouse brain. Neurophotonics 6, 1–11.

Stowe, C. L., Burley, T. A., Allan, H., Vinci, M., Kramer-Marek, G., Ciobota, D.M., Parkinson, G.N., Southworth, T. L., Agliardi, G., Hotblack, A., et al. (2019) Near-infrared dual bioluminescence imaging in mouse models of cancer using infraluciferin. Elife 8, e45801.

Knol-Blankevoort, V.T., Mezzanotte, L., Rabelink, M.J., Löwik, C.W., Kaijzel, E.L. (2016) Development of a Multicolor Bioluminescence Imaging Platform to Simultaneously Investigate Transcription Factor NF-κB Signaling and Apoptosis. Methods Mol Biol. 1461:255-70.

Hall, M. P., Woodroofe, C.C., Wood, M.G., Que, I., van't Root, M., Ridwan, Y., Shi, C., Kirkland, T. A., Encell, L. P., Wood, et al. (2018) Click beetle luciferase mutant and near infrared naphthyl-luciferins for improved bioluminescence imaging. Nat. Commun. 9, 132.

Zambito, G., Hall, M.P., Wood, M.G., Gaspar, N., Ridwan, Y., Stellari, F.F., Shi, C., Kirkland, T.A., Encell, L.P., Löwik, C., Mezzanotte, L. (2020) Red-shifted click beetle luciferase mutant expands the multicolor bioluminescent palette for deep tissue imaging. iScience 24, 101986.

6

Fluorinated PLGA-PEG-mannose nanoparticles for tumor-associated macrophage detection by optical imaging and MRI

Giorgia Zambito[1,2,3 †], Siyuan Deng [4†], Joost Haeck[5], Natasa Gaspar[1,2,6], Roberta Censi[4], Clemens Löwik[1,2], Piera Di Martino[4 *], Laura Mezzanotte [1,2*]

[1] Erasmus Medical Center, Dept. of Radiology and Nuclear Medicine, Rotterdam, 3015 CE, The Netherlands
[2] Erasmus Medical Center, Dept. of Molecular Genetics, Rotterdam, 3015CE, The Netherlands
[3] Medres medical research GmBH, Cologne, 50931, Germany
[4] School of Pharmacy, University of Camerino, 62032, Camerino, Italy
[5] AMIE core facility, Erasmus Medical Center, Rotterdam 3015CE, The Netherlands
[6] Percuros B.V., Leiden, 1333CL, The Netherlands
[†] These authors have contributed equally to this work and share first authorship
***Correspondence:** Laura Mezzanotte, PhD l.mezzanotte@erasmusmc.nl and Piera di Martino, PhD piera.dimartino@unicam.it
Paper submitted in Frontiers, Small Animal Imaging: Technological and Methodological Advances to Improve the Translational Power

ABSTRACT

Tumor-associated macrophages (TAMs) promotes cancer growth and metastasis, but their role in tumor development needs to be fully understood due to the dynamic changes of tumor microenvironment (TME). Here, we report an approach to visualize TAMs by optical imaging and by Fluorine-19 (^{19}F) magnetic resonance imaging (MRI) that is largely applied to track immune cells *in vivo*. TAMs are targeted with PLGA-PEG-mannose nanoparticles (NPs) encapsulating PFCE as MRI contrast agent. These particles are preferentially recognized and phagocytized by TAMs that overexpress the mannose receptor (MRC1/CD206). The PLGA-PEG-mannose NPs are not toxic and they were up-taken by macrophages as confirmed by *in vitro* confocal microscopy. At 48 h after intravenous injection of PLGA-PEG-mannose NPs, 4T1 xenograft mice were imaged and fluorine-19 nuclear magnetic resonance confirmed nanoparticle retention at the tumor site. Because of the lack of ^{19}F background in the body, observed ^{19}F signals are robust and exhibit an excellent degree of specificity. *In vivo* imaging of TAMs in the TME by ^{19}F MRI opens the possibility for detection of cancer at earlier stage and for prompt therapeutic interventions in solid tumors.

Keywords: Cell Tracking; Contrast Media; Fluorine; 19F, Perfluorocarbons; Magnetic Resonance Imaging; Molecular Probes; Tumor-associated macrophages; Breast cancer;

INTRODUCTION

Inflammation is one the major effect of cancer and it plays a pivotal role in cancer progression and metastasis [1]. In healthy conditions, macrophages (Mϕ) exert pro-inflammatory and cytotoxic effect leading the immune response against tumor development[2]. In solid tumors, tumor associated-macrophages (TAMs) are generally skewed away from the classical activation towards an alternative tumor promoting phenotype and becoming the major constituent of tumor malignancy[3,4]. Thus, presence of TAMs in the tumor microenvironment (TME) is correlated with increased tumor metastasis, angiogenesis and tumor aggressiveness[5]. In recent studies, histological sample of necrotic breast cancers have shown high tumor-associated macrophage infiltration correlating with unfortunate prognosis[6]. Indeed, TAMs can efficiently enter the necrotic core of the breast cancer and still functioning in hypoxic-necrotic areas. In this regard, the ability to label and observe TAMs non-invasively and over the time can tremendously help to understand the temporal and spatial localization of this population in the TME[7].

Recently, the magnetic resonance imaging (MRI) technique has been used to image inflammation and to track immune cells in vivo with no need of radiation[8]. In particular, perfluorocarbons (PFCs) are emerging as promising contrast agents for MRI cell tracking [9,10]. This is because, fluorine-based contrast agents are found only in traces in biological tissue meaning that the fluorine background is minimal and that the signal from exogenous fluorine is highly specific in vivo[10]. Amongst PFCs, perfluoro-15-crown-5-ether (PFCE) is one of the most attractive MRI contrast agents because it is FDA approved in a form of emulsion and therefore it is not toxic[11]. However, most of PFCs are not miscible with hydrophilic or hydrophobic solvents due to the strong carbon-fluorine covalent bond and strong electron withdrawing effects of fluorine. Thus, PFCs are typically prepared as lipid-based nano-emulsions with low toxicity and longer circulation time[12]. However, nano-drops of PFCs show limited stability *in vivo* due to the low affinity amongst the PFCs, the continuous phase and the surfactant [7]. In general, the physical structure of nano-emulsion may also restrict the combination with other functional molecules such as drugs, fluorescent tracker or surface ligand for specific targeting. To this purpose, biodegradable organic-based nanocarriers like liposomes, dendrimers, micelles and polymeric NPs act as protector and provide a good stability of the payload [13]. In this context, different strategies can be used for tumor targeting and tumor imaging[14]. For instance, "Passively targeted" nanoparticles (NPs) exploit solely the enhanced permeability and retention (EPR) effect and allow to target cancer systemically. However, the circulation of passively targeted NPs is often prevented by main physiological barriers: the extravasation of the tumor vasculature especially for high-EPR tumors that reduces nanocarrier accumulation; the NPs clearance by mononuclear phagocytic

system (MPS), sinusoidal cells of the liver and Kupffer cells [15]. On the contrary, "actively targeted" nanoparticles can help to overcome such barriers and to deliver greater amount of payload to the desired compartment thanks to the functionalization of the polymeric surface. Amongst nanocarriers, poly-lactic-*co*-glycolic acid (PLGA) an FDA approved copolymer, is one of the most exploited system in pre-clinical research owed to its biodegradability, biosafety, biocompatibility, versatility in formulation and functionalization and long shelf-life. [16,17]

Herein, we have focused on ^{19}F-based PLGA nanoparticles (NPs) to detect TAMs accumulation in humanized mice bearing breast cancer as tumor model (4T1 cells). To this purpose, PLGA Nps have been designed to encapsulate PFCE contrast agent and preserving its magnetic properties [18,19]. In addition, the polymeric shell of PLGA has been functionalized with polyethylene glycol (PEG) chains that enhance the plasmatic half-life of PLGA NPs and prevents the rapid opsonization by the mononuclear phagocyte system (MPS) for *in vivo* purposes. To actively target tumor-associated macrophages, the surface of PLGA-PEG nanoparticles has been also decorated with mannosamine ligand that is preferentially recognized and internalized by TAMs overexpressing mannose receptors (CD206)[20]. In addition, fluorescein isothiocyanate (FITC) has been linked to the polymeric shell of the PLGA-PEG NPs allowing further *in vitro* and *ex vivo* validations. All in all, intravenously injected mannose- decorated ^{19}F based-PLGA-PEG NPs aim to enhance targeting of recruited tumor-associated macrophages in a humanized mouse model of breast cancer by ^{19}F-MRI.

RESULTS

Synthesis and Characterization of polymers

PLGA-PEG-NH_2, PLGA-PEG-COOH, PLGA-PEG-FITC and PLGA-PEG-mannose copolymers were successfully synthesized with a yield of approximately 60% to 85%. The synthesis of PLGA-PEG-mannose copolymer is shown in Figure 1a. Details of the polymer characteristics such as number-average molecular weight (M_n), the molecular weights (M_w) and the polydispersity index (PDI) are provided in **Table 1**. All the resulting copolymers presented PDI approximately of 1.4-1.7 with unimodal and symmetric peak in the GPC. This result confirmed the synthesized copolymer possessed narrow distribution of molecular weight.

The conjugation of mannosamine to PLGA-PEG copolymer was confirmed by by comparing ^{1}H-NMR spectra of PLGA-PEG-mannose to those of PLGA-PEG-COOH (**supplementary Figure 1a**) and D-mannosamine (**supplementary Figure 1b**). The peaks at 1.58 ppm and

5.22 ppm were characteristics of methyl groups and methine groups of glycolic acid (GA) segments, while the peak at 4.82 ppm was attributed to methylene group of lactic acid (LA) segments, which were both contributed by PLGA chains (**supplementary Figure 1a**). The peak observed at 3.64 ppm corresponded to methylene groups of PEG segment. The integration ratio between the characteristic peaks of PEG and PLGA chains reveals that PEG was chemically conjugated on PLGA with mole ratio around 1:1. The peaks of mannosamine overlapped with the peak of PEG (3.62 ppm), therefore only one small peak at 4.11 ppm was detected and attributed to mannosamine [21] . The FITC conjugation molar ratio of PLGA-PEG-FITC copolymer was 85% measured by the fluorescence absorption according to standard curve build by pure FITC solution.

Formulation and Characterization of PLGA-PEG nanoparticles

Formulation of PFCE loaded PLGA-PEG nanoparticles (NPs) is illustrated in figure 1b. NPs showed a mean diameter in the range of ~ 239 nm and ~ 345 nm depending on nanoparticle formulation. PFCE encapsulated nanoparticles showed a slightly higher diameter of ~ 50 nm compared with the empty ones. All the particles were also monodispersed presenting a low PDI. Additionally, all the nanoparticles displayed negative zeta potentials due to the existence of terminal carboxyl groups in the PLGA polymer that is in the deprotonated form at physiological pH [22]. Indeed, zeta potential values were between -31 and -17 mV **(Table 2).** A series of PFCE loaded PLGA-PEG nanoparticles with or without mannosamine as a ligand and FITC as a dye were formulated by emulsion evaporation method. Particle size, PDI and zeta potential of nanoparticles were characterized by DLS and summarized in Table 3. All the nanoparticles exhibited a narrow nanoparticle size distribution ~ 200 and ~ 300 nm. PFCE encapsulated nanoparticles showed a slightly higher diameter of approximately 50 nm compared with the empty ones. Additionally, all the nanoparticles displayed negative zeta potentials due to the existence of terminal carboxyl groups in the PLGA polymer that is in the deprotonated form at physiological pH [30]. Mannosamine decorated PLGA-PEG nanoparticles possessed the less negative zeta potential compared with the ones without mannosamine due to neutralization by mannosamine.

Nanoparticles (NPs) were observed by scanning electron microscopy (SEM) where images confirmed that the PLGA-PFCE nanoparticles had a relatively uniform diameter of ≈200 nm with a spherical shape and smooth surface **(Figure 1C).**

In some cases, nanoparticles showed dented appearance supposedly due to the phase separation of PFCE from nanoparticles during the analysis[23].This finding is therefore an indirect effect of the presence of PFCE within nanoparticles. As depicted in **Figure 1D**, two peaks were highlighted in the spectrum at δ= -75.65 ppm for fluorine atoms of TFA

and at δ= -89.50 ppm for fluorine atoms of PFCE. The amount of PFCE encapsulated was calculated from the integration ratio between PFCE peak and TFA peak. PLGA-PEG and PLGA-PEG-mannose nanoparticles had a comparable fluorine encapsulation efficiency: 65.2% for PLGA-PEG, 67.1% for PLGA-PEG-mannose, and similar load content (6.45 µl/mg. for PLGA-PEG and 6.64 µl/mg for PLGA-PEG-mannose). Quantification and encapsulation efficiency are outlined in **Table 3**.

Cell cytotoxicity and NPs uptake assay of polarized macrophages

Initial studies were performed to assess cell viability when M2-like Raw264.7 macrophages were treated with targeted or untargeted PLGA nanoparticles. Cytotoxicity assay was performed incubating macrophages with different concentration of nanoparticles ranged between 0 and 2.5 mg/ml and incubated for 24 h at 37 °C. Around 100% of cells were not affected by the treatment and all type of nanoparticles were well tolerated **(Figure 2A).** To test if fluorescent targeted or untargeted nanoparticles were preferentially up-taken by macrophages with M2-like phenotype, we first polarized Raw264.7 macrophages into M1-like macrophages, M2-like macrophages, and unpolarized macrophages (M0-like phenotype). Later, cells were incubated with targeted and untargeted PEGylation or not, FITC-PLGA nanoparticles (1 mg/ml) for 6 h. **Figure 2B** shows that targeted and PEGylated PLGA nanoparticles were preferentially up-taken by M2-like polarized macrophages. Particularly for the M0-like phenotype, not significant differences were highlighted by the uptake of the different nanoparticles. For the M1-like phenotype group, targeted-PEG-PLGA NPs particles had greater uptake (~1.20-fold) than un-PEGylated-mannose NPs and also higher uptake than untargeted PEGylated particles (~1.7-fold). For M2-like phenotype group, targeted-PEG-PLGA NPs have roughly a 2.5-fold higher uptake compared to untargeted-pegylated nanoparticles and ~ 8-fold higher than un-PEGylated-mannose NPs. Statistical analysis was performed with one-way ANOVA, for triplicate samples and significance attributed when $P < 0.001$. Taken together, PLGA-PEG-mannose nanoparticles resulted in the highest uptake by M2-like macrophages compared to M0-like and M1-like macrophages, suggesting that both PEGylation and mannose ligand stimulate the cellular uptake. To confirm cellular internalization of NPs, M0, M1 and M2-like Raw 264.7 macrophages were treated with targeted and untargeted nanoparticles conjugated or not with PEG (1 mg/ml). Confocal images of labeled polarized macrophages are shown in **Figure 2c,** where PLGA-PEG nanoparticles conjugated with FITC were stained in green, cell membrane in magenta, lysosomes in red, and nuclei in blue.

In vivo fluorine-19 nuclear magnetic resonance (^{19}F-MRS)

In order to calculate the amount of ^{19}F encapsulated in targeted and untargeted PLGA-PEG NPs, a curve of reference was built using different dilutions of pure ^{19}F ranged between

5 µl and 100 µl (**Figure 3a**). *In vitro* quantification of ^{19}F spins encapsulated in 1mg/ml of targeted and untargeted PLGA-PEG NPs revealed an adequate number of ^{19}F-atoms for further *in vivo* evaluations. In particular 7.01E+19 ^{19}F were detected for PLGA-PEG nanoparticles and 4.95E+19 ^{19}F were detected for PLGA-PEG-mannose nanoparticles.

4T1-breast xenograft mice (n=4 per group) received 1 mg/ml of targeted or untargeted-PLGA-PEG nanoparticles intravenously (200 µl of suspension in PBS). ^{19}F signals from the tumor site were quantified 48 h after NPs injection by MRS. A spectrum of ^{19}F signal was successfully measured from the tumor area of mice injected with targeted PLGA nanoparticle by 7T MRI as shown in **Figure 3b** (top panels). As for untargeted-PLGA-PEG nanoparticles, the signal-to-noise ratio measured from the tumor site was low and fluorine quantification was not possible. This suggests that the targeted-PLGA-PEG nanoparticles have a more efficient accumulation at the tumor site compared to the untargeted-PLGA-PEG nanoparticles.

DISCUSSION

In this study, we have assessed PLGA-PEG NPs decorated with mannose ligand for TAMs detection by ^{19}F-MRI. This approach has exploited the use of different types of PLGA nanoparticles that are not toxic, stable and by definition more resistant to mechanical stress. In addition, polymeric nanoparticles of PLGA offer the advantage to be further functionalized with target ligands. PEGylation and mannosylation show an influence in circulation and cellular uptake of nanoparticles. Actually, first of all, PEGylation of PLGA nanoparticles protects them from complement activation (i.e. opsonization) with longer circulation in the blood stream, with the consequence of an improved opportunity for the drug to be released to the target site. Secondly, mannosylation can act as cellular membrane-docking ligand allowing for nanoparticle internalization in mannose-expressing macrophages especially the M2 macrophages due to overexpression of mannose receptor. Thus, mannose can be used for intracellular delivery of relevant payloads [20,24,25]. Herein, we decided to encapsulate the PFCE perfluorocarbon as contrast agent for ^{19}F-MRI. PLGA nanoparticles used as carrier ensure PFCE stability for long storage, allowing for lyophilize, solubilize in suspensions and freeze the particles. In our study, we could produce PLGA nanoparticles of narrow size the distribution and a size approximately between 330-390 nm irrespective to the nanoparticle formulation (**Table 2).** SEM images for PLGA-PFCE NPs confirmed a However, PLGA-PEG NPs did not provide resolved photos due to the interference of PVA surfactant with the analysis. Thus, images of NPs obtained by TEM would provide more accurate analysis for size and shape of PLGA-PEG NPs. NPs showed minimal toxicity *in vitro* when incubated with macrophages

also for higher concentration like 2.5 mg (**Figure 1 A**). However, it has been shown that vitality of cells is not affected if treated with 20 mg/million cells of PLGA nanoparticles [26]. The ^{19}F-payload of particles is similar amongst the different groups as demonstrated by ^{19}F-MRS and ^{19}F-NMR analyses. All the PFCE-nanoparticles were also able to target TAMs and be internalized by them especially if they were PEGylated and mannosylated **(Figure 2 B and C).** Finally, PFCE used for *in vivo* studies is known to be non-toxic in biological systems. When injected encapsulated in targeted-PEG-PLGA nanoparticles we were able to detect fluorine signals 48h after injections. We observed higher liver retention of nanoparticles *in vivo* most probably due to the continuous uptake by liver like Kupffer cells, liver sinusoidal endothelial cells (LSECs), and hepatic stellate cells (HSCs)[27]. This might be overcome by treating mice with clodronate liposomes before NPs injection and blocking non-specific uptake by Kupffer macrophages in the liver and increasing ^{19}F-signal due to the greater retention of targeted-PLGA NPs in the tumor site [28]. Recently, it has also been demonstrated that an antifouling-polymer coatings may block non-specific uptake of nanoparticles by liver[29]. For untargeted PLGA-nanoparticles, the ^{19}F signals in the tumor did not exceed the background noise arising from the organs. For targeted PLGA-nanoparticles in the tumor site, the ^{19}F signals in the tumor had a weak intensity when measured by MRI *in vivo*, but the concentration of the PFCE was successfully quantified by ^{19}F MRS. We believe that higher magnetic field strengths as 9.5T or 11T MRI equipped with more sophisticated detectors might compensate with the sensitivity of detection allowing to measure fewer amount of fluorine in the tumor. Altogether the results presented in the study prove the efficacy of delivering PLGA-PEG-mannose nanoparticles by TAMs reaching the tumor site *in vivo*. Future studies will focus on accumulation of functionalized PEGylated-nanoparticles delivered by TAMs as a function of tumor growth stage and as a function of the trafficking and timing of TAMs *in vivo*.

Table 1. Mn, Mw and PDI of PLGA-PEG and PLGA-PEG-mannose copolymers

Name	Mw[a] (kDa)	Mn[a] (kDa)	LA:GA[b]	PLGA:PEG[b]	PDI[a]
PLGA-PEG-COOH	14	10	1 : 1	1 : 0.93	1.4
PLGA-PEG-mannose	9.2	7.3	1 : 0.95	1 : 0.82	1.3
PLGA-PEG-NH_2	18.7	12.7	1 : 1	1 : 0.98	1.5
PLGA-PEG-FITC	--	--	1 : 1	1 : 0.92	--

[a] Determined by GPC; [b] Determined by ^{1}H-NMR

Conflict of Interest. The authors declare that the research was conducted in the absence of any commercial or financial relationships that could be construed as a potential conflict of interest.

Table 2. *Particle Size, PDI and Zeta potential of PLGA-PEG nanoparticles.*

Nanoparticles	*Load*	*Particle Size (nm)*	*PDI [iii]*	*Zeta Potential (mV)*
PLGA[i] -PEG	-	258 ±10	0.28 ±0.01	-22.3 ± 0.6
PLGA[i] -PEG	+PFCE[ii]	371 ± 8	0.23 ±0.03	-26.3 ± 0.4
PLGA[i] -PEG-FTIC	-	299 ± 12	0.36 ±0.05	-26.8 ± 0.4
PLGA[i] -PEG-FITC	+PFCE[ii]	345. ± 8	0.20 ±0.01	-24.2 ± 0.2
PLGA[i] -PEG-mannose	-	199 ± 3	0.10 ±0.03	-12.9 ± 0.6
PLGA[i] -PEG-mannose	+PFCE[ii]	386 ± 3	0.23 ±0.00	-17.9 ± 0.1
PLGA[i] -PEG-mannose-FTIC	-	222 ± 4	0.22 ±0.09	-24.2 ± 2.0
PLGA[i] -PEG-mannose-FTIC	+PFCE[ii]	318 ± 4	0.10 ±0.02	-19.6 ± 0.4

[i] PLGA, poly(lactide-co-glycolide)
[ii] Perfluoro-15-crown-5-ether
[iii] Polydispersity index

Table 3. PFCE load content and PFCE encapsulation efficiency PLGA-PEG nanoparticles characterized by *in vitro* ^{19}F-NMR.

	Name	*Number of F-Atoms*	*Load content (μL /mg)*	*Encapsulation Efficiency (%)*
^{19}F-NMR [i]	PLGA-Mannose-FITC- PFCE-	3.14 E+20	6.45	65.2
	PLGA-PEG-mannose-FITC-PFCE	2.82 E+20	6.64	67.1

[i] Values are calculated for 1mg of NPs dissolved in $CDCl_3$ solvent before the analysis at ^{19}F-NMR

Author Contributions. GZ., S.Y., L.M. and P.D.M. designed the experiments, GZ., S.Y., performed the experiments. GZ., S.Y and L.M. wrote the manuscript. GZ., S.Y, N.G., R.C. P.D.M., C.L. and L.M. critically revised the manuscript for important intellectual content. All authors have read and agreed to the published version of the manuscript.

Funding. We acknowledge the funding for this work provided by the European Commission under the H2020 MSCA-RISE award grant number 777682 (CANCER) and under the H2020-MSCA-ITN award, grant number 675743 (ISPIC).

Acknowledgments. This work was supported by the Applied Molecular Imaging Erasmus MC (AMIE) facility. This work was supported also by LECO department from the Erasmus Medical Center. This work was supported by the Applied Molecular Imaging Erasmus MC (AMIE) facility.

REFERENCE

1. Noy, R. & Pollard, J. W. Tumor-associated macrophages: from mechanisms to therapy. *Immunity* **41**, 49–61 (2014).
2. Yang, M., McKay, D., Pollard, J. W. & Lewis, C. E. Diverse Functions of Macrophages in Different Tumor Microenvironments. *Cancer Res.* **78**, 5492–5503 (2018).
3. Mantovani, A., Marchesi, F., Malesci, A., Laghi, L. & Allavena, P. Tumour-associated macrophages as treatment targets in oncology. *Nat. Rev. Clin. Oncol.* **14**, 399–416 (2017).
4. Choi, J., Gyamfi, J., Jang, H. & Koo, J. S. The role of tumor-associated macrophage in breast cancer biology. *Histol. Histopathol.* **33**, 133–145 (2018).
5. Yang, L. & Zhang, Y. Tumor-associated macrophages: from basic research to clinical application. *J. Hematol. Oncol.* **10**, 58 (2017).
6. Yang, M. *et al.* Stromal Infiltration of Tumor-Associated Macrophages Conferring Poor Prognosis of Patients with Basal-Like Breast Carcinoma. *J. Cancer* **9**, 2308–2316 (2018).
7. Srinivas, M., Boehm-Sturm, P., Figdor, C. G., de Vries, I. J. & Hoehn, M. Labeling cells for in vivo tracking using 19F MRI. *Biomaterials* **33**, 8830–8840 (2012).
8. Ahrens, E. T. & Bulte, J. W. M. Tracking immune cells in vivo using magnetic resonance imaging. *Nat. Rev. Immunol.* **13**, 755–763 (2013).
9. Temme, S., Bönner, F., Schrader, J. & Flögel, U. 19F magnetic resonance imaging of endogenous macrophages in inflammation. *Wiley Interdiscip. Rev. Nanomed. Nanobiotechnol.* **4**, 329–343 (2012).
10. Srinivas, M., Heerschap, A., Ahrens, E. T., Figdor, C. G. & de Vries, I. J. M. (19)F MRI for quantitative in vivo cell tracking. *Trends Biotechnol.* **28**, 363–370 (2010).
11. Ahrens, E. T. & Zhong, J. In vivo MRI cell tracking using perfluorocarbon probes and fluorine-19 detection. *NMR Biomed.* **26**, 860–871 (2013).
12. Rho, J. *et al.* Paramagnetic Fluorinated Nanoemulsions for in vivo F-19 MRI. *Mol. Imaging Biol.* **22**, 665–674 (2020).
13. Diou, O. *et al.* Long-circulating perfluorooctyl bromide nanocapsules for tumor imaging by 19FMRI. *Biomaterials* **33**, 5593–5602 (2012).
14. Schleich, N. *et al.* Comparison of active, passive and magnetic targeting to tumors of multifunctional paclitaxel/SPIO-loaded nanoparticles for tumor imaging and therapy. *J. Control. Release* **194**, 82–91 (2014).
15. Blanco, E., Shen, H. & Ferrari, M. Principles of nanoparticle design for overcoming biological barriers to drug delivery. *Nat. Biotechnol.* **33**, 941–951 (2015).
16. Mir, M., Ahmed, N. & Rehman, A. U. Recent applications of PLGA based nanostructures in drug delivery. *Colloids Surf. B. Biointerfaces* **159**, 217–231 (2017).
17. Attia, M. F., Anton, N., Wallyn, J., Omran, Z. & Vandamme, T. F. An overview of active and passive targeting strategies to improve the nanocarriers efficiency to tumour sites. *J. Pharm. Pharmacol.* **71**, 1185–1198 (2019).
18. Zhou, Y. *et al.* Anti-CD206 antibody-conjugated Fe3O4-based PLGA nanoparticles selectively promote tumor-associated macrophages to polarize to the pro-inflammatory subtype. *Oncol Lett* **20**, 298 (2020).
19. Anani, T., Rahmati, S., Sultana, N. & David, A. E. MRI-traceable theranostic nanoparticles for targeted cancer treatment. *Theranostics* **11**, 579–601 (2021).
20. Scodeller, P. *et al.* Precision Targeting of Tumor Macrophages with a CD206 Binding Peptide. *Sci. Rep.* **7**, 14655 (2017).

21. Alonso-Sande, M. *et al.* Development of PLGA-Mannosamine Nanoparticles as Oral Protein Carriers. *Biomacromolecules* **14**, 4046–4052 (2013).
22. Govender, T., Stolnik, S., Garnett, M. C., Illum, L. & Davis, S. S. PLGA nanoparticles prepared by nanoprecipitation: drug loading and release studies of a water soluble drug. *J. Control. Release* **57**, 171–185 (1999).
23. Srinivas, M. *et al.* PLGA-encapsulated perfluorocarbon nanoparticles for simultaneous visualization of distinct cell populations by 19F MRI. *Nanomedicine (Lond).* **10**, 2339–2348 (2015).
24. Yang, R. *et al.* Cancer Cell Membrane-Coated Adjuvant Nanoparticles with Mannose Modification for Effective Anticancer Vaccination. *ACS Nano* **12**, 5121–5129 (2018).
25. Li, Y. *et al.* Targeted Imaging of CD206 Expressing Tumor-Associated M2-like Macrophages Using Mannose-Conjugated Antibiofouling Magnetic Iron Oxide Nanoparticles. *ACS Appl. Bio Mater.* **3**, 4335–4347 (2020).
26. Swider, E. *et al.* Customizing poly(lactic-co-glycolic acid) particles for biomedical applications. *Acta Biomater.* **73**, 38–51 (2018).
27. Park, J.-K. *et al.* Cellular distribution of injected PLGA-nanoparticles in the liver. *Nanomedicine Nanotechnology, Biol. Med.* **12**, 1365–1374 (2016).
28. Schiedner, G. *et al.* Selective depletion or blockade of Kupffer cells leads to enhanced and prolonged hepatic transgene expression using high-capacity adenoviral vectors. *Mol. Ther.* **7**, 35–43 (2003).
29. Nabil, G. *et al.* Nano-engineered delivery systems for cancer imaging and therapy: Recent advances, future direction and patent evaluation. *Drug Discov. Today* **24**, 462–491 (2019).

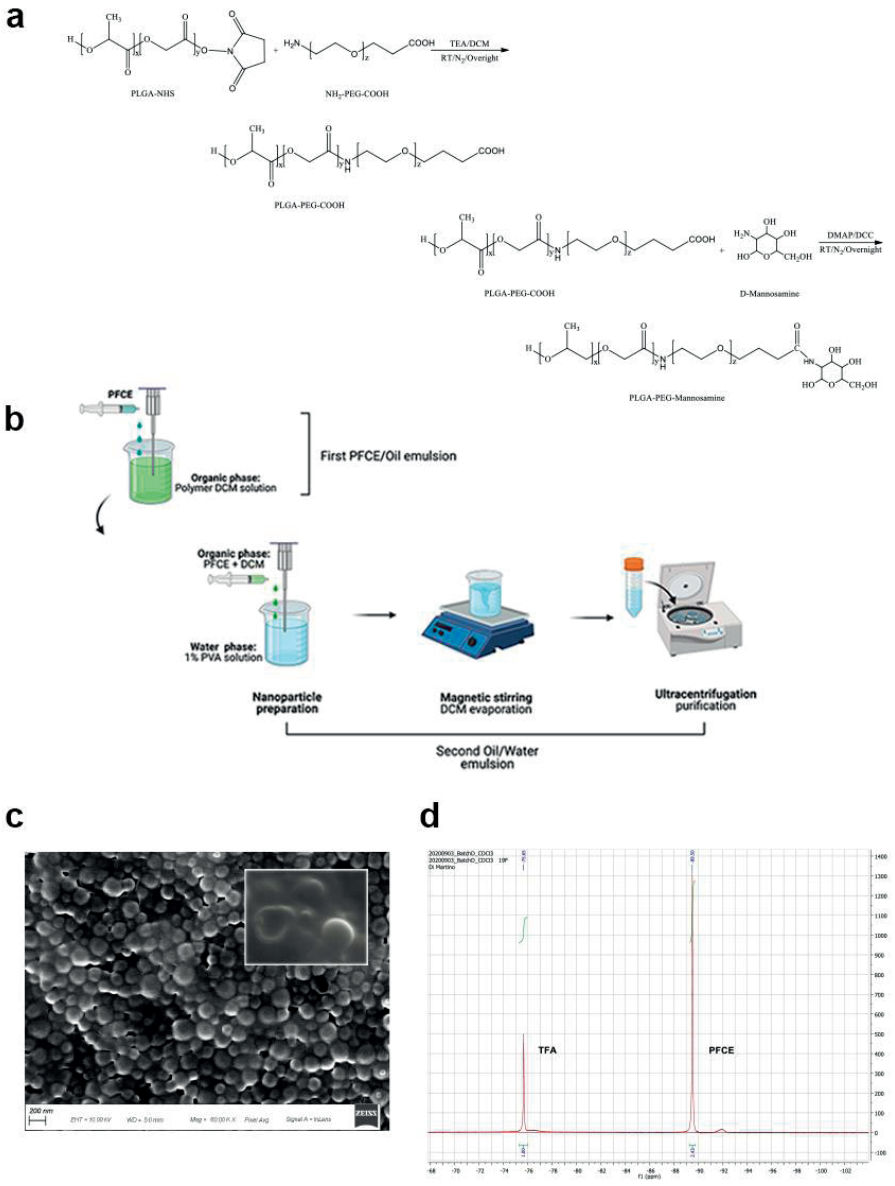

Figure 1 Chemical synthesis and characterization of PLGA-PEG nanoparticles. a) Illustrative chemical synthesis of PLGA-PEG-COOH and PLGA-PEG-mannose copolymers. **b)** Schematic illustration for PFCE/Oil/Water double-emulsion and solvent-evaporation method used to produce PLGA-PEG, PLGA-PEG-mannosamine or PLGA-PEG-FITC nanoparticles. Scanning Electron Microscopy (SEM) of PLGA-PFCE nanoparticles. **c)** ^{19}F-NMR spectrum of PFCE encapsulated PLGA-PEG-FITC-mannose NPs in CDCl3 δ in ppm: -75.65 (3F, CF_3COOH); -89.50 (20F, $C_{10}F_{20}O_5$).

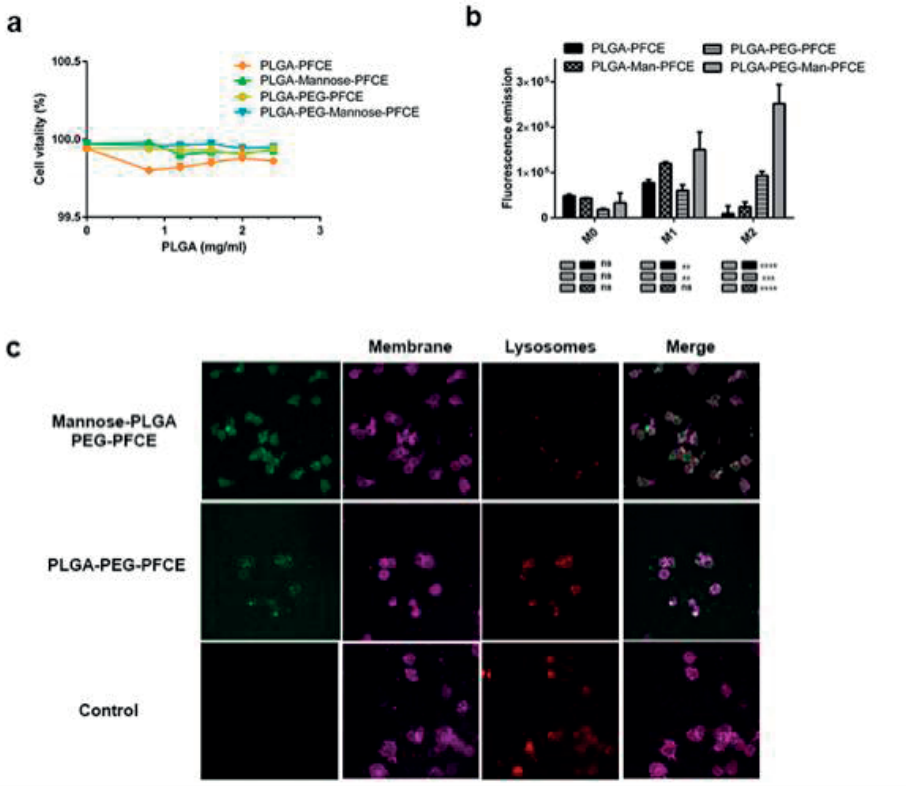

Figure 2 Characterization of nanoparticles in vitro. a) Cytotoxicity tests for Raw264.7 macrophage cells treated for 24 h with PLGA-PFCE, PLGA-PFCE- Mannose, PLGA-PEG-PFCE and PLGA-PEG-mannose-PFCE nanoparticles (final concentration 1mg/ml**). b)** Uptake efficiency of Raw264.7 macrophage cells polarized in and M0 (negative control), M1 (pro-inflammatory), M2 (anti-inflammatory) phenotype and treated for 1 h with PLGA-PFCE, PLGA-PFCE-mannose, PLGA-PEG-PFCE and PLGA-PEG-mannose-PFCE nanoparticles (final concentration 1mg/ml). **c)** Confocal images of polarized M2-polarozed Raw264.7 macrophages treated for 1h with mannose (top panels) and untargeted (middle panels) PLGA-PEG NPs. Negative control for PLGA-PEG nanoparticles is shown in the bottom panels. Nanoparticles are shown in green color (FITC labelled); cell membrane is shown in magenta color; lysosomes are shown in deep-red color.

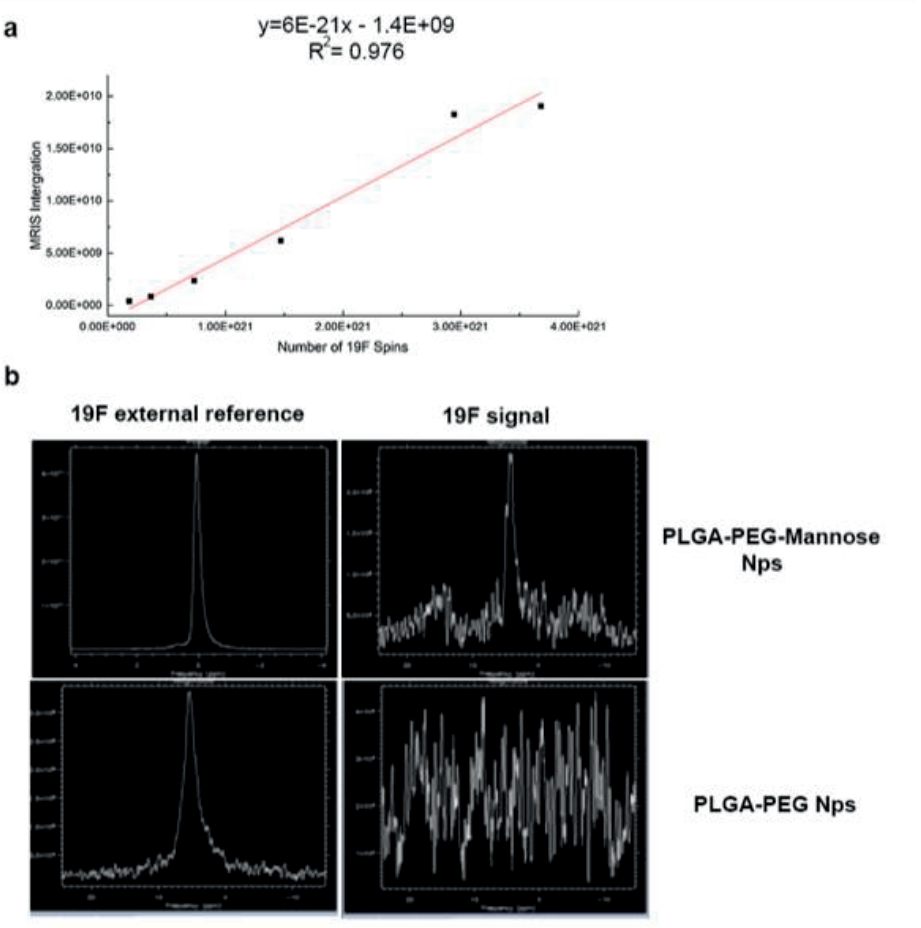

Figure 3. PFCE magnetic resonance measurement by ^{19}F-MRI spectroscopy (MRS). a) Standard curve of pure PFCE contrast agents measured at different dilution volumes ranging from 5 µl and 100 µl. **b)** ^{19}F-MRI spectrum of PFCE detected from 4T1-tumor bearing mice and treated with PLGA-PEG-mannose nanoparticles (top graph) and with PLGA-PEG nanoparticles (bottom graph). Respective external reference tubes (left side of the panels) were used to set up image acquisition methods and for PFCE measurements at the tumor site.

MATERIALS AND METHODS

Materials

Unless stated, chemicals were purchase from Sigma Aldrich (Stenheim, Germany) and used as received. Poly (D,L-lactide-co-glycolide) (PLGA) copolymer (50/50, Resomer RG502H Mw 24000-38000) was purchased from Boehringer Ingelheim (Ingelheim am Rhein, Germany). Perfluoro-15-crown ether (PFCE) was provided by Exfluor Research Corporation (Texas, USA). Agilent Polystyrene calibration kit for GPC characterization was obtained from Agilent Technologies (Santa Clara, U.S.A.). Ultrapure water was produced in the laboratory according to a Milli-Q® system (Merck Millipore, Darmstadt, Germany).

Proton Nuclear Magnetic Resonance Spectroscopy (^{1}H-NMR)

Chemical structures and number-average molecular weight (Mn) of synthesized polymers were characterized by proton nuclear magnetic resonance spectroscopy (1H NMR, Varian Mercury plus 400, Crawley, UK)) using CDCl3 or D2O as solvents. Chemical shifts were referred to the solvent peak (δ = 7.26 ppm for CDCl3, δ = 4.79 ppm for D2O).

Gel Permeation Chromatography (GPC)

Gel permeation chromatography (GPC) was employed to determine the weight average molecular weight (Mw), number average molecular weight (Mn) and the polydispersity index (PDI) of copolymers. GPC measurements were carried out by using a TSK gel G4000HHR column (Tosoh Bioscience, Tokyo, Japan), 7.8 mm ID × 30.0 cm L, pore size 5 µm. Polystyrenes of defined molecular weights ranging from 580 to 377400 Da were used as calibration standards. The eluent was tetrahydrofuran (THF), the elution rate was 1.0 mL/min and the column temperature was 35 °C. The samples were dissolved in THF at a concentration of 5 mg/ml.

Synthesis and Characterization of Polymers: PLGA-PEG-COOH, PLGA-PEG-FITC and PLGA-PEG-mannosamine

Carboxyl terminal groups of PLGA were activated and converted to PLGA-NHS for the subsequent conjugation with polyethylene glycol (PEG). Briefly, 2 g PLGA 503H polymer was dissolved in 10 mL anhydrous dichloromethane (DCM) followed by adding an excess of N-hydroxy succinimide (NHS, 46.0 mg, 0.4 mmol) and N,N'-dicyclohexylcarbodiimide (DCC,82.5 mg, 0.4 mmol). The reaction was stirred at room temperature overnight, under the N2 atmosphere. To purify, PLGA-NHS was precipitated in diethyl ether and washed by cold mixture of diethyl ether and methanol three times to remove the residual NHS.

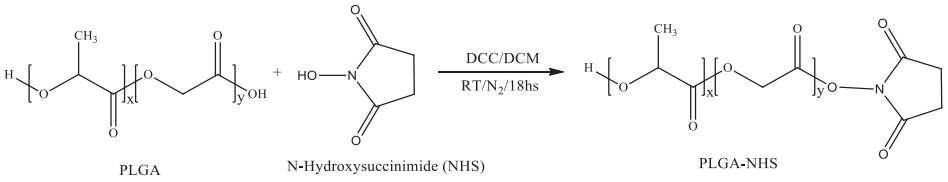

Chemical synthesis scheme of PLGA-NHS

PLGA-PEG copolymers with carboxyl terminal groups and amino terminal groups were synthesized by conjugated amino groups of NH_2-PEG-COOH and NH2-PEG-NH_2 correspondingly to the N-hydroxysuccinimide esters of resulting PLGA-NHS. In details, PLGA-NHS (500 mg, 0.015 mmol) was dissolved in 5 mL anhydrous DCM. Then NH_2-PEG-COOH or NH2-PEG-NH_2 (44.1 mg, 0.015 mmol) was added in the DCM solution with trimethylamine (TEA, 13.3 µL, 0.09 mmol) as catalyst. The reaction was processed at room temperature overnight, under N_2 atmosphere. PLGA-PEG copolymer was precipitated with a cold mixture of diethyl ether and methanol and washed 3 times by the same solvents, then dried by desiccator under vacuum. number-average molecular weight (M_n), the molecular weights (M_w) and the polydispersity index (PDI) were characterized by gel permeation chromatography (GPC, TSK gel G4000HHR column (Tosoh Bioscience, Tokyo, Japan). Mn and chemical structures were determined by proton nuclear magnetic resonance spectroscopy (^{1}H-NMR, arian Mercury plus 400, Crawley, UK).

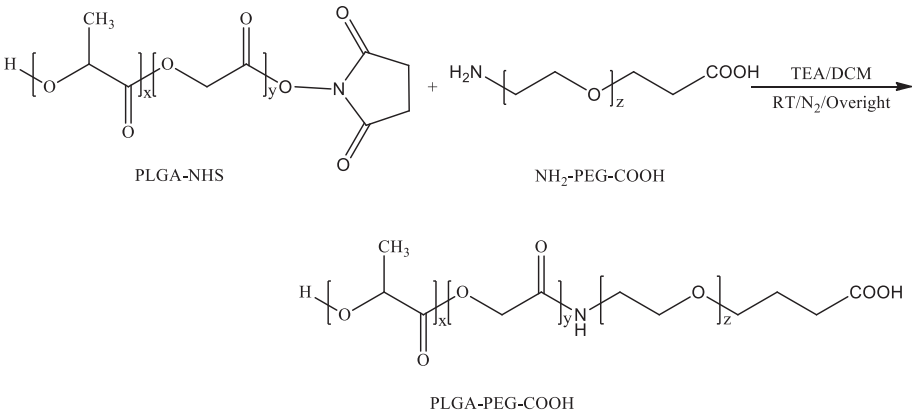

Chemical synthesis scheme of PLGA-PEG-COOH

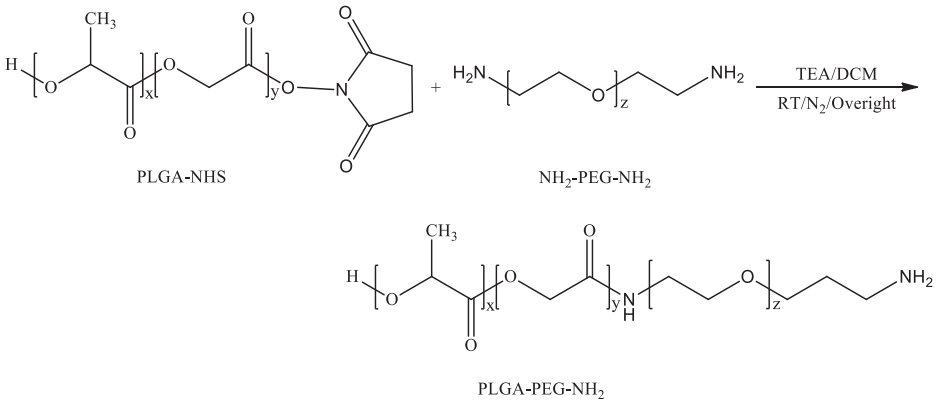

Chemical synthesis scheme of PLGA-PEG-NH_2

D-mannosamine was covalently conjugated to the acid terminal groups of PLGA-PEG-COOH copolymer to yield PLGA-PEG-mannosamine copolymer. Briefly, the synthesized PLGA-PEG-COOH copolymers (200 mg, 0.006 mmol) were dissolved in 2.5 mL D-mannosamine solution in Dimethyl formamide (DMF) at a concentration of 0.025M. Then, 4-dimethylaminopyridine (DMAP, 7.3 mg, 0.06 mmol) and DCC (123.8 mg, 0.6 mmol) were added stepwise. The reaction mixture was stirred at room temperature overnight under nitrogen atmosphere. PLGA-PEG-mannosamine was precipitated in a cold mixture of diethyl ether and methanol, dried by desiccator under vacuum. Mn, Mw and PDI were characterized by GPC, and chemical structures were determined by ^{1}H-NMR spectroscopy.

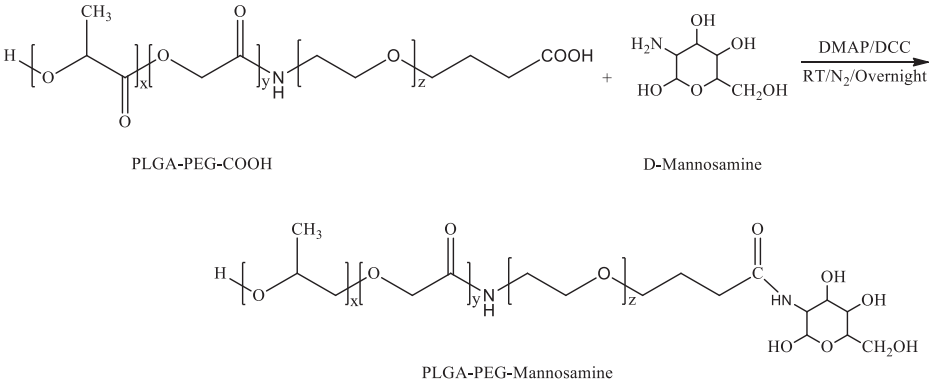

Chemical synthesis scheme of PLGA-PEG-mannosamine

Fluorescein isothiocyanate (FITC) was conjugated to PLGA-PEG-NH_2 to yield fluorescently labeled PLGA-PEG nanoparticles. FITC (4.21 mg, 0.011 mmol) and PLGA-PEG-NH_2 (100 mg, 0.0027 mmol) were dissolved in 2.5 mL anhydrous dimethylsulfoxide (DMSO) at

room temperature overnight. To purify, the reaction mixture was dialyzed against DMSO and water sequentially (Mw cutoff = 12 - 24 kDa), then isolated by lyophilization as a yellow powder. The FITC conjugation was characterized by measurement of fluorescence absorption at an excitation wavelength of 490 nm and an emission wavelength of 530 nm using Spectramax (iD3, Molecular Devices, USA). The FITC conjugation yield was calculated according to Formula 1.

Nanoparticle formulation

Nanoparticles were formulated by double emulsion solvent-extraction evaporation method using PLGA-PEG, PLGA-PEG-mannosamine or PLGA-PEG-FITC copolymers[14]. Nanoparticles encapsulating PFCE (890 µl) were prepared using 90 mg of PLGA-PEG copolymers, in a single emulsion technique using 3 ml of DCM as solvent. Organic phase was then added dropwise to 18 ml of aqueous 1% (w/v) polyvinyl alcohol (PVA) as surfactant and emulsified for 20 min at 13500 rpm by homogenization (Ultra-Turrax® T25 digital, IKA, Staufen, Germany). Particles were washed extensively 3 times with distilled water by ultracentrifugation for 20 min at 4 °C and at 10.000g (Avanti JXN-26, Beckman Coulter Life Sciences). Nanoparticles were then cryoprotected with sucrose (7%) and freeze-dried for 24h. Lyophilizates were stored at -20 °C. PFCE unloaded nanoparticles were prepared by single O/W emulsion method in the same conditions as described above.

Size and zeta potential

Zeta potential, polydispersity index (PDI) and size of the nanoparticles were characterized by dynamic light scattering (DLS) at fixed at fixed 90° scattering angle at 25 by Malvern Zetasizer 2000 (Malvern, UK). Suspensions were diluted in distilled water. Measurements were performed in triplicate at room temperature.

Scanning electron microscopy (SEM)

Nanoparticle morphology was determined by a field emission-scanning electron microscope (FE -SEM Zeiss Sigma 300, Zeiss, Germany). SEM sample stage was prepared by placing a double-sided adhesive carbon tape on an aluminum stub. One small drop of 1 mg/mL nanoparticle sample suspended in ultrapure water was placed on the sample stage and then dried at 37 overnight. Subsequently, the dried sample was sputtered under vacuum with a chromium layer of approximately 100 Å thickness (Quorum Q150T ES, Quorum Technologies, UK) prior to analysis.

Determination of PFCE encapsulation efficacy by ^{19}F NMR

PFCE load content and encapsulation efficiency of PLGA-PEG, and PLGA-PEG-MN nanoparticles was determined by Fluorine-19 nuclear magnetic resonance spectros-

copy (19F-NMR). Lyophilized nanoparticles were dissolved in $CDCl_3$ containing 0.1 M trifluoroacetic acid (TFA) as internal standard. The amount of PFCE was calculated by the integration ratio between PFCE peak to TFA peak. Fluorine contents were calculated according to the **Formula 1** and **Formula 2**.

$$\text{PFCE load content} = \frac{\textit{PFCE volume loaded in nanoparticles}}{\textit{Weight of nanoparticles}} \qquad \textbf{\textit{Formula 1}}$$

$$\text{PFCE encapsulation efficency \%} = \frac{\textit{PFCE encapsulated volume}}{\textit{PFCE total volume}} \times 100 \qquad \textbf{\textit{Formula 2}}$$

Cell culture

Murine macrophage Raw 264.7 cell line and 4T1 cells (murine mammary carcinoma cells) purchased from (ATCC®) were cultured in complete DMEM medium (Sigma, St. Louis, Mo, USA) supplemented with 10% fetal bovine serum (FBS) and 1% of penicillin and streptomycin and incubated at 37 °C with 5% CO_2. When cell confluence reached around 80%, dead cells were washed away with PBS (Lonza) and live cells were detached by cell scraper. Cells were centrifuged and re-suspended with 8 ml of fresh DMEM medium. Cell counting was performed using BioRad TC20 cell counter.

Cell cytotoxicity and uptake assay of polarized macrophages

Cytotoxicity of targeted or untargeted PLGA or PLGA-PEG nanoparticles was tested for Raw 264.7 cells by Pierce LDH assay kit (Thermo Scientific, city and state) and following manufacturer's instructions. Cells were treated with nanoparticles at different concentrations ranging from 0 to 2.5 mg/ml and incubated for 24 h. For uptake assay, Raw 264.7 cells were first polarized for anti-tumorigenic (M1) or pro-tumorigenic (M2) phenotypes. M1 phenotype was made by incubating cells for 24h with lipopolysaccharide (LPS) (100 ng/ml) and Interferon-gamma (IFN-ɣ) (50 ng/ml). M2 phenotype was made by incubating cells with Interleukin-4 (IL-4) (20 ng/ml) for 24 h to obtain M2 highly expressing CD206 receptor. After polarization, cells were seeded in 24-well plates (8×10^4 cells per well) and incubated with targeted or un-targeted PLGA-PEG nanoparticles (1 mg/ml). Incubation was performed for 1 h, 6 h and 24 h at 37 . After the incubation time, wells were gently washed with PBS to discard particles not up taken and green fluorescence of FITC was measured by selecting excitation wavelength at 490 nm an emission wavelength of 530 nm by Spectramax (iD3 serie, Molecular Devices). Raw 264.7 cells not polarized (M0 phenotype) were used as control and all the tests were performed multiple times in triplicate.

Fluorescence microscopy

Internalization of PLGA nanoparticles targeted (PLGA-FITC-PEG-Mannose loaded with PFCE) or untargeted (PLGA-FITC-PEG loaded with PFCE) nanoparticles was confirmed

by confocal microscopy. Raw 264.7 cells were seeded in a six well plate (80.000 cells per well). After cell attachment, cells were treated with targeted or untargeted nanoparticles (1mg/ml) for 1h. Wells were then washed three times and lysosomes were stained by deep red LysoTracker™ dye (Thermo Fisher Scientific) incubated for 20 minutes before cell fixation. Cells were then washed gently with PBS three times and fixated with 4% paraformaldehyde (PFA) for 20 minutes. After PBS wash, cell membrane was stained by PKH26 red fluorescent cell membrane label kit (Sigma-Aldrich, City, state) and nuclei were stained with Vectashield mounting-DAPI blue fluorescent dye (LSBio). Fluorescent NPs uptaken by Raw 264.7 cells were imaged by Leica SP5 confocal microscope equipped with Ar-He/Ne lasers (Leica Microsystems, Wetzlar, Germany). A 63x magnification with oil immersion objective (Carl Zeiss, Oberkochen, Germany) was used for cell imaging. Nanoparticles, cell membranes and lysosomes were visualized with respective channels at 488 nm (green), 561 nm (red) and 633 nm (deep-red).

In vitro Fluorine-19 Magnetic Resonance Spectroscopy (^{19}F-MRS)

Eppendorf tubes loaded with different concentrations of PFCE ranging from 5 µl to 100 µl were used to create a calibration curve. An MR 901 Discovery 7T magnet (Agilent Technologies, Santa Clara, CA, USA) with a preclinical front-end (GE Healthcare, Little Chalfont, UK) was used for MRS acquisition. The system is equipped with a gradient set with a maximum gradient strength of 300 mT m-1, a rise-time of 600 T m-1 s-1 and an inner diameter of 310 mm. For transmission and reception, an in-house-built dual tuned 1H/19F single channel surface coil with a diameter of 2 cm was used. The 19F MRS spectrum was recorded using a EchoSCI sequence (TR/TE = 1250/15 ms, NEX = 128, FOV = 6 cm, slice thickness = 2,5 cm). MRS processing was performed in SAGE 7.6.2 (GE Healthcare, Little Chalfont, UK) on the MR 901 Discovery system. For processing of the data, time domain signals were apodized with a 10 Hz line broadening function, after which the signal was zerofilled to 4096 points. Subsequently the time domain signal was Fourier transformed and the resulting spectrum was properly phased to show an absorption mode resonance line. 19F in the sample was quantified by reference to a standard curve, which was obtained by measuring a dilution series of PFCE with known ^{19}F content.

Mouse model

BALB/c mice (6-8-week years old) were provided access to food and water ad libitum and were hosted in the animal facility at the Erasmus MC (Rotterdam, The Netherlands). All experiments were performed according to the guidelines for animal care of the Erasmus MC Animal Experiments Committee. For tumor mouse model, $8x10^4$ of LUC2 luciferase-expressing 4T1 breast cancer cells were injected subcutaneously in the left flank of the mice (n=4 mice for each group). This cell line has been chosen because is a late state of

breast cancer and exhibits necrosis. Tumor growth was measured by calipers and by bioluminescence imaging by IVIS spectrum imager (model, Perkin Elmer, city, state).

In vivo Fluorine-19 Magnetic Resonance Spectroscopy (^{19}F-MRS)

^{1}H and ^{19}F images were acquired 48 h after injection of 1 mg/ml of targeted (PLGA- PEG -FITC-Mannose loaded with PFCE) or untargeted (PLGA -PEG-FITC loaded with PFCE) nanoparticles by 7T MRI system (Bruker Biospin, city, Germany). All the subcutaneous breast tumors have a diameter ranging between ~0.6 and ~0.8 mm^3 of diameter. *In vivo* imaging was done using a custom built dual ^{1}H/^{19}F coil for *in vivo* imaging. Mice (n=4 for each group) were anesthetized using 1.5%. isoflurane (Isoflutek, Laboratorios Karizoo). Body temperature was monitored and regulated during imaging. Reference tube of known ^{19}F concentration (7.01E+19 ^{19}F for PLGA-PEG-Mannose concentrated 1 mg/ml; and 4.95E+19 ^{19}F for PLGA-PEG nanoparticles) was placed alongside the mouse to optimize quantification of fluorine detected at the tumor site.

Magnetic resonance spectrometry was used to measure the 19F content per cell. The ^{19}F MRS spectrum was recorded using a EchoSCI sequence (TR/TE = 1250/15 ms, NEX = 128, FOV = 6 cm, slice thickness = 2.5 cm). MRS processing was performed in SAGE 7.6.2 (GE Healthcare, Little Chalfont, UK) on the MR 901 Discovery system. For processing of the data, time domain signals were apodized with a 10 Hz line broadening function, after which the signal was zerofilled to 4096 points. Subsequently the time domain signal was Fourier transformed and the resulting spectrum was properly phased to show an absorption mode resonance line. ^{19}F in the sample was quantified by reference to a standard curve, which was obtained by measuring a dilution series of PFCE with known ^{19}F content.

Statistical analysis

The data are presented as mean ± standard deviation (SD). *In vitro* and *in vivo* tests were performed using Graphpad 7 software and One-way ANOVA and T-test analysis of variance were used to analyze the differences between the groups. Significance was attributed when $P < 0.001$ (*) for *in vitro* tests and $P < 0.05$ (*) for *in vivo* tests.

Supplementary Material

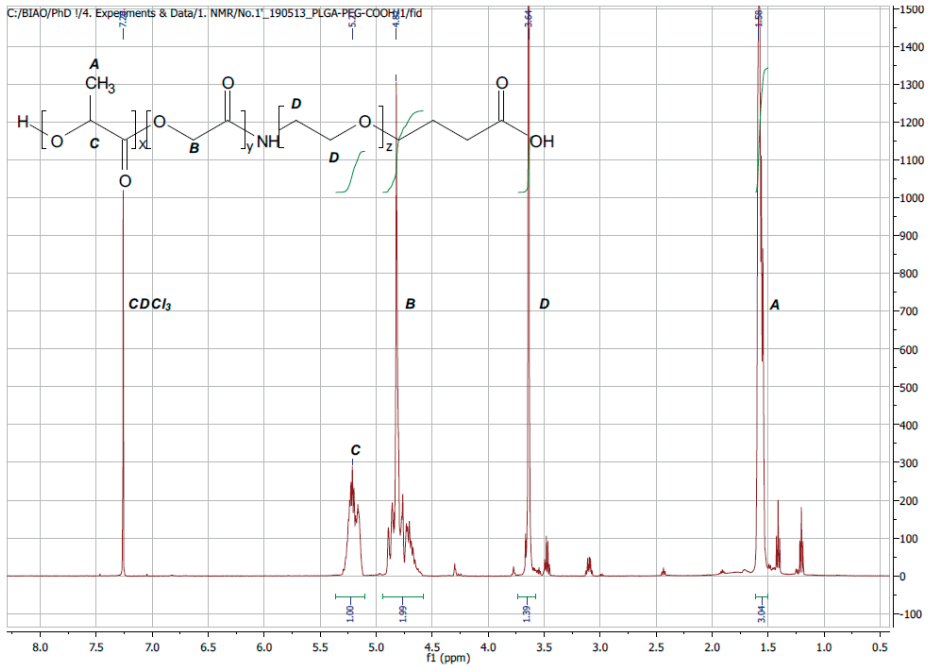

Supplementary Figure 1a. ^{1}H-NMR spectrum of PLGA-PEG polymer in $CDCl_3$, δ in ppm: 1.58 (3H, -O-CH(C<u>H</u>$_3$)-); 4.82 (2H, -O-C<u>H</u>$_2$-C(=O)-);5.21 (-O-C<u>H</u>(CH$_3$)-).

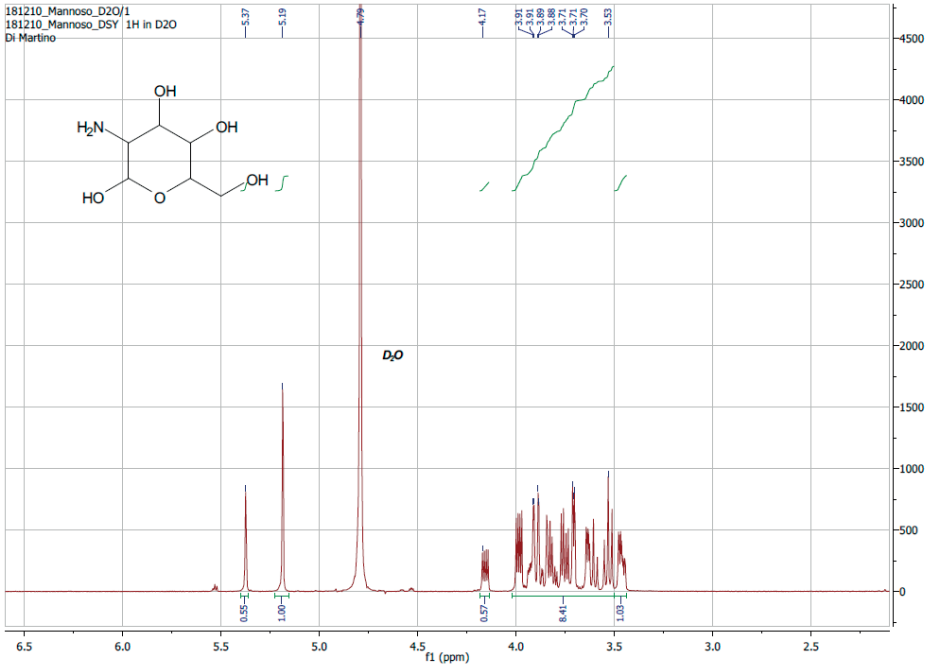

Supplementary Figure 1b. ^{1}H-NMR spectrum of Mannosamine in D_2O, δ in ppm.

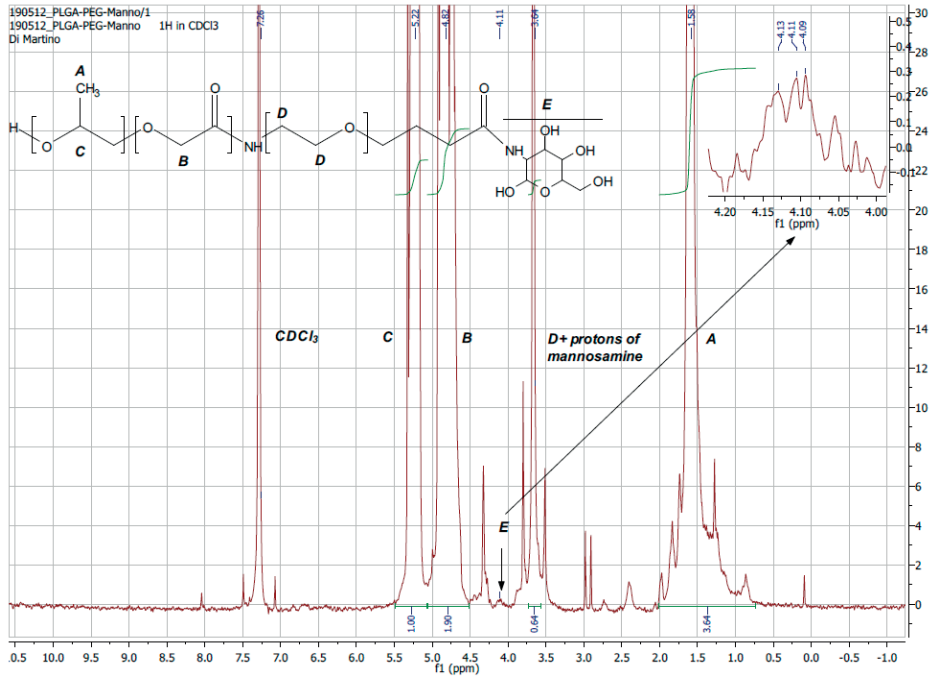

Supplementary Figure 1c. ^{1}H-NMR spectrum of PLGA-PEG-mannosamine polymer in $CDCl_3$, δ in ppm: 1.58 (3H, -O-CH($C\underline{H}_3$)-);3.64 (4H, -$C\underline{H}_2$-$C\underline{H}_2$-O-) 4.1-4.2 (protons of conjugated mannosamine); 4.82 (2H, -O-$C\underline{H}_2$-C(=O)-);5.21 (-O-C$\underline{H}$(CH_3)-).

General discussion
Future perspectives
Nederlandse samenvatting
Summary
About the author
List of publications
Portfolio
Dankwoord (Acknowledgements)

GENERAL DISCUSSION

Within the thesis, we have examined two different approaches to label cells, either by indirect methods using bioluminescent reporter genes or by direct methods using PLGA-nanoparticles decorated with the ligand of interest. Bioluminescence and MRI were used as non-invasive imaging modalities for in vivo validation.

In chapter 1, a broad introduction on Bioluminescence and MRI as molecular imaging techniques is given. Pre-clinical applications and cell targeting strategies are also described.

Colorful bioluminescence palette and new emerging technologies for deep tissue imaging

Bioluminescence imaging has been widely applied in preclinical research either for imaging cells or to exploit the light output for other imaging purposes[1]. In general, BL applications rely on luciferase/luciferin enzymatic reaction with specific emission spectra and recently with more robust photon outputs[2]. The ongoing discovery of novel natural bioluminescent luciferases and the production of optimized synthetic luciferins will expand the BL toolbox for more challenging in vivo applications. In **chapter 2**, we describe important research developments for BL including the generation of optimized luciferase/luciferin systems for more sensitive and accurate in vivo imaging. We discussed the recent improvements not only for terrestrial and marine luciferases that are the most used for mammalian studies but we also discussed the recent advancements for BL bacteria and fungi. The last ones are worthy to mention due to their independence on exogenous administration of substrate which makes the systems of particular interest[3,4]. Another attractive application mentioned is the use of D-luciferin caged substrates that allow the real-time detection of enzymatic activity and to study protein uptake[5,6]. Further recent BL biotechnologies emerging in recent years including bioluminescent nanoparticles (quantum dots and two-step BRET probes)[7], multiplex BL in deep tissues[8], gene editing solutions with a BL tag[9], and photo-uncaging technology[10] are also described.

Finally, we discussed the future directions of bioluminescence imaging including the following subjects: the detection of protein-protein interactions (i.e. antibody/target) and the design of more accurate BRET biosensor systems that may be further used to monitor therapeutic intervention in the future or to detect the delivery of bio-compounds in living animals. Furthermore, the synthetic efforts and computational modeling on substrate design and luciferase affinity will identify BL pairs more reliable for the detection of fewer cells in free-living animals. Due to the plethora of emerging luciferase/luciferin

pairs the research community must consider the properties of the recently published bioluminescent reports especially when a multicolor BL is performed. It is clear that choosing the appropriate BL systems for *in vitro* and *in vivo* detection can be crucial. However, there are still factors complicating BLI results such as ATP dependency, luciferin bioavailability, and luciferase stability in serum. Finally, the improvement of luciferase/luciferin performance in vivo together with the optimization of new software with more sensitive photon detector systems (CCD camera) or the development of sophisticated algorithm will be a promising advancement for more accurate analysis and interpretation of data. These next-generation tools will considerably reduce inconsistent data generated by inaccurate experimental settings.

In chapter 3, valuable guidance on different BL systems is provided. Luciferase/substrate pairs have been analyzed and studied with specific parameters: equimolar expression of luciferases in cells, injection of substrates respecting substrate solubility and tolerability in mice, and record of the maximum attainable signal based on previous literature. Photon yields and spectral characterization of the most used D-luciferin-dependent luciferases (Luc2, CBG99, CBR2, and Akaluc) in preclinical research were reported. Spectral data were collected after in vitro and in vivo administration of D-luciferin analogs (D-LH2, NH_2-NpLH2, Cycluc1, and Akalumine-HCl). The list of in vivo emission intensities resulted from the study provides valuable information for the research community working on BLI, especially when applying multiplex BLI in vitro and in vivo. Thus, based on the analysis we were able to recommend BL pairs that can work more efficiently and can be used for simultaneous visualization of cells. I envision that this will not only reduce the time for selecting the appropriate BL pair, but will also reduce the number of experimental tests on animals and possibly also the time per imaging session.

The demand for near-infrared shifted probes for imaging dense tissue or for the visualization of fewer cells in deep tissue *in vivo* has incredibly increased and novel luciferase/luciferin pairs emitting in the near-infrared (NIR) window are, therefore, essential if tracking of multiple cell types or biological events is required in the same animal model.

In chapter 4, we describe the generation of a novel dual-color luciferase system consisting of two click beetle luciferase mutants both emitting NIR light. One is the novel CBG2 luciferase mutant that has been engineered from the original green CBG99 luciferase. CBG2 (λ=650nm) can emit NIR photons with NH_2-NpLH2 luciferin and can be paired with CBR2 luciferase (λ=730nm), that also uses NH_2-NpLH2 luciferin as a substrate, for dual-color BLI in vivo. This system enables to record semiquantitative data from the lungs as a deep-tissue model in vivo by reducing light attenuation. Notably, the administration of

NH_2-NpLH2 luciferin as a unique substrate not only provides high sensitivity but also reduces the time of imaging sessions and the number of animals needed per experiment.

One limitation of the study is a partial attenuation of light of CBG2 luciferase due to the absorption of some emitted "green" photons by tissues in vivo. Indeed, we recorded a partial attenuation of "green" photons that resulted in a shift of the spectral peak to ~680-700 nm in the lungs. Nevertheless, the dual-color system can be considered effective and applicable in vivo because the spectra of CBG2 and CBR2 can still be adequately spectrally separated which allowed to discriminate the light output of both click-beetle luciferases. The discrimination of the light output was calculated by the spectral unmixing algorithm tool as part of the IVIS imaging device software.

CBG2/NH_2-NpLH2 can also be applied with other bioluminescence systems to perform multicolor bioluminescence imaging. We attempted to pair CBG2/NH_2-NpLH2 (λ=~680 nm) with Akaluc/Akalumine-HCl pair (λ=650 nm). This setup will effectively probe more than one cellular process, each producing specific BL signals upon sequential administration of each substrate in vivo. However, the sequential substrate administration will require the clearance of the first substrate but provides maximal light emission for each luciferase, thereby reducing spectral interference from each luciferase. This example shows the importance of building a bioluminescent pair working with one single substrate to produce more accurate data. However, a triple color system is feasible if CBG2/CBR2 with NH_2-NpLH2 (λ= 680 nm and 730 nm, respectively) are coupled with another bright system as Nanoluc/Hydrofurimazine (λ=460 nm) which is a coelenterazine-depend system and does not interfere with D-luciferin-dependent systems as click-beetle luciferases. This represents an encouraging approach for multicolor visualizations of cells in vivo and in the same living animal. The implementation of the visualization and the quantification of multicolor BL signals will boost novel discoveries in life sciences and can speed up drug discovery and future treatments.

In chapter 5, we provide a detailed protocol on how to perform dual color imaging and resolve mixed spectral images when HEK-CBG2 (λ=660 nm) and HEK-CBR2 (λ=730 nm) cells are injected simultaneously in vivo. The experimental set-up and the use of the spectral unmixing algorithm are explained. The experimental procedure will help to separate and quantify single spectral emissions enabling the visualization of multiple cell types in deep tissue. The protocol may also be extended to perform in vivo multicolor BLI where another luciferase/luciferin system can be added. For instance, our system made of CBG2/CBR2 and NH_2-NpLH2 can be paired with another orthogonal system like Nanoluc marine luciferase. Nanoluc has a specific affinity for coelenterazine-like substrates but not for D-luciferin-like substrates and therefore, produces specific

BL signals. This approach can be considered for a triple-color BLI application that will ensure a good spectral separation for each luciferase used in vivo.

Tuning the functionality of PLGA-nanoparticles for in vivo Tumor-associated macrophage visualization

As described **in chapter 1**, tumor cells and immune cells can be visualized using indirect and direct labeling strategies. Inflammatory cells as macrophages are attractive targets because they are recognized to play increasingly crucial roles in cancer growth, progression, and metastasis and are indicated as tumor-associated macrophages (TAMs) [11]. Indeed, macrophages can differentiate upon stimulation by specific chemical factors as chemokines, growth factors and cytokines released in the (tumor) micro-environment and they can change their functional state reversibly in pro-inflammatory (classical activation; M1 like phenotype) or anti-inflammatory (alternative activation; M2 like phenotype) form. However, this is only an oversimplification because macrophages can show both characteristics belonging to the main phenotypes[12]. Moreover, their phagocytic nature and their ability to reach promptly the inflamed or cancer sites, make them an attractive target for cell imaging and therapeutic aims[13]. Imaging both pro-inflammatory or anti-inflammatory phenotypes will give more insight into macrophage behavior in their environment and it will contribute to design new therapeutic interventions.

Targeted delivery approaches to image and treat cancer have shown a steep rise over the past decades[14–16,17]. The choice of the most efficient delivery approach is quite challenging because the desired system must be capable of specifically targeting diseased cells without affecting the normal healthy cells/tissues. On the other hand, formulated nanocarriers used as delivery systems must pass through several physiological and biological barriers in the body before it can reach its target. Choosing between passive targeting and active targeting of cells is not trivial. As explained in **chapter 1,** passive targeting relies on the Enhanced Permeability and Retention (EPR) effect and therefore nanocarriers are delivered to the desired target (usually cancer site) driven by the leaky tumor vasculature. Indeed, it is well known that under certain conditions like hypoxia and inflammation the endothelium of blood vessels can become more permeable. This leaky vasculature lets nano-system reach the tumor stroma and the impaired lymphatic drainage contributes to nanocarriers retention[17]. However, the characteristic of nanocarriers used for passive targeting relies mainly on the *size*, because the optimal size range is around 20-200nm[18,19,20]. The EPR effect seems highly variable and heterogeneous amongst patients due to differences in tumor growth, vascular distribution and intra-tumoral blood flow. Indeed, greater sizes will cause the entrapment of nanocarrier by Reticuloendothelial System (RES) like monocytes, macrophages and dendritic cells[21].

Another characteristic that can affect the passive targeting of cells is the circulation time. The hydrophobic surface and the charged system can also influence the uptake from RES and determining their opsonization. Thus, a possible solution is to modify the nanocarrier surface by attaching PEG chains which confer stealth properties and longer circulation time[22].

The chemical structure of nanocarriers has a crucial impact on nanocarrier retention into specific organs/tissues and prevents off-target interactions when introducing a targeting ligand. These characteristics are critical to the active targeting that increases significantly the accumulation of the payload in the target site. In the case of targeting tumor-associated macrophages both passive and active targeting have been performed. For active targeting, there is a large spectrum of ligands mainly based on monoclonal antibodies, peptides, oligomers, or small molecules like mannose and legumain. The ligands mostly aim to reduce the number of TAMs by inhibiting macrophage recruitment, reprogramming TAMs towards an anti-tumoral phenotype, initiating of immune response and blocking the tumor-promoting functions of TAMs. These strategies are all aimed to increase the accumulation of the payload compared to the passive delivery in preclinical analysis[23].

In chapter 6, we describe the formulation of fluorinated PLGA-nanoparticles for the active targeting of macrophages in breast cancer. Breast cancer is the leading cause of cancer mortality in women over the past 25 years and the identification of new strategies for early-stage diagnosis and therapy can contribute to design new therapeutic interventions. The aggressive 4T1 mouse breast cancer model we used has been previously described in which syngeneic 4T1 tumor cells are injected subcutaneously and will rapidly form solid tumors. These solid 4T1 breast cancer tumors develop hypoxic and necrotic areas [25,26] which increases significantly the recruitment of hypoxic TAMs promoting tumor progression and delaying the antitumor immune response [27].

To target TAMs in the tumor microenvironment, mannose-decorated PLGA nanoparticles have been employed. Since activated TAMs have upregulated mannose receptors, the mannose ligand will act as a cellular membrane-docking ligand to increase the cellular uptake by activated TAMs. The polymeric PLGA structure was also chemically conjugated to polyethylene glycol (PEG) chains and to the fluorescein isothiocyanate (FITC) conferring optical properties. PLGA-nanoparticles decorated or not with mannose ligand had a size ranging between 320 and 370 nm and reaching a narrow size distribution. As MRI contrast agent, cyclic perfluoro-15-crown-5-ether (PFCE) was chosen amongst the other perfluorocarbons because it has 20 equivalent ^{19}F atoms resulting in a specific single resonance peak when ^{19}F-NMR measurement is performed. PFCE is not toxic and is

mostly used in a form of nano-emulsion. However, functionalization of nano-emulsions requires complex chemistry and often needs a lipid shell for better stability such as phospholipids which confers longer circulation time[28]. Herein, we decided to stabilize PFCE using a PLGA-PEG shell that is easy to formulate and functionalize instead of a lipid coating. PLGA nanoparticles can be easily customized allowing high encapsulation of the contrast agent and importantly allowing surface decoration with an active ligand. Biodegradable PLGA has previously been used as carriers for the controlled delivery of macromolecular therapeutics including proteins, peptides, vaccines, genes, antigens and growth factors[29,30]. Thus, PLGA has several advantages and is FDA-approved for human use and stability for long-term storage.

Another important feature of ^{19}F-based imaging, is the lack of background when performing imaging in vivo. Indeed, the accumulation of ^{19}F-labelled immune cells at the inflammation sites generates "hot spots" which are detectable by spin-density weighted ^{19}F-MRI with no background signal due to the absence of endogenous fluorine in the body. On the other side, ^{19}F MRI imaging has detection limits and low sensitivity in vivo and therefore, it requires a larger accumulation of the tracer in targeted particles compared to iron oxide particles[24]. One solution can be increasing the concentration of nanoparticles injected which can result in a toxic bioproduct in vivo. In some cases, it is also possible to pre-label immune cells with nanoparticles ex-vivo and to inject them i.v., enhancing the efficacy of cell labeling. However, this strategy was beyond our aim because we wanted to create an injectable system closest to clinical protocols. Moreover, direct labeling of immune cells *ex vivo* is challenging particularly for terminally differentiated cells since the signal may be diluted because of cell proliferation or cell death. Recently, another strategy has been shown to improve ^{19}F MRI sensitivity in vivo by decreasing the lengthy ^{19}F longitudinal relaxation time (T_1) of PFC and enhancing the paramagnetic relaxation. For instance, an iron-bound fluorinated β-diketone (FDK) chelator can be used for a shortened T_1 imaging increasing the signal-to-noise ratio (SNR) [28].

All in all, mannose decorated-PLGA nanoparticles demonstrated their capability to actively target TAMs and to reach the tumor site. We found that the background noise registered from the surrounding organs was particularly high making detection of untargeted PLGA nanoparticles not feasible. Nevertheless, we could detect a single ^{19}F peak from the 4T1 tumor after injection of targeted-particles by ^{19}F MRS. We believe that a more advanced magnetic field strength and detector coil design might contribute to increase the SNR allowing to detect fewer amount of fluorine in the tumor. In addition, high particle retention was observed in the liver most probably due to the uptake by liver cells like Kupffer cells, liver sinusoidal endothelial cells (LSECs) and hepatic stellate cells (HSCs)[31]. Resident macrophages play a pivotal role in tissue homeostasis and body

defense. Therefore, the presence of circulating resident macrophages and the continuous changes of macrophage phenotype in response to environmental stimuli may also interfere with unspecific nanoparticle uptake. However, the depletion of resident macrophages using for instance clodronate liposomes, has shown to increase the risk of infections. Ultimately, a combination of strategies for example, depletion and re-education of TAMs towards a pro-inflammatory phenotype and using different nanocarriers may be a promising way to achieve significant results. A deeper understanding of macrophage tissue distribution and their plasticity will be essential for refining existing targeting strategies.

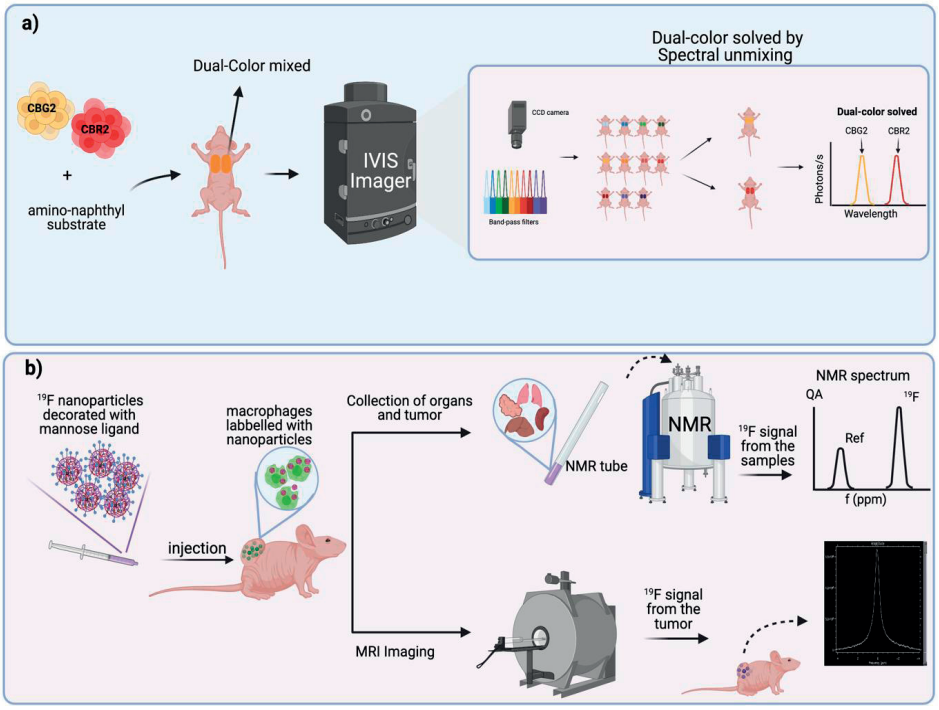

Illustration for Multimodal imaging of immune cells.

a) Sensitive in vivo dual-color bioluminescence with a novel red-shifted CBG2-luciferase cell line. CBG2-cells (λ=680nm) and CBR2-cells (λ=730nm) are injected i.v. and amino-naphthyl luciferin (NH_2-NpLH2) is injected i.p. into nude mice. CBG2 and CBR2 cells are colocalized and mixed BL signals arise from the lungs (orange color). Mice are placed in the IVIS image spectrum device. The device is equipped with a sensitive CCD camera that measures the BL outputs. The use of the spectral unmixing tool enables resolving the dual-color. Respective spectra of CBG2-cells (yellow color) and CBR2-cells (red color) are separated. Separated emission spectra are then registered and quantified. For more details**, chapters 2,3,4 and 5** can be consulted.

b) Fluorinated-PLGA nanoparticle for in vivo macrophage detection. Mannose decorated ^{19}F containing PLGA-nanoparticles are injected i.v. into mice. MRI imaging is performed 48h after nanoparticle injection to allow the targeting of Tumor-associated macrophages (TAMs). Fluorine (^{19}F) signals are detected in the solid breast tumor and quantified by ^{19}F-Magnetic Resonance Spectroscopy (MRS). Alternatively, tumors and relevant organs can be excised and ex-vivo analysis can be performed by ^{19}F-Nuclear Magnetic Resonance (NMR). The ^{19}F content of each sample can be measured by integration ratio with an internal reference to draw an NMR spectrum. For more details, **chapter 6** can be consulted.

FUTURE PERSPECTIVES

In this thesis, we generated new tools to indirectly or directly label immune cells for *in vivo* imaging. The rising interest in bioluminescence for preclinical applications emphasized the need to evaluate several luciferase/D-luciferin analog systems and their applicability for deep-tissue imaging or for multiplex BL application in vivo. We found that CBG2/CBR2 with NH_2-NpLH2 substrate can be used efficiently for NIR dual-color bioluminescence imaging of the lungs as a deep tissue model. Moreover, due to the great brightness of the system in vivo, the imaging time was greatly reduced to 6 min minimizing the discomfort of animals. For this purpose, it would be highly interesting to exploit this pair to test the possibility to image small cell depots in deep organs or lymph nodes. Moreover, the use of CBG2/CBR2 with NH_2-NpLH2 together with another orthogonal luciferase/luciferin systems specific for coelenterazine-like substrates will give the benefit to perform sensitive triple-color BLI *in vivo*. The realization of the triple-color BLI will be favorable to visualize functional state, activation and localization of immune cells in the same animal model. Finally, **in chapter 5** we have provided a protocol to perform spectral unmixing of two-cell populations in a mouse model. The spectral unmixing tool enables to separate successfully the light outputs emitted by two co-localized luciferases. Due to the brightness and sensitivity of the system, it would be interesting to validate the spectral unmixing tool in larger animal models such as rats, hamsters, or ferrets. Moreover, the development of imager equipped with CCD detectors having high quantum efficiency for photons above 700 nm should further improve sensitivity when using these novel NIR luciferase/luciferin systems. Ultimately, the further co-evolution of BL enzymes and substrates will be a promising approach to design brighter and/or NIR synthetic biological light. The computational modeling is also contributing to the design of new BL systems and the optimization of existing ones. I expect that the expanding bioluminescent toolbox will enable in vivo single-cell imaging, monitoring of endogenous protein levels for instance using bright and quantitative NanoLuc technology, monitoring enzymatic activities and other molecular events via novel caged-luciferase systems.

Within this thesis, I have also shown that besides targeting cells with luciferase reporter genes, immune cells can also be labeled with nanocarriers as delivery strategies. **In chapter 6** we attempted to label immune cells, and in particular tumor-associated macrophages (TAMs), by mannose-targeted PLGA-nanoparticles. Labeled TAMs were quantified non-invasively in vivo in the tumor site by ^{19}F-MRS thanks to the PFCE contrast agent encapsulated into the particles. In general, macrophages play a crucial role in the clearance of nanocarriers so, it will be interesting to investigate and compare the cellular uptake of our nanoparticles by resident macrophages like Kupffer cells, liver

sinusoidal endothelial cells (LSECs), and hepatic stellate cells (HSCs). This could help to get more insight on nanoparticle uptake and on the possible circulation time.

Although ^{19}F-MRI has the advantage of high spatial-resolution and also superior tissue penetration, its relative high sensitivity still requires substantial improvements compared to other imaging techniques like optical imaging techniques. Given the linear relationship between signal intensity and PFCE concentration (as well as voxel size), it is possible to optimize the protocol to increase the final concentration of PFCE encapsulated or injected nanoparticles. However, higher doses of injected nanoparticles (more than 5 mg/ml) should be limited in mouse models for safety concerns. Besides, it will be highly beneficial to collect additional information on nanoparticle accumulation by ^{19}F-nuclear magnetic resonance (NMR) for further ex-vivo quantification on the amount of fluorine detected in tumor, liver, spleen and, lungs. I envision that the optimization of targeted-PLGA-nanoparticles encapsulating different perfluorocarbons (PFCs) with specific ^{19}F spectral frequencies and decorated to target specific immune cells, could be promising to visualize the exact cell bio-distribution non-invasively. Overall, the recent developments to optimize nanoparticle formulations with high payloads and the realization of advanced magnetic field strength with sensitive detector coils will offer new promises for labeled cell imaging by ^{19}F MRI.

In conclusion with this thesis, we bring new information on sensitive dual-color BLI for deep-tissue imaging and on the active targeting of immune cells by ^{19}F-MRI. The outcome of our study should be used to address specific questions on *in vivo* target of cells and to design and optimize new cellular imaging tools. Hopefully, the collective efforts between different fields such as biochemistry, immunology, and radiology will lead to the achievement of the ultimate goal: the effective tracking of multiple immune cells in vivo as a future diagnostic tool for cancer.

REFERENCES

1. Mezzanotte, L., van 't Root, M., Karatas, H., Goun, E. A. & Löwik, C. W. G. M. In Vivo Molecular Bioluminescence Imaging: New Tools and Applications. *Trends Biotechnol.* **35**, 640–652 (2017).
2. Xu, T. *et al.* The Expanding Toolbox of In Vivo Bioluminescent Imaging. *Front. Oncol.* **6**, 150 (2016).
3. Kotlobay, A. A. *et al.* Genetically encodable bioluminescent system from fungi. *Proc. Natl. Acad. Sci.* **115**, 12728 LP – 12732 (2018).
4. Gregor, C., Gwosch, K. C., Sahl, S. J. & Hell, S. W. Strongly enhanced bacterial bioluminescence with the ilux operon for single-cell imaging. *Proc. Natl. Acad. Sci.* **115**, 962 LP – 967 (2018).
5. Maric, T. *et al.* Bioluminescent-based imaging and quantification of glucose uptake in vivo. *Nat. Methods* **16**, 526–532 (2019).
6. Bazhin, A. A. *et al.* A bioluminescent probe for longitudinal monitoring of mitochondrial membrane potential. *Nat. Chem. Biol.* **16**, 1385–1393 (2020).
7. Lu, L. *et al.* NIR-II bioluminescence for in vivo high contrast imaging and in situ ATP-mediated metastases tracing. *Nat. Commun.* **11**, 4192 (2020).
8. Zambito, G. *et al.* Red-shifted click beetle luciferase mutant expands the multicolor bioluminescent palette for deep tissue imaging. *iScience* **24**, (2021).
9. Amoasii, L. *et al.* In vivo non-invasive monitoring of dystrophin correction in a new Duchenne muscular dystrophy reporter mouse. *Nat. Commun.* **10**, 4537 (2019).
10. Karatas, H. *et al.* Real-Time Imaging and Quantification of Peptide Uptake in Vitro and in Vivo. *ACS Chem. Biol.* **14**, 2197–2205 (2019).
11. Yang, R., Sarkar, S., Yong, V. W. & Dunn, J. F. In Vivo MR Imaging of Tumor-Associated Macrophages: The Next Frontier in Cancer Imaging. *Magn. Reson. Insights* **11**, 1178623X18771974-1178623X18771974 (2018).
12. Yang, M., McKay, D., Pollard, J. W. & Lewis, C. E. Diverse Functions of Macrophages in Different Tumor Microenvironments. *Cancer Res.* **78**, 5492–5503 (2018).
13. Choi, J., Gyamfi, J., Jang, H. & Koo, J. S. The role of tumor-associated macrophage in breast cancer biology. *Histol. Histopathol.* **33**, 133–145 (2018).
14. Mukherjee, S., Sonanini, D., Maurer, A. & Daldrup-Link, H. E. The yin and yang of imaging tumor associated macrophages with PET and MRI. *Theranostics* **9**, 7730–7748 (2019).
15. Mantovani, A., Marchesi, F., Malesci, A., Laghi, L. & Allavena, P. Tumour-associated macrophages as treatment targets in oncology. *Nat. Rev. Clin. Oncol.* **14**, 399–416 (2017).
16. Makela, A. V, Gaudet, J. M. & Foster, P. J. Quantifying tumor associated macrophages in breast cancer: a comparison of iron and fluorine-based MRI cell tracking. *Sci. Rep.* **7**, 42109 (2017).
17. Attia, M. F., Anton, N., Wallyn, J., Omran, Z. & Vandamme, T. F. An overview of active and passive targeting strategies to improve the nanocarriers efficiency to tumour sites. *J. Pharm. Pharmacol.* **71**, 1185–1198 (2019).
18. Miller, M. A. *et al.* Tumour-associated macrophages act as a slow-release reservoir of nano-therapeutic Pt(IV) pro-drug. *Nat. Commun.* **6**, 8692 (2015).
19. Danhier, F., Feron, O. & Préat, V. To exploit the tumor microenvironment: Passive and active tumor targeting of nanocarriers for anti-cancer drug delivery. *J. Control. Release* **148**, 135–146 (2010).
20. Martinez, F. O., Sica, A., Mantovani, A. & Locati, M. Macrophage activation and polarization. *Front. Biosci.* **13**, 453–461 (2008).

21. Tang, Y. *et al.* Overcoming the Reticuloendothelial System Barrier to Drug Delivery with a 'Don't-Eat-Us' Strategy. *ACS Nano* **13**, 13015–13026 (2019).
22. Suk, J. S., Xu, Q., Kim, N., Hanes, J. & Ensign, L. M. PEGylation as a strategy for improving nanoparticle-based drug and gene delivery. *Adv. Drug Deliv. Rev.* **99**, 28–51 (2016).
23. Binnemars-Postma, K., Storm, G. & Prakash, J. Nanomedicine Strategies to Target Tumor-Associated Macrophages. *International Journal of Molecular Sciences* vol. 18 (2017).
24. Makela, A. V & Foster, P. J. Imaging macrophage distribution and density in mammary tumors and lung metastases using fluorine-19 MRI cell tracking. *Magn. Reson. Med.* **80**, 1138–1147 (2018).
25. Bastian, A. *et al.* A small molecule with anticancer and antimetastatic activities induces rapid mitochondrial-associated necrosis in breast cancer. *J. Pharmacol. Exp. Ther.* **353**, 392–404 (2015).
26. Serganova, I. *et al.* Metabolic imaging: a link between lactate dehydrogenase A, lactate, and tumor phenotype. *Clin. cancer Res. an Off. J. Am. Assoc. Cancer Res.* **17**, 6250–6261 (2011).
27. Singh, Y. *et al.* Targeting tumor associated macrophages (TAMs) via nanocarriers. *J. Control. Release* **254**, 92–106 (2017).
28. Rho, J. *et al.* Paramagnetic Fluorinated Nanoemulsions for in vivo F-19 MRI. *Mol. Imaging Biol.* **22**, 665–674 (2020).
29. Vasir, J. K. & Labhasetwar, V. Biodegradable nanoparticles for cytosolic delivery of therapeutics. *Adv. Drug Deliv. Rev.* **59**, 718–728 (2007).
30. Caputo, A., Sparnacci, K., Ensoli, B. & Tondelli, L. Functional polymeric nano/microparticles for surface adsorption and delivery of protein and DNA vaccines. *Curr. Drug Deliv.* **5**, 230–242 (2008).
31. Park, J.-K. *et al.* Cellular distribution of injected PLGA-nanoparticles in the liver. *Nanomedicine Nanotechnology, Biol. Med.* **12**, 1365–1374 (2016).

NEDERLANDSE SAMENVATTING

Via verschillende preklinische studies is in deze thesis beoogd cellen te labelen en deze in vivo te visualiseren. Het einddoel was om de mogelijkheden om bioluminescentie (BL) te gebruiken als optische moleculaire beeldvormingstechniek uit te breiden en om nanodeeltjes te ontwikkelen voor magnetische resonantie beeldvorming (MRI) van immuuncellen. In hoofdstuk 1 is een introductie gegeven van deze twee beeldvormendende modaliteiten alsook de verschillende strategieën om cellen te labelen en af te beelden in een en hetzelfde muismodel.

Bioluminescentie en beeldvorming ervan bij het zeer gevoelig zichtbaar maken van cellen in vivo.

Bioluminescentie is een niet-invasieve optische techniek die wordt gebruikt om cellen te labelen. Het is een veel gebruikte techniek om cellen in hun natuurlijke omgeving te visualiseren en om moleculaire mechanismen, zoals genexpressie, eiwit-eiwit interactie maar ook om celdeling, celdifferentiatie en celdood te volgen. Bioluminescentie is een natuurlijk proces en vindt plaats wanneer een luciferase-enzym een luciferinesubstraat bindt en de oxidatie ervan katalyseert. Het terugvallen van het geoxideerde luciferine (aangeslagen toestand) zorgt voor het vrijkomen van een lichtquantum (een foton) en deze kan worden gedetecteerd door een zeer gevoelige CCD-camera. Bioluminescentie heeft als groot voordeel dat het een relatief goedkope en gemakkelijk toepasbare techniek is. Tegenwoordig en mede door ons onderzoek, zijn de bioluminescente kleurpaletten van het uitgezonden licht uitgebreid waardoor specifieke luciferasen die een bepaalde kleur licht uitzenden kunnen worden gekozen op basis van het onderzoeksdoel. Cruciale parameters waarmee rekening gehouden dient te worden voordat een experiment opgezet wordt zijn bijvoorbeeld de grootte van het luciferase, uitgezonde golflengte van het licht, thermostabiliteit, optimale pH en cofactoren benodigd voor de reactie zoals Mg^{2+}, ATP en O_2. In Hoofdstuk 2 wordt een overzicht gegeven van de nieuwste genetisch gemanipuleerde luciferasen en ook nieuwe synthetische luciferines. Een luciferase met zijn luciferine substraat noemen we een bioluminiscentie-systeem. De generatie “slimmere” bioluminescentie-systemen zoals b.v. Nanoluc, een blauwemitterende marine luciferase met nieuwe furmazine luciferine analogen heeft een reeks aan toepassingen voor gevoelige in vivo BLI mogelijk gemaakt. Verdere verbeteringen en toepassingen van dit systeem zullen zich breed verspreiden zeker gezien het feit dat Nanoluc-systemen gemakkelijk kunnen worden gecombineerd met terrestrische luciferasen zoals het vuurvliegjes luciferase (Fluc) dat een ander substraat gebruikt. Hierdoor is het mogelijk om twee type cellen of processen zichtbaar te maken in een en hetzelfde dier. Een ander voordeel van op marine gebaseerde luciferase sytemen is dat ze geen ATP als cofactor vereisen, dit in tegenstelling tot de terrestrische luciferasen. Dit

geeft de unieke mogelijkheid om bijvoorbeeld extracellulaire moleculaire processen of entiteiten zoals membraanreceptoren of immuunantigenen te bestuderen.

Bij beeldvorming van 2 verschillende celpopulaties is de keuze van de twee luciferase-systemen van groot belang. Zo zijn de grootte van het luciferase, de uitgezonden golflengte die de kleur en penetratie van het licht bepaald, de thermostabiliteit van het enzym, de optimale pH van de reactie en de behoefte aan cofactoren (Mg^{2+}, ATP and O_2) factoren om rekening mee te houden in de keuze voor de twee beste luciferase/luciferine-paren. In hoofdstuk 2 worden ook schimmel- en bacteriële luciferasen beschreven en hun biologische toepassingen. Het is ook mogelijk om het luciferase substraat, D-luciferine, te koppelen aan een specifieke kleine moleculen ("caged" substraten) waarbij het luciferine alleen vrijkomt en een reactie kan aangaan met het luciferase als het kleine molecuul eraf geknipt wordt of eraf valt als er een interactie plaatsvindt met het kleine molecuul. Hierdoor is het mogelijk om in real-time, afhankelijk van het specifieke molecuul wat er aan gekoppeld zit, bepaalde enzymatische activiteit of opname van bepaalde stoffen b.v glucose of eiwitten zichtbaar te maken in proefdieren. Ook bespreken we andere nieuwe bioluminescentie technieken die de afgelopen jaren ontwikkeld zijn, zoals bijvoorbeeld bioluminescente nanodeeltjes waarbij minder diep penetrerend bioluminescentielicht wordt overgedragen op een oranje-rood fluorescerend eiwit (BRET) waarvan het licht dieper door de weefsels dringt, maar ook oplossingen voor het manipuleren van genen of eiwitten door er een bioluminescent "vlaggetje" (tag) aan te hangen.

Omdat de keuze van het meest geschikte luciferase/luciferine bioluminescentie-systeem voor in vitro en in vivo studies cruciaal is, bieden we hiervoor in hoofdstuk 3 een waardevolle leidraad en beschrijven we de belangrijkste bioluminescente systemen die gebruikmaken van D-luciferine analogen. Hier beschrijven we de spectrale in vitro en in vivo karakteriseringen (welke golflengte van lichtemissie) van verschillende luciferasen met verschillencde subtraten en verdere in vivo validaties met verdere overwegingen en conclusies voor het gebruik van meerkleurige bioluminescente beeldvorming in vivo. Hieruit wordt duidelijk dat voor in vivo detectie van twee celpopulaties in diepe weefsels het beste luciferasen /luciferinesystemen geselecteerd kunnen worden die rood of nabij-infrarood licht uitzenden. Dit omdat de lichtabsorptie van rood en nabij-infrarood licht door weefselcomponenten, m.n. door hemoglobine en melanine, aanzienlijk minder is ten opzichte van blauw of groen licht, waardoor de detectie van licht in vivo toeneemt.

Hiertoe zijn bioluminescente luciferasen gemuteerd zodat ze licht uitzenden van hogere golflengten in het zogenaamde optimale "bio-optische venster" met golflengten tussen de 600 nm–800 nm. Een prachtig voorbeeld van de kracht van een "rood-verschoven" lu-

ciferase/luciferinepaar is het visualiseren van individuele tumorcellen in de longen van muizen en het detecteren van kleine aantallen neuronen in de vrij bewegende dieren.

In hoofdstuk 4 zijn we de uitdaging aangegaan om een bioluminescent-systeem te creëren waarin twee verschillende luciferasen met slechts één enkel substraat worden gebruikt voor twee kleurige in vivo bioluminescentie beeldvorming. Hiertoe hebben we een nieuwe kniptor groen (click beetle green) mutant, genaamd CBG2, gemaakt die in combinatie met het door ons eerder ontwikkeld NH_2-NpLH2-substraat kan worden gebruikt voor nabij infrarood BLI-beeldvorming omdat het licht uitzendt met een golfengte van 660 nm. Het mooie is dat CBG2 in combinatie met NH_2-NpLH2-substraat kan worden samen gebruikt met het door ons eerder gepubliceerde nabij click beetle infraroodsysteem (CBR2) dat hetzelfde NH_2-NpLH2 substraat gebruikt maar licht uitzendt met een golflengte van 730 nm. De beide systemen kunnen worden gebruikt voor tweekleurige in vivo nabij infrarood (NIR) BLI in een en dezelfde muis. Deze combinatie van systemen maakt het mogelijk om semi-kwantitatieve gegevens te verschaffen van getransplanteerde cellen in de longen, als diep weefselmodel in vivo, en de absorptie van licht in vivo te verminderen waardoor je sterkere signalen krijgt. Met deze toepassing wordt ook de noodzaak tot het gebruik van meerdere toedieningen van substraten voorkomen, waardoor de beeldvormingssessie verkort wordt en het gebruik van dieren verfijnd wordt. In vivo is het gebruik van het tweekleurige paar effectief en goed toepasbaar om twee cel populaties van elkaar te onderscheiden omdat de spectra van CBG2 en CBR2 voldoende spectrale scheidingen behouden om ze van elkaar te kunnen onderscheiden. De onderscheiding van de verschillende golflengten van het uitgezonden licht kan worden berekend met behulp van een spectraal ontmengingsalgoritme dat onderdeel is van de IVIS-beeldapparatuur software. CBG2/NH_2-NpLH2 kan ook worden toegepast met andere bioluminescentiesystemen om een specifieke meerkleurige bioluminescentie-beeldvorming uit te voeren, zoals marine luciferase/luciferine maar dan moet men wel 2 verschillende substraten gebruiken.

In hoofdstuk 5 bieden we een gedetailleerd protocol en waardevolle aanbevelingen hoe de spectrale unmixing-tool gebruikt kan worden. Dit helpt onderzoekers bij het beter scheiden en kwantificeren van twee verschillende bioluminescente cel populaties zodra ze gelijktijdig in vivo worden geïnjecteerd. Deze tool heeft een ongelooflijke potentie omdat het niet alleen kan worden toegepast voor diepe weefselmodellen zoals hier uitgelegd, maar ook voor andere toepassingen zoals het afbeelden van kleinere gebieden als lymfeklieren of om een kleiner aantal cellen in hun natuurlijke omgeving af te beelden.

Het belang van het richten op tumor-geassocieerde macrofagen bij kanker

Zoals in hoofdstuk 1 beschreven kunnen tumorcellen en immuuncellen samenwerken om het groeiproces van de tumor en metastase in de micro-omgeving van de tumor te intensiveren. Onder de immuuncellen zijn tumor-geassocieerde macrofagen aantrekkelijke doelwitten omdat hun timing en ruimtelijke lokalisatie in de micro-omgeving van de tumor essentiële informatie kan verschaffen aangaande de groei van kanker. Tumorgeassocieerde macrofagen (TAMs) zijn macrofagen die in de tumoromgeving zijn gedifferentieerd en een ontstekingsremmend fenotype vertonen. Dit gebeurd door specifieke chemische factoren zoals chemokinen, groeifactoren en cytokinen die vrijkomen in de tumor micro-omgeving die er voor zorgen dat pro-inflammatoire macrofagen veranderen in anti-inflammatoire macrofagen. De ontstekingsremmende macrofagen onderdrukken de immuunrespons tegen de tumor door de cytotoxische T-cellen (CD8+) te remmen en ze versterken nieuwe bloedvatvorming (angiogenese) en metastasering. De TAMs zijn dan ook een aantrekkelijk doelwit voor beeldvorming en therapeutische doeleinden met name door hun vermogen om hun vermogen om allerlei materiaal op te nemen (fagocytose) en om hun vermogen om snel de ontstoken- of kankerlocaties te bereiken. Het in beeld brengen van zowel pro-inflammatoire als ontstekingsremmende macrofagen zal meer inzicht geven in het gedrag van macrofagen in hun natuurlijke omgeving en zal bijdragen aan het ontwerpen van nieuwe therapeutische interventies.

In hoofdstuk 6 beschrijven we het genereren van fluor bevattende PLGA-nanodeeltjes voor het zichtbaar maken van macrofagen in MRI (Magnetic Resonance Imaging) bij borstkanker. Borstkanker is de grootste oorzaak van kankersterfte bij vrouwen in de afgelopen 25 jaar en er wordt actief gewerkt aan het identificeren van nieuwe strategieën voor vroege diagnose en therapie. Een van de kenmerken van borstkanker als snelgroeiende solide tumor is de ontwikkeling van zuurstofarme (hypoxische) en necrotische gebieden, omdat de slechte kwaliteit bloedvaten de zuurstofvoorziening niet kunnen bijhouden. Om het dode necrotische materiaal op te ruimen neemt de rekrutering van TAM's in de tumor aanzienlijk toe en kunnen ze bovendien de hypoxische omgevingen goed verdragen. Om selectief op TAM's als doelwit te gebruiken, werden PLGA-nanodeeltjes (PLGA-NPs) ingezet omdat zij stabiel, niet toxisch en bestand zijn tegen mechanische belasting. Er werden PEG-ketens gekoppeld aan de polymere structuur van het nanodeeltje om opsonisatie te voorkomen en de circulatietijd te verlengen. Om cellulaire opname door TAM's te verhogen zijn de PEG-ketens chemisch geconjugeerd aan een mannose-molecuul die fungeerde als ligand voor de mannose-receptoren die verhoogd tot expressie komen op TAMs. Verder is er ook een groen fluorescerend FITC (fluoresceïne-isothiocyanaat) gekoppeld aan de PEG-ketens om ook beeldvormingsvalidaties met een fluorescentiemicroscoop mogelijk te maken. Zoals gezegd bevatten de nanodeeltjes fluor-19 als MRI-contrastmiddel. Hiervoor werd cyclische perfluoro-15-crown-5-ether (PFCE) gekozen uit

de andere perfluorkoolstoffen (PFC's) omdat het 20 equivalente ^{19}F-atomen bevat, wat resulteert in één specifieke resonantiepiek bij de ^{19}F NMR-meting. PFCE in de vorm van een nano-emulsie is niet toxisch en door de FDA goedgekeurd voor gebruik in mensen. Bovendien zorgen de PLGA-NPs voor een beschermend schild van de PFCE waardoor ze ook hun stabiliteit behouden. Bovendien verbeteren de PLGA-NPs de inkapselingsefficiëntie en PFCE-afgifte in de tumor, waardoor het PFCE-signaal wordt verhoogd en de beeldvormingsresultaten worden verbeterd. PLGA-NP's bieden ook het voordeel dat ze makkelijk chemisch gemodificeerd kunnen worden waardoor een flexibel aanpasbaar nano-dragersysteem ontworpen en geproduceerd kan worden dat in vivo specifiek op bepaalde cellen gericht kan worden.

In dit proefschrift hebben we ons gericht op de karakterisering van Mannose-PLGA-PEG nanodeeltjes in vitro en hebben we de mogelijke toxiciteit ervan op cellen getest door TAM's te behandelen met verschillende concentraties van nanodeeltjes. Ook hebben we de cellulaire opname van de nanodeeltjes bevestigd door confocale microscopie. Ten slotte werden PFCE-signalen ook gedetecteerd en gemeten vanuit de tumorlocaties door middel van ^{19}F-Magnetic Resonance Spectroscopy (MRS).

Conclusie

Al met al hebben we nieuwe, nauwkeurige en gevoelige in vivo bioluminescent hulpmiddelen gecreëerd voor BL-beeldvorming in twee kleuren die het mogelijk maakt om afzonderlijk 2 celpopulaties die co-gelokaliseerd zijn in diep weefsel te visualiseren en te kwantificeren. Ook hebben we nieuwe fluor-19 bevattende PLGA nanodeeltjes met aan de buitenkant mannose ontworpen en gekarakteriseerd die het mogelijk maakt om tumor-geassocieerde macrofagen in de micro-omgeving van de tumor te detecteren met de mogelijkheid om ze ook te gebruiken om medicijnen af te leveren. Met behulp van deze nanodeeltjes waarmee we TAMs kunnen detecteren kunnen we een beter begrip krijgen van de verdeling en lokalisatie van TAMs in verschillende stadia van de kanker wat essentieel is voor het verfijnen van doelgerichte strategieën en effectievere therapieën in de nabije toekomst.

SOMMARIO

In questa tesi abbiamo usato diversi studi preclinici per distinguere e visualizzare le cellule del sistema immunitario *in vivo*. L'obiettivo finale e' di espandere gli strumenti utili ad eseguire la bioluminescenza (BL) come tecnica di imaging molecolare ottico e la risonanza magnetica (MR). Nel **capitolo 1** viene fornita un'introduzione a queste due modalità di imaging insieme alle diverse strategie per distinguere e visualizzare le cellule in un unico modello di topo.

Bioluminescenza e sua applicazione per l'imaging di cellule *in vivo.*

La bioluminescenza è una tecnica ottica non invasiva utilizzata per etichettare le cellule. Questa è una tecnica ampiamente utilizzata per visualizzare le cellule nel loro ambiente nativo e per monitorare i meccanismi molecolari come l'espressione genica, l'interazione proteina-proteina e la distribuzione cellulare. La produzione di bioluminescenza avviene in natura quando l'enzima "luciferasi" si lega al substrato "luciferina" e ne catalizza l'ossidazione. Pertanto, il rilassamento della luciferina ossidata dal suo stato eccitato determina il rilascio di un quanto di luce (un fotone) che può essere rilevato da una telecamera molto sensibile. La bioluminescenza ha il grande vantaggio di essere una tecnica economica e facile da usare. Oggigiorno le palette bioluminescenti sono state ampiamente ampliate permettendo di utilizzare luciferasi specifiche e più adatte allo scopo della ricerca.

Nel capitolo 2 sono descritte le più recenti luciferasi ingegnerizzate insieme a nuove luciferine sintetiche. La generazione di sistemi più luminosi come per esempio la luciferasi marina Nanoluc ad emissione blu ha aperto un elenco di applicazioni per una BL piu' sensibile *in vivo*. I miglioramenti di questo sistema avranno un uso molto diffuso perché i sistemi Nanoluc possono essere facilmente accoppiati con luciferasi terrestri come FLuc permettendo di visualizzare due popolazioni cellulari nello stesso animale. Un altro vantaggio dei sistemi basati sulla luciferasi marina è che non richiedono ATP come cofattore a differenza delle luciferasi terrestri. Questo ha il vantaggio unico di studiare, ad esempio, eventi molecolari extracellulari come i recettori di membrana o gli antigeni immunitari. D'altra parte, la scelta di due sistemi di luciferasi per l'imaging di due popolazioni cellulari è cruciale e può influenzare i risultati della ricerca. La dimensione della luciferasi, la lunghezza d'onda emessa, la termostabilità enzimatica, il pH ottimale della reazione e la necessità di cofattori ($Mg^{2+,}$ ATP e O_2) sono parametri da considerare prima di scegliere le due migliori coppie luciferasi / luciferina.

Nel capitolo 2 sono state descritte anche luciferasi derivate da funghi e batteriche per la loro indipendenza dalla somministrazione esogena di substrato che le rende di par-

ticolare interesse per applicazioni biologiche. Substrati con D-luciferina chimicamente sequestrata consentono la rilevazione in tempo reale dell'attività enzimatica e lo studio sull'assorbimento delle proteine. Abbiamo anche coperto le recenti biotecnologie BL emerse negli ultimi anni, tra cui: nanoparticelle bioluminescenti (quantum dots e sonde BRET a due fasi), BL multiplex nei tessuti profondi, soluzioni di modifica genica con tag bioluminescente e tecnologia photo-uncaging. Data l'estrema importanza nel selezionare il sistema di luciferasi / luciferina opportuno per studi *in vitro e in vivo*, nel **capitolo 3** abbiamo descritto i principali sistemi bioluminescenti che utilizzano analoghi di D-luciferina. le considerazioni sulle curve di emissione generate *in vitro ed in vivo* sono state descritte insieme a ulteriori considerazioni e conclusioni per l'imaging bioluminescente multicolore (BLI). Quando e' necessario visualizzare due popolazioni cellulari nei tessuti profondi vengono spesso preferiti sistemi di luciferasi / luciferina emissione nel rosso o infrarosso. Questo perché l'assorbimento della luce da parte dei componenti del tessuto (emoglobina, melanina, ecc.) sarà notevolmente ridotto migliorando la rilevazione della luce durante l'imaging *in vivo*. Per superare questo problema, le luciferasi bioluminescenti sono state mutate per emettere lunghezze d'onda nella cosiddetta "finestra bio-ottica" (λ = 600 nm – 800 nm). Una straordinaria applicazione della coppia luciferasi-luciferina che emette luce rossa o infrarossa è la visualizzazione di singole cellule tumorali nei polmoni di topi o la rilevazione di un piccolo numero di neuroni nel cervello.

Nel capitolo 4, abbiamo creato un sistema bioluminescente in cui vengono utilizzate due luciferasi con un unico substrato per l'imaging di bioluminescenza a due colori *in vivo*. Abbiamo introdotto un nuovo mutante derivato da una lucciola denominata CBG2 che emette luce nell' infrarosso. CBG2 con il substrato NH_2-NpLH2 (λ = 660 nm) può essere integrato con il sistema CBR2 / NH_2-NpLH2 (λ = 730 nm) e utilizzato per bioluminescenza nell' infrarosso (NIR) in vivo. Il sistema consente di registrare dati semi-quantitativi dai polmoni usato come modello di tessuto profondo. Questa applicazione eviterà la somministrazione multipla di substrati rendendo la sessione di imaging più breve, riducendo il numero di animali usati e rendendo piu' facile l'interpretazione dei dati. La coppia bicolore può essere considerata efficace e applicabile in vivo perché gli spettri di CBG2 e CBR2 si mantengono separati permettendo di discriminare la singola emissione luminosa di CBG2 o CBR2. Questo e' reso possibile grazie all'utilizzo di un algoritmo che permette lo "spectral unmixing" cioe' la separazione di piu' spettri bioluminescenti *in vitro ed in vivo*. **Nel capitolo 5**, un protocollo dettagliato e ulteriori raccomandazioni sono descitte per eseguire "lo spectral unmixing". Questo strumento ha un'incredibile potenzialità perché può essere applicato non solo nei modelli di tessuto profondo ma avra' anche un'ulteriore applicabilità per l'imaging di aree più piccole come linfonodi o per l'immaging di un numero molto piccolo di cellule nel loro ambiente nativo.

L'importanza di selezionare e monitorare macrofagi associati al tumore (TAMs)

Come descritto nel **capitolo 1**, le cellule tumorali e le cellule immunitarie possono cooperare per intensificare il processo di crescita del tumore e per creare metastasi. Tra queste cellule immunitarie, i macrofagi associati al tumore (TAMs) sono bersagli interessanti perché la loro tempistica e la loro localizzazione spaziale nel microambiente tumorale possono fornire informazioni cruciali sulla diagnostica e cura del cancro. I TAMs sono macrofagi differenziati con un fenotipo anti-nfiammatorio. Infatti, i macrofagi pro-infiammatori possono evadere la loro attivazione classica su stimolazione da parte di fattori chimici specifici come chemochine, fattori di crescita e citochine rilasciate nel microambiente. Pertanto, i TAMs possono cambiare il loro stato funzionale in modo reversibile da pro-infiammatorio ad antinfiammatorio (attivazione alternativa). L'attivazione anti-nfiammatoria sopprime la risposta immunitaria bloccando ad esempio i linfociti T citotossici (CD8 +) e accelerando il processo di angiogenesi e di metastasi. Inoltre, per la loro natura fagocitica e la loro capacità di raggiungere prontamente i siti infiammati o tumorali, i TAMs sono un bersaglio importante per l'imaging cellulare a scopo terapeutico. Nel **capitolo 6** e' descritta la formulazione di nanoparticelle PLGA che incapsulano 19-F fluoro e che riconoscono i macrofagi indirizzati verso il cancro al seno e ne permettono la visualizzazione mediante risonanza magnetica (MRI). Il cancro al seno è la principale causa di mortalità nelle donne negli ultimi 25 anni e l'identificazione di nuove strategie per la diagnosi e la terapia in fase iniziale è ancora in corso. Una delle caratteristiche del cancro al seno è lo sviluppo di aree ipossiche (a bassa concentrazione di ossigeno) e necrotiche che aumentano significativamente il reclutamento di macrofagi associati al tumore (TAMs) nel sito del tumore.

Per selezionare e visualizzare i TAMs, le nanoparticelle di PLGA (PLGA-NP) sono state utilizzate perché non sono tossiche, sono stabili e resistenti alle sollecitazioni meccaniche. Le catene PEG sono state coniugate alla struttura polimerica per sfuggire alla degradazione prematura delle particelle e aumentarne il tempo di circolazione. Le catene di PEG sono state coniugate chimicamente al mannosio che agisce come ligando alla membrana cellulare dei TAMs. Inoltre, la proteina fluorescente verde FITC (fluoresceina isotiocianato) è stata legata alle catene di PEG per consentire ulteriori investigazioni con l'uso della fluorescenza. Il perfluoro-15-corona-5-etere ciclico (PFCE) è stato scelto tra gli altri perfluorocarburi (PFC) come agente di contrasto per MRI perché risulta in un picco di risonanza singolo e specifico. Non è tossico ed è approvato dalla FDA (Agenzia per gli alimenti ed i medicinali) per uso umano sotto forma di nano-emulsione. Pertanto, le nanoparticelle di PLGA garantiscono un guscio protettivo per gli agenti PFCE mantenendone la stabilità. Inoltre, il PLGA migliora l'efficienza dell'incapsulamento e il rilascio di PFCE nel sito del tumore aumentando il segnale e migliorando i risultati di imaging. I PLGA-NP offrono anche il vantaggio di essere modificati chimicamente con-

sentendo di progettare e produrre un sistema nanocarrier personalizzabile e sono in grado di selezionare le cellule *in vivo*. All'interno di questa tesi, ci siamo concentrati sulla caratterizzazione delle nanoparticelle di Mannosio-PLGA-PEG *in vitro* e abbiamo testato la tossicità delle cellule trattando i TAMs con diversa concentrazione di nanoparticelle. Infine, i segnali di PFCE sono stati rilevati e misurati anche dai siti del tumore mediante la spettroscopia di risonanza magnetica 19F (MRS).

In conclusione, questa tesi include una serie di studi incentrati sulla caratterizzazione di strumenti bioluminescenti *in vivo* per visualizzare due tipi cellulari diversi co-localizzati nei tessuti profondi. Ciò consentirà il rilevamento simultaneo di due popolazioni cellulari nello stesso ambiente e la quantificazione dei rispettivi segnali bioluminescenti. Abbiamo anche progettato e caratterizzato nanoparticelle come strategia per indirizzare e rilevare i macrofagi associati al tumore nel microambiente tumorale *in vivo*. In questa direzione, lo studio ed il monitoraggio della distribuzione e della localizzazione dei macrofagi saranno essenziali per perfezionare le future strategie di targeting cellulare e sviluppare trattamenti antitumorali piu' mirati.

ABOUT THE AUTHOR

Giorgia Zambito was born on August 10th, 1987 in Palermo, Italy. After getting the diploma of secondary school in classical studies, she studied Biological Sciences and she carried out her Master of Science (MSc.) in Cell and Molecular Biology both at the University of Palermo. She performed half of the MSc. program at the Giga research center of Liege (Belgium) thanks to the Erasmus European Exchange program scholarship (2013-2014). During that year, she investigated and wrote her report on the alternative splicing of mRNA in breast cancer cells. In 2015, she obtained her Master's degree (*summa cum laude*) and later, she started an internship on apoptotic effects of natural compounds on melanoma cells at the National Institute of Research in Palermo until June 2016.

In September 2016, she joined the optical molecular imaging (OMIR) group at the Erasmus medical center (EMC) under the supervision of Dr. Laura Mezzanotte. As early-stage researcher, she was introduced to the optical imaging field applied to track immune cells. This project was in collaboration with the department of Immunology of the University of Leiden (LUMC). In January 2017, she started her Ph.D. project on new tools for multimodal imaging of immune cells and she was hired by Medres research company (Cologne, Germany) in collaboration with EMC. During her Ph.D. she was awarded for best poster for the category of new probes for bioluminescent imaging at the EMIM 2018 conference and she was invited speaker at the World Molecular Imaging Conference 2019. She is member of the European Molecular Imaging Society, of the ESMI study group on small animal standardization study and she is co-founding member of the Dutch young Molecular Imaging Community (DyMIC). After her PhD studies Giorgia, she pursued a postdoctoral position at the EMC in 2021 in the OMIR group at the EMC.

PHD PORTFOLIO

Name Ph.D. student	**Giorgia Zambito**
Erasmus MC Department	**Radiology & Nuclear Medicine**
Research School	**Molecular Medicine**
Promotor	**Prof. Dr. C.W.G.M. Löwik**
Co-promotor	**Dr. L. Mezzanotte**

Courses	***Year***	***ECTs***
Laboratory Animal Science (art.9)	2017	3
Translational Imaging Workshop in Molecular imaging (AMIE)	2017	1.4
Academic English course	2017	1
Monocytes: origins, destinations, functions and diagnostic targets	2017	1
Practical Radiation Protection: 5B level	2017	1
Basic Introduction Course on SPSS	2018	1
Course Scientific Integrity	2018	0.5
Biomedical English Writing and Communications	2018	2.5
Graph pad prism version 6 course	2018	0.3
Cell health and metabolism assay in 3D and organ-on-a chip	202	0.3
Career Development for PhD Candidates	2019	0.15
Photoshop and Illustrator CC 2018 Workshop	2020	0.3
Excel basic course	2020	0.3
Excel advanced course	2020	0.4
Subtotal		**13.15**
Conferences and symposia	**Year**	**ECTs**
European Society for Molecular Imaging Summer Workshop (ESMI-TopimTech)-poster presentation	2017	1.25
European Optical imaging user meeting –Perkin Elmer	2017	0.5
European Molecular Imaging Meeting Conference (EMIM)-poster presentation	2018	1.25
Cancer meeting-Immunotherapy approaches to improving cancer outcome and quality of like - oral presentation	2018	1.25
International Symposium on Bioluminescence and Chemiluminescence	2018	1
Stem Cells, Organoids and Regenerative Medicine symposium	2018	1
14th European Molecular Imaging Meeting (EMIM)	2019	1
The 2nd Summer School of the Malopolska Centre of Biotechnology - invited speaker	2019	1.25
World Molecular Imaging Congress (WMIC) - oral presentation	2019	1.25
Topim - winter school - IMAGING IMMUNITY: from nanoscale to macroscale - poster presentation	2020	1.25
EMIM 2020 15th European Molecular Imaging Meeting - poster presentation	2020	1.25
Annual Course on Molecular Medicine	2017-2021	2.8
Subtotal		**15**

Teaching and other activities	Year	ECTs
Weekly Molecular Genetics Department Work Discussion Meeting	2017-2021	1.5
Monthly radiology joined meeting	2017-2021	1
Weekly meeting Laboratory Journal	2017-2021	1
Weekly research group meeting	2017-2021	1
Supervision of trainees	2017-2021	5
Subtotal		**9.5**
Total		**39.65**

Posters

- **G. Zambito,** N. Gaspar, Y. Ridwan, C. Löwik, L. Mezzanotte "Combining luciferases and novel D-luciferin analogues for accurate multicolor bioluminescence imaging". At the European Society for Molecular Imaging Summer Workshop (ESMI Topim Tech). Chania, Crete, Greece, 10-15 July 2017.
- **G. Zambito,** N. Gaspar, Y.Ridwan, C. Löwik, L. Mezzanotte. "Evaluating different luciferase reporter genes combined with novel D-luciferin analogues for BLI: an updated version". At the 13th European Molecular Imaging Meeting. San Sebastian, Spain, 20-23 March 2018.
  (*Poster awarded in the category: New Probes for optical imaging and photoacoustic).*
- **G. Zambito**, S. Deng, N. Gaspar, C. Lowik, P. Di Martino, L. Mezzanotte, "Mannosylated PLGA nanoparticles for tumor macrophage detection by 19F MRI" Presented at the TOPIM 2020, Les Houches, France. 12-17-January 2020
- **G. Zambito**, S. Deng, J.Haeck, N. Gaspar, R. Censi, C. Löwik, U.Himmelreich, P. Di Martino, L. Mezzanotte "Mannosylated PLGA nanoparticles for tumor macrophage detection by 19F MRI" presented at the EMIM 2020, virtual conference. 24-28 August 2020.

Oral presentations

- **Giorgia Zambito**, M.P. Hall, N. Gaspar, Y. Ridwan, C. Shi, Th.A. Kirkland, L.P. Encell, K.V. Wood, C. Lowik and L. Mezzanotte. "A novel click-beetle mutant for near infrared dual color bioluminescence imaging in deep tissue" Presented at World Molecular Imaging Congress, Montreal, Canada, 4-7 September 2019.
- **Invited speaker** for category "Optical imaging and its applications in tumor microenviroment" Malopolska Centre of Biotechnology, Zakopane, Poland, 23-24 May 2019.
- **Giorgia Zambito**, Siyuan Deng, Joost Haeck, Natasa Gaspar, Uwe Himmelreich, Roberta Censi, Clemens Löwik, Piera Di Martino, Laura Mezzanotte "Fluorinated PLGA-PEG-mannose nanoparticles for tumor-associated macrophage detection by optical imaging and MRI" European Association for Cancer Research (EACR), 30 June 2021

LIST OF PUBLICATIONS

- **Zambito G.** and Mezzanotte L. Dual color near infrared bioluminescence imaging of two cell populations in mice. Star Protocols, 2021. *(submitted)*
- Siyuan Deng, Maria Rosa Gigliobianco, Yimin Mijiti, Marco Minicucci, Manuela Cortese, Campisi Barbara, Dario Voinovich, Michela Battistelli, Sara Salucci, Pietro Gobbi, Giulio Lupidi, **Giorgia Zambito**, Laura Mezzanotte, Roberta Censi and Piera Di Martino. Development and Characterization of a Novel Redox-responsive Nanocapsule as Potential Intracellular Delivery System. *(submitted)*
- **Zambito G.**, Deng S., Haeck J., Gaspar N., Censi R., Löwik C., Himmelreich U., Di Martino P., Mezzanotte L. Fluorinated Mannose-PLGA nanoparticles for tumor-associated macrophage detection by optical imaging and MRI. Frontiers in medicine on translational imaging, 2021 *(manuscript in preparation).*
- **Zambito G**., Chawda C., Mezzanotte L. Emerging Tools for Bioluminescence Imaging. Current Opinion in Chemical Biology. 2021
- Gaspar N, Walker JR, **Zambito G**, Marella-Panth K, Lowik C, Kirkland TA, Mezzanotte L. Evaluation of NanoLuc substrates for bioluminescence imaging of transferred cells in mice. J Photochem Photobiol B. 2021 Jan 26; 216:112128.
- Costagliola di Polidoro A, **Zambito G**, Haeck J, Mezzanotte L, Lamfers M, Netti PA, Torino E. Theranostic Design of Angiopep-2 Conjugated Hyaluronic Acid Nanoparticles (Thera-ANG-cHANPs) for Dual Targeting and Boosted Imaging of Glioma Cells. Cancers (Basel). 2021 Jan 28; 13(3):503.
- Deng S, Iscaro A, **Zambito G**, Mijiti Y, Minicucci M, Essand M, Lowik C, Muthana M, Censi R, Mezzanotte L, Di Martino P. Development of a New Hyaluronic Acid Based Redox-Responsive Nanohydrogel for the Encapsulation of Oncolytic Viruses for Cancer Immunotherapy. Nanomaterials (Basel). 2021 Jan 8; 11(1):144.
- **Zambito G**, Hall MP, Wood MG, Gaspar N, Ridwan Y, Stellari FF, Shi C, Kirkland TA, Encell LP, Löwik C, Mezzanotte L. Red-shifted click beetle luciferase mutant expands the multicolor bioluminescent palette for deep tissue imaging. iScience. 2020 Dec 26; 24(1):101986.
- **Zambito G**, Gaspar N, Ridwan Y, Hall MP, Shi C, Kirkland TA, Encell LP, Löwik C, Mezzanotte L. Evaluating Brightness and Spectral Properties of Click Beetle and Firefly Luciferases Using Luciferin Analogues: Identification of Preferred Pairings of Luciferase and Substrate for In Vivo Bioluminescence Imaging. Mol Imaging Biol. 2020 Dec; 22(6):1523-1531.
- Gaspar N, **Zambito G**, Dautzenberg IJC, Cramer SJ, Hoeben RC, Lowik C, Walker JR, Kirkland TA, Smith TP, van Weerden WM, de Vrij J, Mezzanotte L. NanoBiT System and Hydrofurimazine for Optimized Detection of Viral Infection in Mice-A Novel in Vivo Imaging Platform. Int J Mol Sci. 2020 Aug 15;21(16):5863.

- Gaspar N, **Zambito G**, Löwik CMWG, Mezzanotte L. Active Nano-targeting of Macrophages. Curr Pharm Des. 2019;25(17):1951-1961.
- Kleinovink JW, Mezzanotte L, **Zambito G**, Fransen MF, Cruz LJ, Verbeek JS, Chan A, Ossendorp F, Löwik C. A Dual-Color Bioluminescence Reporter Mouse for Simultaneous in vivo Imaging of T Cell Localization and Function. Front Immunol. 2018 Jan 8; 9:3097.

DANKWOORD (ACKNOWLEDGEMENTS)

«**e quindi uscimmo a riveder le stelle**»
- Inferno 34, Divina Commedia, Dante Alighieri.

«**and thence we came forth to see again the stars**»
Inferno 34, The Divine Comedy, Dante Alighieri.

It is hard to realize that this crazy, long and exciting journey came to the end. So many times, I fell and stood up again! I felt discouraged one day and I felt optimistic the day after. Overcoming this roller-coaster of feelings has only been possible with the support of my friends, family, and colleagues.

First of all, thank you Prof. Clemens for being my supervisor and for all your time in guiding me. Thank you for your immense knowledge and your inspiring opinion on the newly published papers. Thank you also for the wonderful boat trips with the whole group in Leiden. That was so much fun!

Laura, no words are enough to thank you for the time and efforts spent in supervising, teaching, guiding me, and giving so many suggestions. Thanks for your optimism and all the comforting words when I was disheartened. You were always comprehensive and supported me a lot.

OMIR colleagues: Natasa, Marc, Kranthi, Roisin, and Chintan: it was great having you as my colleagues. Thank you guys for the time spent together inside and outside the lab. For the post-work beers, the picnics in the park and for the fun we had together. Good luck with your future careers!!

All the colleagues from the Genetics and Radiology departments: thank you all for the chatting time in front of the coffee machine. This helped me a lot to break my lab days.

My co-authors and the Promega team: Mary, Lance, Ce, and Thomas. Thank you for your time in reviewing the manuscripts.

Dustin and Giulia: thanks for your hard work in the lab. It was fun being your supervisor. You are great workers ;)

Yanto: Bedankt voor je tijd! Thank you for your time and for teaching me all the tricks for mouse imaging. After 5 years, my Dutch is still not good but I know you believe in me and my potentiality…ahahah I hope one day we could talk about food and recipes in Dutch.

Lauretta: thank you for being my paranymph. You spent so much time supporting me mentally and psychologically in the last 5 years that I am so glad to have met you! Thank you for the board-game nights, for the guitar sessions, and the aperitivi at your place. So much fun with you!!

Alvja, my paranymph… che dire? Grazie di cuore amica Alvis!! Sei arrivata a Rotterdam e ne abbiamo combinate di tutti i colori. Grazie per il tuo supporto, per i tuoi consigli, per il tuo sostegno e per avermi sempre dato coraggio. Ti prometto che faro' lo stesso con te J

Siyuan: ciao mia bella Siyuan! Without you, the nanoparticle paper would not have been possible. Thank you for the time spent together forcing me to work hard in the lab until 20:00. I was suffering and complaining all the time but you taught me to never give up when experiments are not working as expected. That is science, right??? I hope to see you soon. I wish you the best in your future!

Amerigo: "Giorgis devi stare calma". Tu sapevi che l'apparenza inganna e che dietro ai miei sorrisi si nascondeva un esaurimento nervoso (:D). Grazie per le tue parole, per il tuo supporto e per avermi introdotto al mondo delle nanoparticelle svelandomi tutti i segreti che conoscevi. Grazie per le birre, le cene, i pranzi sul prato durante il lunch break e per tutti gli stupidi video che facevi e che condividevi con me. Mi manchi tantissimo amico mio!

Giannis: my greek/italian friend. Thank you so much for the coffee breaks and your amazing dinners. I wish you good luck with your thesis and with your future!! In bocca al lupo J

Angelaaa: signorinella mia ci siamo conosciute in laboratorio e poi siamo diventate amiche. Grazie mille per il tempo passato insieme. Sei una persona speciale e non vedo l'ora di venirti a trovare a Napoli. Mi manchi!

To all the friends from Nijmegen: zia Betty, Mora, Lorenz, Nader, Giek, Michele, Daniela, Martina, Lauretta, Jordi, Marco. Grazie per le serate passate insieme. Per le giocate notturne a Risk-Game of Thrones, per le chiacchierate e per i parties. Vi ricorderò con grande affetto e vi auguro il meglio.

Zia Betty: sei pazzeska! Grazie per il tuo supporto, per le chiacchierate ignoranti e per il tempo passato assieme. Per i concerti e la nuova musica che mi hai fatto conoscere. In bocca al lupo per tutto zia!!

Geert and Annemiek: thank you for the time spent together and for sharing with me your precious collection of funky beers. I wish you guys all the best!!

Peter, Deborah, Yvet, Chao and Elisavet: Thank you for the time spent together and for your suggestions about the PhD life J

Sandrina e Giacomini: ciao amiciiii!! Thank you for your support and for the special friendship we developed in these years. I will never forget the time spent together and the trips around Sicily and in Madrid…It was so much fun with you guys!! I miss you a lot and I hope to see you soon!

Gli italiani a Rotterdam: Cristiana, Marco, Chiara, Ghitto. Spero che i nostri barbecues, pizze e gin tonics non saranno mai abbastanza. Grazie ragazzi!!

Gli amici di Palermo: Dariella, Serenuzza, Desi, Lo Cullo, Annarita, Silvia, Giammi e Sampi (il mio collega del cuore). Grazie per il tempo passato assieme. Ogni volta è una gioia ritrovarsi a Palermo!

Ma anche Gianni, Claudia, Chicca, Marco, Fulvio, Bonga, Fausto, Tina e Ciro, La Barba, Frenci, Budda, Fede, Aldo, Tullio, Lo Sicco, Maister, Canna, Cilla, Vito e Anna e tanti altri che sicuramente ho scordato. Grazie a tutti voi e per il tempo passato insieme!

Robi e Stefi: ragazze vi adoro! Grazie per esserci sempre state. Per le chat, i messaggi vocali, e per tutti i gossips condivisi…Vi voglio bene e vi auguro il meglio!

Chiaretta, amica del mio cuore: cosa posso dire? Ci conosciamo da secoli e averti nella mia vita mi riempie il cuore di gioia. Sei un tesoro, mi hai sempre ascoltata e supportata pur vivendo lontane. Il bene che ti voglio è immenso e sei una persona splendida. Grazie per questa longeva amicizia…Prosit!!

La mia famiglia, grazie per il vostro supporto e per le foto che mi avete mandato al mare quando io invece ero in laboratorio a lavorare :P

Ringrazio anche mio Padre per il suo sostegno e per le chiacchierate spensierate al telefono. So che per te è difficile stare lontani ma grazie per avermi capita e sostenuta.

Vorrei anche ricordare mia zia Anna: zia sei sempre stata orgogliosa di me ed interessata al mio lavoro. Grazie per le chiacchierate in campagna e per tutte le cene di Natale che hai organizzato. Mi manchi tantissimo zia <3

Gabri, Vinci e Charlie-amore: grazie per avermi supportato e sopportato in questi anni. Sorellina mia che dire, sei una sorella fantastica e un'amica d'oro. Grazie per tutto quello che hai fatto e continui a fare per me! Vi voglio bene ragazzi e vi auguro il meglio!

Mamma: grazie per tutto il supporto che mi hai dato ed i sacrifici che hai fatto per me. Non ci saranno mai abbastanza parole per descriverti la mia gratitudine. E' grazie a te che sono diventata quella che sono adesso! Ti voglio bene Mamy <3

Questa tesi la dedico a te perché tu mi hai insegnato a non arrendermi mai.

Mio caro Gius: grazie per la tua pazienza, la tua positività, le tue parole di conforto e per esserci sempre stato. Grazie per il supporto ed il sostegno che mi hai dato. Ti auguro di realizzare tutti i tuoi obiettivi e tutti i tuoi sogni. Sei una persona davvero speciale ed io sono fortunata ad averti accanto! Ti amo.